Universidade do Minho
Escola de Ciências

Ângela Beatriz Martins Pinto Leite

A peptide-mediated drug delivery system to target macrophages in cancer therapy

October 2023

A peptide-mediated drug delivery system to target macrophages in cancer therapy

Ângela Beatriz Martins Pinto Leite

UMinho | 2023

FCT
Fundação para a Ciência e a Tecnologia
MINISTÉRIO DA CIÊNCIA, TECNOLOGIA E ENSINO SUPERIOR

NORTE2020

PORTUGAL 2020

UNIÃO EUROPEIA
Fundo Europeu de Desenvolvimento Regional

Universidade do Minho
Escola de Ciências

Ângela Beatriz Martins Pinto Leite

A peptide-mediated drug delivery system to target macrophages in cancer therapy

Master Thesis
Master in Chemical Analysis and Characterization Techniques

Work done under the guidance of
Professor Susana Paula Graça da Costa
and
Professor Maria Manuela Marques Raposo

October 2023

DIREITOS DE AUTOR E CONDIÇÕES DE UTILIZAÇÃO DO TRABALHO POR TERCEIROS

Este é um trabalho académico que pode ser utilizado por terceiros desde que respeitadas as regras e boas práticas internacionalmente aceites, no que concerne aos direitos de autor e direitos conexos. Assim, o presente trabalho pode ser utilizado nos termos previstos na licença abaixo indicada. Caso o utilizador necessite de permissão para poder fazer um uso do trabalho em condições não previstas no licenciamento indicado, deverá contactar o autor, através do RepositoriUM da Universidade do Minho.

Atribuição-NãoComercial-SemDerivações
CC BY-NC-ND

https://creativecommons.org/licenses/by-nc-nd/4.0/

ACKNOWLEDGMENTS

This dissertation wouldn't be possible without the help and support of several people, to whom I express my sincere appreciation.

Primarily, I would like to thank Professor Susana Costa for introducing me to this fascinating project, which contributed to my professional and personal growth. I am grateful for the guidance and encouragement given throughout this academic year and for teaching me that despite unexpected setbacks, there's always a potential to turn things around.

I would also like to thank Professor Manuela Raposo for the opportunity granted to carry out this project and for the knowledge, help and support provided.

I would like to thank the Centre of Chemistry at the University of Minho, for allowing this project to be carried out, and the Fundação para a Ciência e Tecnologia (FCT) for funding the project PTDC/QUI-OUT/3143/2021, in which this work was included.

I would like to thank Doctor Juan Gallo, Ana and Andreia for the welcome to the INL, for introducing me to the world of nanoparticles and their usage in drug delivery systems.

I would like to thank Dr. Elisa Pinto for her commitment to obtaining NMR spectra and Ricardo Machado for the MS spectra.

I would also like to thank my colleagues from Laboratories 40 and 1, Mariana, Francisca, Nuna, Raquel and Erika, for the pleasant working environment, for the snack breaks and for all the motivation given, and especially Sónia, for inspiring me every day.

A very special thank you to Cátia Martins, who accompanied me in this project since day one, for showing me what dedication looks like, and for tirelessly helping me when I needed it most, which contributed to making this journey more memorable.

I would like to thank my partners in crime, Magnésio, Prata, Irídio and Zircónio, who even though we have been apart this year, we have never stopped supporting each other.

Finally, a big thank you to my parents, for always believing in my potential and for helping me achieve everything I have achieved so far, and especially José Costa, who at this point is also part of my family, for the words of motivation that always gave me strength to continue and for showing me that calmly, everything can be done.

STATEMENT OF INTEGRITY

I hereby declare having conducted this academic work with integrity. I confirm that I have not used plagiarism or any form of undue use of information or falsification of results along the process leading to its elaboration. I further declare that I have fully acknowledged the Code of Ethical Conduct of the University of Minho.

ABSTRACT

A peptide-mediated drug delivery system to target macrophages in cancer therapy

Tumour-associated macrophages (TAMs) are immune cells that perform essential roles within the tumour microenvironment. These macrophages can change their functional characteristics in response to local environmental cues, switching between an M1 phenotype (anti-tumour) or an M2 phenotype (tumour-promoting). Unfortunately, TAMs are largely polarized into the M2 phenotype, contributing to tumour growth and immunosuppression. Therefore, strategies to modulate and reprogram M2 macrophages towards an M1 phenotype have been explored as potential approaches to boost anti-cancer immune responses and enhance the effectiveness of cancer therapies. Recent studies have reported that the peptide M2pep (YEQDPWGVKWWY) preferentially binds to M2 macrophages, making it a promising candidate for targeted drug delivery and bioimaging.

The aim of this work was the development of a new magnetic drug delivery system capable of specifically targeting M2 TAMs and reprogramming their phenotype from predominantly M2 to M1, thereby triggering an immune response against cancer. To achieve this, M2pep was selected due to its ability to target M2 TAMs and was covalently linked to different phospholipids (DPPE and DOPE) for further conjugation with lipid-coated magnetic solid lipid nanoparticles (mSLNs). Peptide synthesis was performed by microwave-assisted solid phase peptide synthesis (MW-SPPS), while conjugation of peptides to phospholipids was performed by solid-phase or solution synthesis. The structure of these conjugates was confirmed by MS, UV-Vis absorption and FTIR. Subsequently, the synthesis of the mSLNs as well as the incorporation of M2pep-lipid conjugates was carried out by a green and simple method, and characterized by DLS, ICP-AES, TEM, UV-Vis and fluorescence spectroscopy.

Furthermore, to confirm the selectivity of M2pep towards M2 TAMs using fluorescence-based techniques, the M2pep was conjugated to a fluorophore (Rhodamine B). This peptide was prepared and coupled to Rhodamine B by MW-SPPS. The obtained probe was purified by semi-preparative HPLC and characterized by MS, UV-Vis absorption and fluorescence spectroscopy.

Keywords: Cancer therapy; M2pep; magnetic drug delivery system, peptide labelling, tumour-associated macrophages.

RESUMO

Um sistema de entrega de fármacos mediado por péptidos dirigido para macrófagos na terapia do cancro

Os macrófagos associados a tumores (TAMs) são células imunológicas que desempenham funções essenciais no microambiente tumoral. Estes macrófagos podem alterar as suas características funcionais em resposta a estímulos ambientais, alternando entre um fenótipo M1 (anti-tumoral) ou um fenótipo M2 (pro-tumoral). Infelizmente, os TAMs são amplamente polarizados no fenótipo M2, contribuindo para o crescimento tumoral. Portanto, têm sido exploradas estratégias para modular e reprogramar macrófagos M2 em direção ao fenótipo M1 de modo a aumentar as respostas imunes anticancerígenas e a eficácia das terapias contra o cancro. Estudos recentes revelaram que o péptido M2pep (YEQDPWGVKWWY) se liga preferencialmente a macrófagos M2, tornando-o um candidato promissor para a administração direcionada de fármacos e produção de bioimagens.

O objetivo deste trabalho foi o desenvolvimento de um novo sistema magnético de entrega de fármacos capaz de atingir especificamente os macrófagos M2 e reprogramar o seu fenótipo para M1, desencadeando assim uma resposta imunitária contra o cancro. Para conseguir isto, o M2pep foi escolhido devido à sua capacidade de visar o fenótipo M2 e foi ligado covalentemente a diferentes fosfolípidos (DPPE e DOPE) para a sua integração no invólucro lipídico de nanopartículas lipídicas sólidas magnéticas (mSLNs). A síntese de péptidos foi realizada por síntese peptídica em fase sólida assistida por micro-ondas (MW-SPPS), enquanto a conjugação com os fosfolípidos foi realizada por síntese em fase sólida ou em solução. A estrutura destes conjugados foi confirmada por EM, absorção UV-Vis e FT-IV. Posteriormente, a síntese das mSLNs bem como a incorporação dos conjugados M2pep-lípido foi realizada por um método simples e verde, e foram caracterizadas por DLS, TEM, ICP-AES, UV-Vis e espectroscopia de fluorescência.

Além disso, para confirmar a seletividade do M2pep em relação aos macrófagos M2 usando técnicas baseadas em fluorescência, o M2pep foi acoplado com um fluoróforo (Rodamina B), por MW-SPPS. A sonda obtida foi purificada por HPLC semi-preparativo e caracterizada por EM, espectroscopia de absorção UV-Vis e de fluorescência.

Palavras-chave: Terapia do cancro; M2pep; sistema magnético de entrega de fármacos, marcação de péptidos, macrófagos associados a tumores.

CONTENTS

LIST OF ABBREVIATIONS, ACRONYMS, AND SYMBOLS

Abs	Absorbance
ACN	Acetonitrile
AcOEt	Ethyl acetate
Al	Albumine
AMF	Alternating magnetic field
ARG	Arginase
Asp	Aspartic acid
a.u.	Arbitrary units
Boc	*tert*-Butoxycarbonyl group
Cy5	Pentamethine cyanine
d	Duplet
DCM	Dichloromethane
DDS	Drug delivery system
D_h	Hydrodynamic diameter
DIC	*N,N*-Diisopropylcarbodiimide
DiO	3,3'-Dioctadecyloxacarbocyanine perchlorate
DIPEA	*N,N*-Diisopropylethylamine
DLS	Dynamic light scattering
DMF	*N,N'*-Dimethylformamide
DMSO-d_6	Deuterated dimethylsulfoxide
DOPE	1,2-dioleoyl-*sn*-glycero-3-phosphoethanolamine
DOX	Doxorubicin
DPPE	1,2-dipalmitoyl-*sn*-glycero-3-phosphoethanolamine
DSPE	1,2-distearoyl- *sn*-glycero-3-phosphoethanolamine
EDC.HCl	*N*-ethyl-*N*'-(3-dimethylaminopropyl) carbodiimide hydrochloride
EPR	Enhanced permeability retention
equiv.	Equivalent(s)
ESI	Electrospray ionization
FDA	Food and Drug Administration

FGF	Fibroblast growth factor
Fmoc	9-Fluorenylmethyloxycarbonyl
FTIR	Fourier-transform infrared spectroscopy
Gln	Glutamine
Glu	Glutamic acid
Gly	Glycine
HGF	Hepatocyte growth factor
HPLC	High performance liquid chromatography
ICP-AES	Inductively coupled plasma atomic emission spectroscopy
IGF	Insulin-like growth factor
iNOS	Inducible nitric oxide synthase
J	Coupling constant
Lys	Lysine
m	Multiplet
MDD	Magnetic drug delivery
MeOH	Methanol
MH	Magnetic hyperthermia
MIONs	Magnetic iron oxide nanoparticles
mLNVs	Magnetic lipid nanocomposite vehicles
MNPs	Magnetic nanoparticles
MRI	Magnetic resonance imaging
MS	Mass spectrometry
mSLNs	Magnetic solid lipid nanoparticles
MW_{calc}	Calculated molecular weight
MW-SPPS	Microwave-assisted solid-phase peptide synthesis
m/z	Mass to charge ratio
NHS	*N*-hydroxysuccinimide
nk	Natural killer
NPs	Nanoparticles
OA	Oleic acid

Oxyma	Ethyl 2-cyano-2-(hydroxyimino)acetate
PAC	Poly(ethylene glycol)-hydrazone-C18
PEG	Poly(ethylene glycol)
PHC	Poly(ethylene glycol)-amide-C18
PI	Polydispersity index
PLC	Preparative layer chromatography
PLGA	Poly(lactic-co-glycolic acid)
Pro	Proline
R_f	Retention factor
RhoB	Rhodamine B
ROS	Reactive oxygen species
s	Singlet
SA	Succinic anhydride
SLNs	Solid lipid nanoparticles
SPIONs	Supermagnetic iron oxide nanoparticles
SPPS	Solid-phase peptide synthesis
TA	Tannic acid
TAMs	Tumour-associated macrophages
tBu	*tert*-Butyl group
TEM	Transmission electron microscopy
TFA	Trifluoroacetic acid
TIS	Triisopropylsilane
TLC	Thin-layer chromatography
TME	Tumour microenvironment
TNBC	Triple-negative breast cancer
Trp	Tryptophan
Trt	Trityl group
Tyr	Tyrosine
UV-vis	Ultraviolet–visible
WHO	World Health Organization

Zpot	Zeta potential
^{1}H NMR	Proton nuclear magnetic resonance
$\boldsymbol{\delta}$	Chemical shift
$\boldsymbol{\lambda_{em}}$	Emission wavelength
$\boldsymbol{\lambda_{abs}}$	Absorption wavelength
$\boldsymbol{\lambda_{exc}}$	Excitation wavelength

LIST OF FIGURES

LIST OF SCHEMES

LIST OF TABLES

SCIENTIFIC COMMUNICATIONS/PROCEEDINGS

Part of the work developed during this dissertation gave rise to a proceeding and an electronic communication in an international congress and a national poster communication:

Conference Proceeding

Ângela B. M. P. Leite; Cátia D. F. Martins; M. Manuela M. Raposo; Susana P. G. Costa. Preparation of a Fluorescent Peptide Substrate to Target Tumour-associated Macrophages. Proceedings of the 27th International Electronic Conference on Synthetic Organic Chemistry. *Chem. Proc.* **2023** (Accepted).

Electronic Communication

Ângela B. M. P. Leite; Cátia D. F. Martins; M. Manuela M. Raposo; Susana P. G. Costa. Preparation of a Fluorescent Peptide Substrate to Target Tumour-associated Macrophages. 27th International Electronic Conference on Synthetic Organic Chemistry. 15-30 November 2023 (Accepted).

Poster Communication

Ângela B. M. P. Leite; Cátia D. F. Martins; M. Manuela M. Raposo; Susana P. G. Costa. Solid-phase synthesis of a M2 macrophage-targeting peptide. P03, 6th Symposium on Medicinal Chemistry of the University of Minho, Braga, Portugal, 15th June **2023**.

Chapter 1

Introduction

1. Introduction

1.1 Cancer Immunotherapy

Cancer is a malignant illness that involves free and accelerated cellular proliferation of abnormal and dysfunctional cells as a result of epigenetic and genetic modifications.[1] This heterogeneous disease is responsible for a large number of deaths every year, being the second-leading cause of death worldwide.[2] According to previously disclosed data,[3] more than 19,3 million new cancer cases have been diagnosed and registered, with an estimated 10 million fatalities in 2020. The World Health Organization (WHO) also predicts a 60% rise in the incidence of new cancer cases worldwide over the next 20 years.[4]

Current cancer treatment options include surgical intervention, chemotherapy and radiotherapy or a combination of these procedures.[5] These therapies include a number of downsides and non-specific side effects, including nausea, heart or brain damage, and losses of fertility, that seriously lower patients' quality of life and reduce the amount of effective dosage that can be administered.[2] In order to improve treatment outcomes and the quality of life for cancer patients, it is important to create strategies that can target cancer cells selectively while causing the least amount of harm to healthy organs.[6]

Therapies that particularly target the immune system rather than cancer cells have recently been developed, to avoid the side effects of common cancer therapies. These new therapies work by interacting with molecules involved in immune cell activation in order to reverse cancer-induced immunotolerance and trigger an anti-tumour immune response, in other words, uses the immune system of the body itself to identify and combat cancer cells.[7] Numerous ways to target the processes that trigger these immune reactions have been made possible by immunotherapy's fast development.[8]

Enhancing immune cell activation and addressing immune pathway dysfunction in the tumour microenvironment (TME) are the two basic methods used in cancer immunotherapy.[8] When the tumour has grown to a size where tumour-induced interactions predominate, TME will be formed. Numerous investigations have revealed that

inflammatory cells such neutrophils and macrophages are present in the majority of human tumours.[9]

1.1.1. Macrophages

Immunology plays a central role in biomedical research, with a focus on macrophages as essential immune system components.[10] Macrophages are known for their role in elimination of microorganisms and their significance extends beyond defense against external invaders, involving various stages of inflammation.[11] They respond strongly to secondary infections, producing important immune system molecules like insulin-like growth factor (IGF), fibroblast growth factor (FGF), hepatocyte growth factor (HGF), that are essential for maintaining the normal functioning of cells, tissues, and organs.[12]

Macrophages are recognized as versatile cells with several important functions, including phagocytosis to help clear the body of dead cells or other debris, role the adaptive immune response by presenting antigens to other immune cells, production of pro-inflammatory cytokines to help regulate immune responses, and therefore, regulation of inflammation, and tissue repair and promoting the growth of new tissue (**Figure 1**). Thus, its importance in the treatment of cellular damage and to trigger innate immunity is undeniable.[12,13]

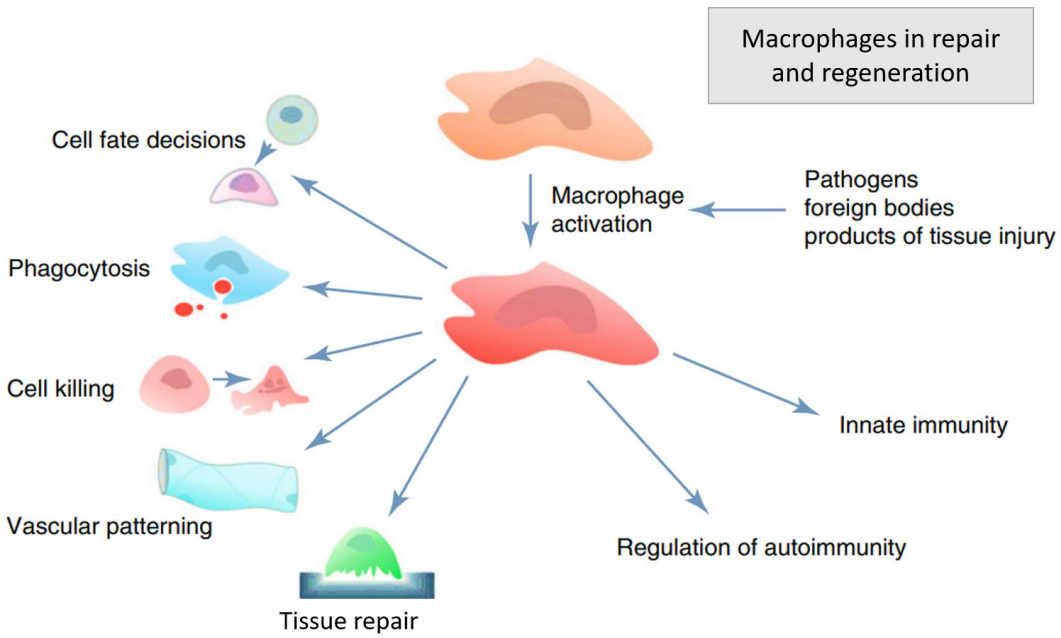

Figure 1. *The role of macrophages in repair and regeneration. (Figure adapted from reference 12)*

Considering that nearly all organs contain macrophages and that these cells have a range of varied subpopulations, the capacity of macrophages to adapt to various microenvironments is notable in infections and cancer.[14,15] In many cases, macrophages are recruited to the TME in response to signals from cancer cells. These macrophages, known as tumour-associated macrophages (TAMs), can have diverse functions that influence tumour behavior as well as its immune responses as being abundant in this environment,[16] making the characterization of different types of TAM's crucial for a comprehensive understanding of their roles and potential therapeutic interventions.[17]

Overall, macrophages hold immense significance in immunology, and specifically, TAMs are gaining attention as potential targets in cancer therapy due to their multifaceted functions.[18]

1.2 Tumour-Associated Macrophages (TAMs)

Tumour-associated macrophages (TAMs), found in the TME play a significant role in promoting tumour cells by suppressing antitumour immune responses. TAMs directly enhance tumour cell growth through angiogenesis by forming new blood vessels or disrupt immune cell interactions within the TME, leading to tumour proliferation.[9,19] The presence of TAMs is generally associated with a poor prognosis in solid tumours,[20] representing one of the primary groups of immune cells that infiltrate tumours and may even occupy up to 50% of the tumour mass (**Figure 2**).[5]

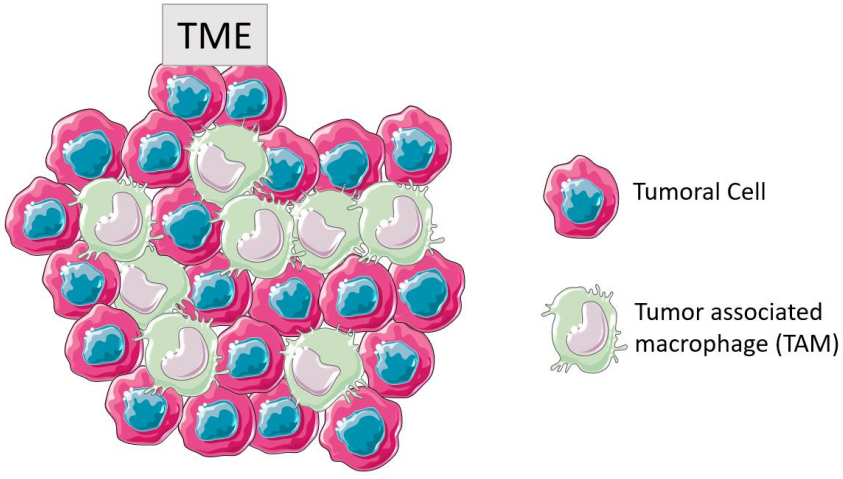

Figure 2. *Tumour-associated macrophages (TAMs) in tumour microenvironment (TME).*

TAMs contribute directly to the formation of blood vessel networks, supplying nutrients and oxygen, what causes further tumour growth, which facilitates the transition of premalignant tumours to the malignant stage. This complex interplay highlights how important TAMs are for the development of tumours.[14]

As a result, TAMs cannot be ignored in tumour progression and are a viable new target for cancer therapy. They can be divided into M1 and M2 macrophage types that coexist in the TME, and because of their plasticity, TAMs can switch from one type to another depending on the environment they are in.[15]

1.2.1. Macrophage polarization

As the tumour subsequently increases in size and an intratumoural vascular network forms, monocytes that were created in the bone marrow that circulate in the blood stream, migrate towards affected tissues, infiltrating into the tumour, and mature into TAMs.[14]

Depending on the cytokine balance, that regulate the immune responses of the TME, TAMs polarize into two functional phenotypes, M1-like macrophage or classically activated macrophages, which are pro-inflammatory, and antitumour immunity, and M2-like macrophage or alternatively activated macrophages, which are anti-inflammatory, immunosuppressive and tumour promoting (**Scheme 1**).[18,21]

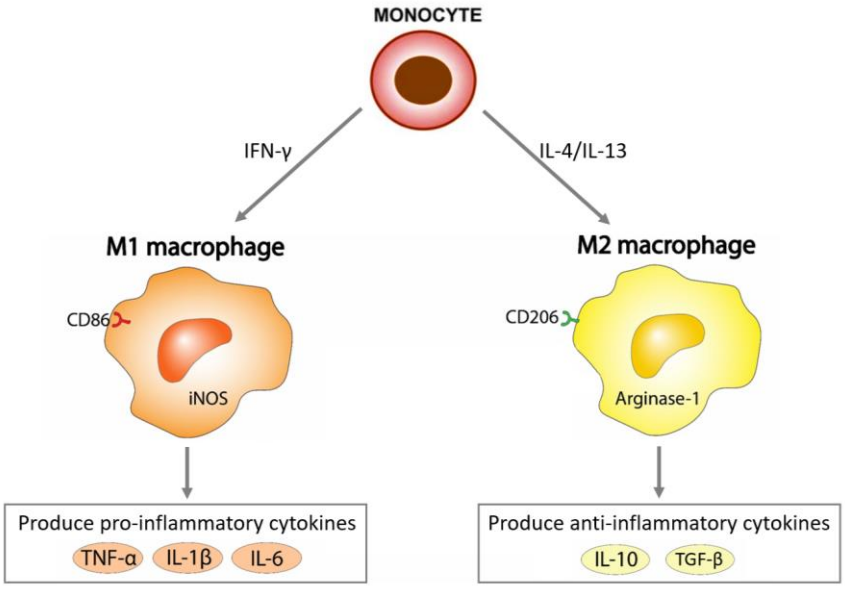

***Scheme 1**. Differentiation of monocytes into polarized macrophage subsets when exposed to different cytokines. (Figure adapted from reference 17)*

Macrophages have traditionally been considered anti-tumourigenic (M1-like) when they produce high levels of pro-inflammatory cytokines (IL-1β, IL-6 and TNF-α), including the production of reactive oxygen species (ROS), that create an environment that inhibits tumour growth. This M1-like TAMs help enhance the overall immune response against tumours by the recruitment and activation of other immune cells, like cytotoxic T cells and natural killer cells (NK cells), which are crucial for recognizing and eliminating cancer cells. They often express an inducible nitric oxide synthase (iNOS) and a CD86 marker that interacts with its corresponding receptor, CD28, on T cells. Their polarization is typically induced by pro-inflammatory signals, like cytokines IFN-γ (**Scheme 1**).[20,22,23]

The M2-like macrophages synthesize anti-inflammatory cytokines (IL-10 and TGF-β), that contributes to tissue repair, angiogenesis (formation of new blood vessels), creating an environment that provides growth factors and immunosuppression, that inhibits immune responses against the tumour. They can inhibit the activity of T cells and NK cells, creating a microenvironment that can protect tumour cells from the immune attack, supporting tumour growth and metastasis. These M2 macrophages express markers like the mannose receptor (CD206) and arginase-1 (ARG-1), and they polarize by inducing IL-4, IL-13, and other anti-inflammatory signals (**Scheme 1**).[15,20,22]

Although these two subtypes of TAMs coexist, higher levels of M2 macrophage infiltration in tumours have often been linked to poor prognosis because their presence indicates a more immunosuppressive and tumour-promoting microenvironment.[5] Additionally, TAMs resembling a pro-tumour M2-like phenotype embrace up to 50% of the tumour mass in some types of cancer.[22] Therefore, lowering the number of M2-like TAMs can alleviate the immunosuppressive TME, stimulate the host immune system, and eventually prevent tumour growth.[5]

Plasticity of these macrophages gives them the ability to repolarize from M1 into M2 macrophage, or vice versa. This unique feature gives the possibility to reprogram the types of TAMs, from an immunosuppressive M2-like state to a pro-inflammatory M1-like.[9] The polarization of M2 to M1 macrophages can enhance the immune response against cancer cells, and eventually prevent tumour growth (**Scheme 2**).[21]

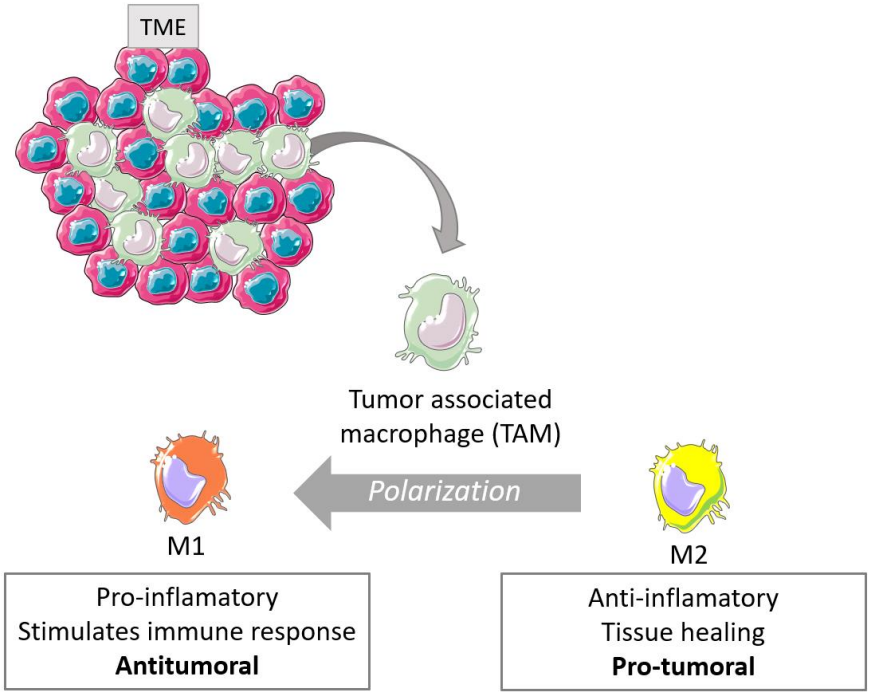

Scheme 2. *Differentiation of tumour-associated macrophages (TAMs) in M1 and M2 phenotypes, with different functions and that manage to polarize into one another.*

TAMs have been targeted with drugs to either deplete them or transform their tumour-supportive M2-like phenotype into the anti-tumour M1-like phenotype. However, because TAMs have low rates of mutation, which could eventually lead to treatment resistance, it is difficult to deliver drugs to them. To address these difficulties, many ligands that target M2 macrophages, like mannose, have been investigated as components of drug carriers. When conjugated with a drug, mannose, a ligand for the mannose receptor (CD206), has been demonstrated to have high affinity for TAMs and improve drug absorption.[24]

As is shown in **Figure 3**, a mannose conjugated lipid-coated nanoparticles with zoledronic acid (Zol), that has been shown selective cytotoxicity to TAMs, wrapped with a extracellular pH-sensitive poly(ethylene glycol) (PEG) shield, accumulated in tumours, eliminating TAMs, decreasing the expression of anti-inflammatory cytokine IL-10 which shows the diminution of the M2 macrophages population, and specifically restraining tumour growth with no significant changes in the main organs.[25]

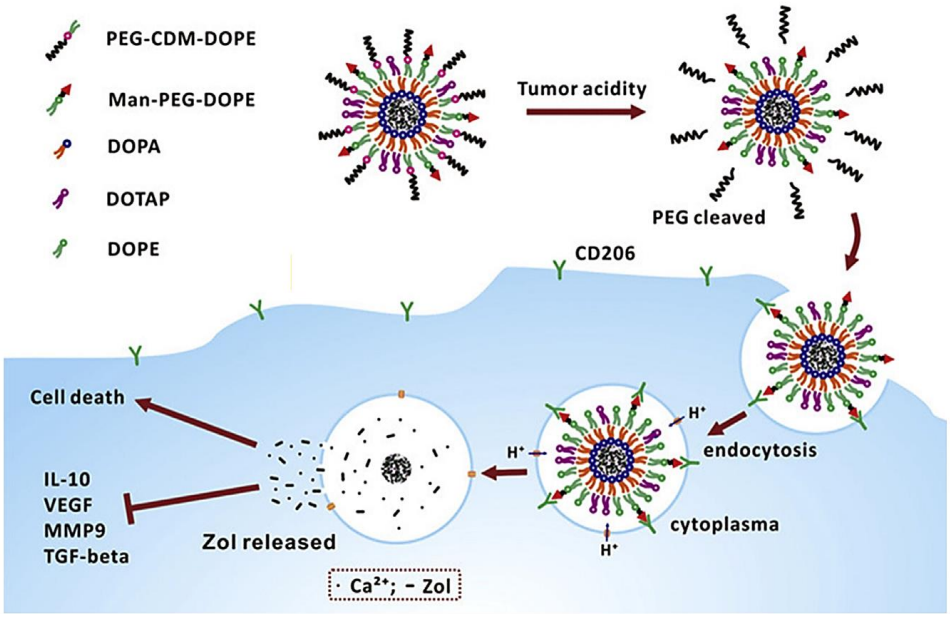

Figure 3. *Lipid-coated nanoparticles with zoledronic acid (Zol) containing conjugated mannose targeting TAMs. (Figure adapted from reference 15)*

Given the significance of TAMs in regulating tumour immunity, there is a considerable interest in developing additional therapeutic approaches that target macrophages, specifically those that are responsible for TAMs pro-tumour activity (M2).[20] Current research focuses on a number of macrophage-targeting agents that prevent macrophage recruitment into tumour tissues, block macrophage differentiation into the M2 pro-tumoural phenotype, or even prevent their repolarization.[14]

1.2.1.1 M2 Macrophage-Targeting Peptide

The significance of M2 macrophages in chronic inflammation and cancer is becoming better understood, and a key goal of macrophage-targeted therapy is the capacity to modify particular fractions of macrophage populations.[26] There have been efforts to administer drugs to TAMs in an effort to deplete them or change their pro-tumour M2-like phenotype into the anti-tumour M1-like phenotype.[24] However, there are currently a few targeting entities that are selective for M2 macrophages, as mannose, which has been conjugated to drug nanocarriers for M2 macrophage delivery, previously shown in **Figure 3**.[25] Yet, the mannose receptor is highly expressed in other cell types, like dendritic cells. The aim is to create an M2-targeted compound that can selectively target TAMs but not other cells.[26]

To increase the selectivity of TAM targeting, a targeting peptide with a 12 amino acid sequence YEQDPWGVKWWY (M2pep) (**Figure 4**), which shows selective binding and internalization in M2 macrophages and minimal M1 macrophage interaction, was identified by Cieslewicz *et al.*,[26] from the biopanning of a peptide phage library.[27] They adopted a peptide library selection strategy since, in comparison to proteins and antibodies, peptides are smaller and can subsequently better penetrate tissues to reach target cells, offering higher binding affinities and specificities for their receptors. Peptide ligands are normally less immunogenic, easier to produce and the existence of several functional groups of amino acids allows conjugation to cargo more flexible.[28] The short half-life of the peptides that may in some cases lower the affinity for the target, is considered as one of their limitations.[27]

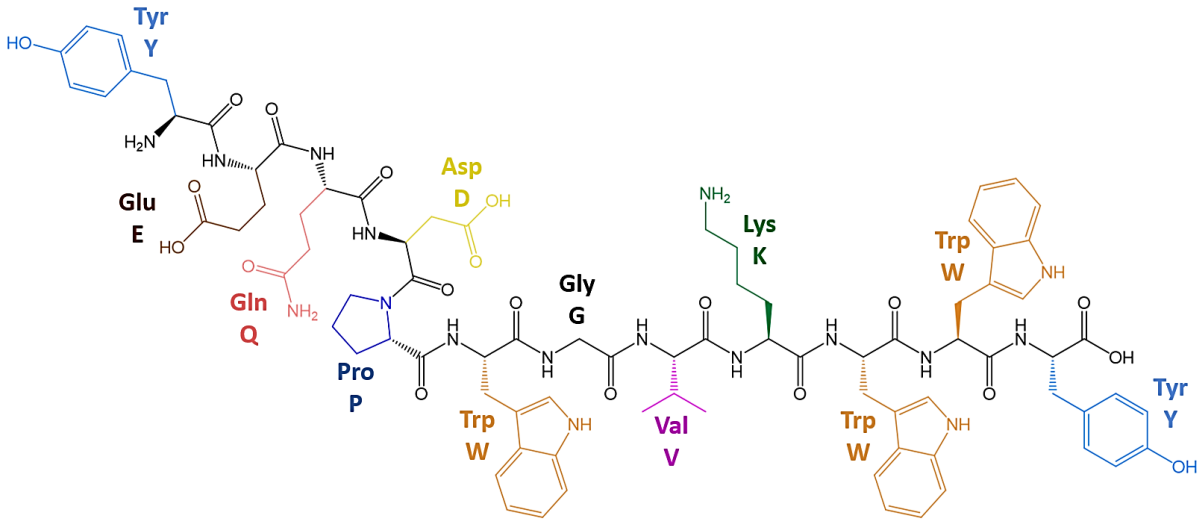

Figure 4. *Structure of the M2 macrophage-targeting peptide (M2pep).*

Since it has already been established that macrophage depletion alone may not be sufficient to completely eradicate cancer, in this work,[26] M2pep was employed to target and deliver a proapoptotic peptide that induces apoptosis - KLA peptide - as a promising alternative to the traditional ligands to isolate M2 macrophages. The results showed that M2pep preferentially binds and accumulates in murine TAMs compared to other cells, like resting macrophages, neutrophils and stromal cells. It has also been demonstrated slower tumour growth in the M2pepKLA treatment group, which indicates that targeted M2 macrophages TAMs in combination with other anticancer agents may improve cancer therapy.[26]

However, the combination of drug loading capacity and the desire of M2 macrophage-binding remains to be improved.[24] In order to get around these limitations, nanomedicines can be modified to carry both chemotherapeutic agents and target peptides, such M2pep, for effectively target TAMs and potentialize the anti-tumour effect of chemotherapy, with less side effects.[22,29]

1.3 Drug Delivery Systems (DDS)

Cancer remains a serious global health problem despite the significant advances made during the past decades. Traditional cancer treatment approaches, like chemotherapy and radiotherapy, have experienced breakthroughs, but these methods still have drawbacks such drug resistance, lack of selectivity and side effects. The idea of producing selective cytotoxic effects on cancer cells is fundamental to the development of improved cancer treatments. This includes reducing damage to healthy tissues while stopping or slowing tumour growth.[30]

These limitations may be overcome through nanotechnology, notably in the delivery of chemotherapeutic agents, like Doxil[31] and Abraxane[32]. The difficulty lies in creating and delivering drugs that specifically target cancer cells while causing the least amount of damage to healthy tissues. These nanotechnology-based approaches aim to overcome the challenges associated with conventional cancer therapies by providing targeted drug delivery and enhanced treatment efficacy.[8]

A successful drug delivery system (DDS) aims to control drug release, with consequential increased circulation time with high stability and improved bioavailability, and optimize drug concentration at the target site and minimal toxicity.[33,34] Innovations in nanotechnology have lined the way for targeted therapeutics, like target-specific nanocarriers, reducing side effects and increasing accuracy in targeting organs or cells.[6,35,36]

Nanomedicine in drug delivery is promising for developing drug-loaded nanoparticles as a perfect solution to afford higher efficacy for cancer therapy, addressing drug selectivity and a precise cancer treatment,[6] furthermore these nanoparticles are versatile for diagnostics tools, sensors, and tissue engineering.[4,37]

1.3.1 Magnetic Drug Delivery (mDD)

Nanoparticles (NPs) have garnered substantial interest from formulation scientists in the field of drug delivery due to their distinctive physicochemical properties and ultra-small particle size (1 to 100 nm), facilitating their ability to cross biological barriers.[30,33] These NPs have unique physical and optical properties and chemical stability, enabling targeted drug delivery to organs, tissues, and even individual cancer cells.[29] These characteristics enhance the bioactivity of therapeutic compounds by lowering the concentration needed, thereby potentially increasing effectiveness and reducing negative effects on healthy tissues.[4] So, nanomaterials can efficiently transport substantial drug doses to localized regions, lowering cytotoxicity and unwanted side effects associated with excessive dosing in undesirable areas.[38–40]

In recent decades, significant strides have been made in the advancement of nanomaterials for effective delivery of anticancer drugs, with magnetic drug delivery systems (MDDs) standing out for their potential clinical applications, using magnetic nanoparticles (MNPs).[41] MNPs have gained attention as versatile tools for diagnosis, monitoring, and therapy due to their relative straightforward synthesis, purification, functionalization, and characterization, together with their usually good biodegradability and diagnostic platform potential, confer major advantages for their use in cancer theranostics, integrating both diagnostics and therapy to provide and precise cancer treatment strategies. Combining these two approaches can help adapt each patient's therapy needs within an personalized design of therapeutic strategy, with a greater probability of a positive outcome while simultaneously minimizing adverse effects.[42,43]

MNPs, which form the main core of MDDs (**Figure 5**), can be easily magnetized under external magnetic fields to release drugs *via* vibration or heat.[41] The most commonly used MNPs in the biomedical field are superparamagnetic iron oxide nanoparticles (SPIONs), such as magnetite (Fe_3O_4) and maghemite (γFe_2O_3) which present high biocompatibility and lower toxicity compared to other metal structures, like gold nanoparticles and carbon nanotubes, addressing degradation and elimination concerns.[4,44,45]

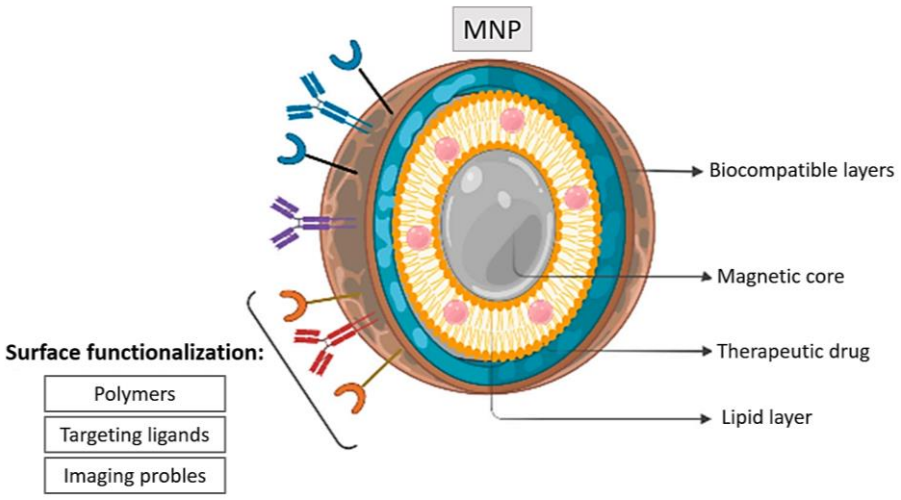

Figure 5. *Structure of a magnetic nanoparticle (MNP), with a magnetic core-shell encapsulated by a biocompatible coating, where drugs are loaded into. (Figure adapted from reference 4)*

These superparamagnetic properties offer control through the application of alternating magnetic fields (AMF). Selective AMF use can force the MNPs to induce local heat, enabling tumour ablation and controlled drug release without invasive procedures.[46,47] These nanoparticles, with their physicochemical traits, small size, and biointeraction potential, serve as magnetic resonance imaging (MRI) contrast agents, hyperthermia inducers by magnetic heating and DDS for cancer treatment (**Figure 6**).[4]

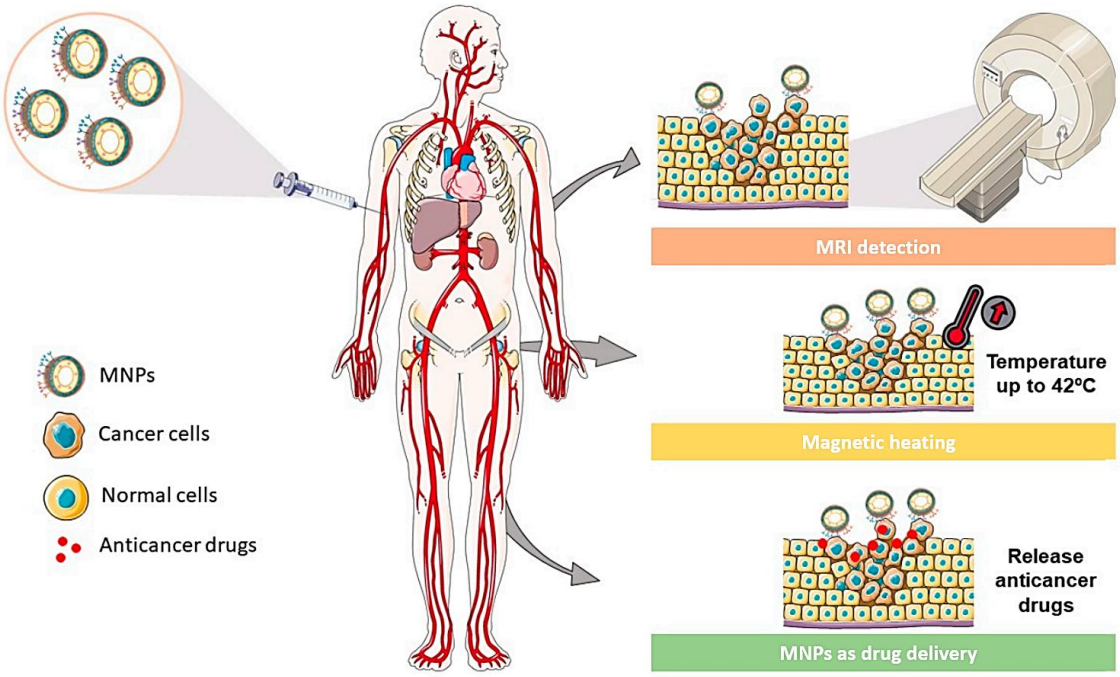

Figure 6. *Magnetic nanoparticle (MNP) applications in diagnosis and treatment of cancer. (Figure adapted from reference 4)*

Magnetic resonance imaging (MRI) is a non-invasive diagnostic tool that utilizes magnetism and radio pulses to create images of internal tissues and organs, providing clear illustrations of soft tissues.[48] MNPs serve as multifunctional MRI contrast agents, offering potential for specific tissue localization,[49] including tumours, like in **Figure 6**.[4] Furthermore, hyperthermia is a cancer therapy approach in which the temperature increases throughout the target tissue causing it to reduce the viability of cancerous cells.[41,46] It has been established that employing MNPs containing drugs could increase the effectiveness of magnetic hyperthermia (MH), by applying an external AMF to induce heat and activate a controlled drug release to the desired specific sites (MH-induced drug delivery)[50,51] or even by endogenous stimuli such as pH changes, since TME has a lower pH than normal physiological values.[52] Therefore, MNPs are well applied as tracking probes and contrast agents in diagnosing in MRI, and as heat-producing particles in MH therapy.[4,53]

Therefore, MNPs as a MDDs are a cost-effective way of delivering drugs to the desired specific sites, with a possibility to obtain large concentrations of anticancer chemicals controlled, causing no toxicity because of the controlled drug release over time.[38,54]

These magnetic nanocarriers performance depends on factors like composition, morphology, and coating. Surface functionalization with targeted ligands reduces toxicity in areas that should not be affected and enhances therapeutic efficacy in targeted sites.[55] Traditional synthesis methods yield MNPs usually with a magnetic core-shell structure and polymer coating, suitable for loading chemotherapeutics and improving stability (**Figure 5**). Additionally, selectivity of MNPs can be improved with their functionalization, such as imaging probes and targeting ligands.[4]

Optimal coating selection is crucial for drug loading and controlled release. Coatings like lipids, polymers and surfactants enhance biocompatibility, systemic circulation, and target reach, while reducing toxicity in healthy tissues. With this purpose, different types of nanomaterials have been developed, such as inorganic and polymeric nanoparticles and lipid-based nanosystems.[22,54,56]

1.3.2 Solid Lipid Nanoparticles (SLNs)

Various strategies have been explored to enhance targeting precision and minimize the toxicity of chemotherapy agents. Among these approaches, different DDS have been thoroughly investigated, including micelles, dendrimers, liposomes, emulsions, solid lipid nanoparticles (SLNs), and polymeric nanoparticles.[57,58] Among these, SLNs based on solid lipids have gained attention for cancer therapy. They offer controlled drug release and reduced toxicity, compared to inorganic and polymeric nanoparticles, making them a promising option for enhancing chemotherapy effectiveness in such diseases.[4]

Lipid-based nanocarriers, notably SLNs, stand out among nanocarriers due to their biocompatibility and biodegradability, large-scale production, and bioavailability. These carriers offer advantages like enhanced drug solubility and absorption, reducing side effects and enabling drug delivery past physiological barriers.[30,59]

SLNs are composed of a lipid matrix that remains solid at room and body temperatures, along with surfactants used as stabilizing and solvating agents. A representation of stabilized SLNs with a neutral surfactant is shown in **Figure 7**. These lipid-based nanocarriers properties, such as size, surface charge, stability, and drug release profile, can be tailored through varying lipid and surfactant compositions. In preparation of SLNs, fatty acids and triglycerides, fatty alcohols, and waxes, are commonly used.[30] The small size of the formulations (10 to 1000 nm range),[60] the large surface-to-volume ratio, and the high drug encapsulation efficiency are the key benefits of SLNs. The selection of the lipids can also influence the biodegradability, stability, and affinity by drugs and other elements (metals, dyes, etc.).[4]

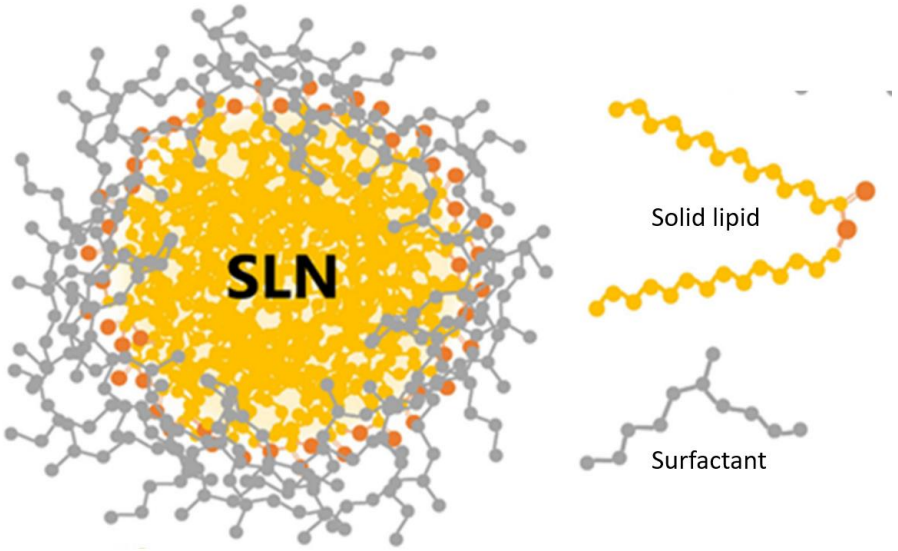

Figure 7. *Schematic representation of stabilized SLNs with a neutral surfactant. (Figure adapted from reference 30)*

These lipid NPs offer simplicity, scalability, and cost-efficiency in drug delivery capable of encapsulating both hydrophobic and hydrophilic chemotherapeutic drugs.[59,61] Not only can SLNs encapsulate single or multiple drug candidates, facilitating multidrug co-delivery strategies, but they also serve as a platform for functionalization, enabling specific targeting and accumulation in tumour regions.[62] Beyond the encapsulation of anticancer drugs, SLNs have already been used to encapsulate magnetic particles.[4]

Recent advancements in cancer treatment involve the utilization of MNPs and SLNs, either individually or combined, resulting in magnetic solid lipid nanoparticles (mSLNs). These mSLNs exhibit exceptional performance and potential in various applications like diagnosis, drug delivery, and other therapeutic approaches. mSLNs are composed of inorganic magnetic nanoparticles embedded within solid lipid nano-matrices. A schematic interpretation of mSLNs can be seen in **Figure 8**. These nanomaterials demonstrate colloidal stability and water solvation through the use of different surfactants during their synthesis.[4]

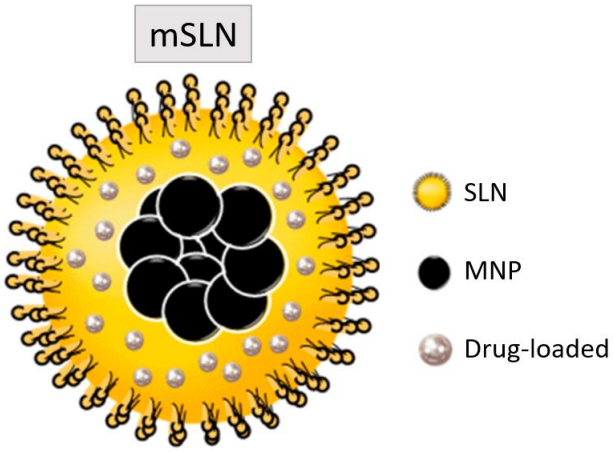

Figure 8. *Representation of a magnetic solid lipid nanoparticle (mSLN). (Figure adapted from reference 4)*

The small size and high entrapment efficiency of mSLNs synergistically enhance their capabilities, combining the advantages of both nanocarriers types.[63] mSLNs are versatile due to the MNPs, finding applications in diagnostics (MRI) and cancer therapy (MH).[64] The hyperthermia approach enhances drug release control, increasing cytotoxicity against cancer cells compared to standalone SLNs or MNPs.[4] These lipid nanocomposites can co-encapsulate imaging probes, like SPIONs and chemotherapeutic agents, exhibit enhanced cell membrane affinity and synergistic functionality. This arises from lipid matrix capabilities, including drug encapsulation and surface functionalization, combined with SPIONs' magnetic properties.[57]

Magnetic nanocarriers offer enhanced drug accumulation in tumours through passive and active targeting approaches. Passive targeting exploits the enhanced permeability and retention (EPR)"effect, which enables the accumulation of different kinds of NPs in the tumour tissue more than they do in normal tissues,[47,65] while active targeting involves external magnetic fields or surface modifications with ligand-receptor interactions, where the MNP surface holds specific ligands for the surface receptors present in cancer cells. Moreover, incorporating chemotherapeutic drugs in mSLN formulation allows a synergistic combination of MH and chemotherapy.[4,8]

Active targeting approaches in drug delivery and imaging, especially in cancer, have expanded due to advances in molecular engineering and screening techniques that produce new targeting ligands for different cell targets. Antibodies, proteins, peptides, and small

molecules are all employed as targeting agents in various DDS.[6] MNPs recently have emerged incorporating fluorophores for simultaneous fluorescence and magnetic scanning, enabling improved *in situ* monitoring. These theranostic NPs hold potential for real-time cancer monitoring and treatment, utilizing both MRI and fluorescence scanning.[38]

Altogether, mSLNs exhibit promise due to their favorable biocompatibility, enhanced thermo-responsiveness compared to SLNs, effective tumour targeting, and high drug encapsulation efficiency.[66,67]

García-Hevia *et al*. recently described a green and direct method to make a mSLN from Carnauba wax (**Figure 9**).[33] This natural compound is available commercially and approved for human use. The authors presented an efficient magnetic lipid-based hybrid nanosystem to simultaneously incorporate MNPs and anti-cancer drugs for the combinatorial thermo-chemoterapeutic treatment, for treating melanoma tumours. The researchers have developed a novel approach for creating magnetic lipid nanocomposite vehicles (mLNVs) that exhibit potent antitumoural activity while maintaining low toxicity. This proposed nanostructure employs a natural hydrophobic matrix composed of Carnauba wax, known for its high melting point, making it a promising choice for a DDS due to its stability of use and reduced drug leakage.[33]

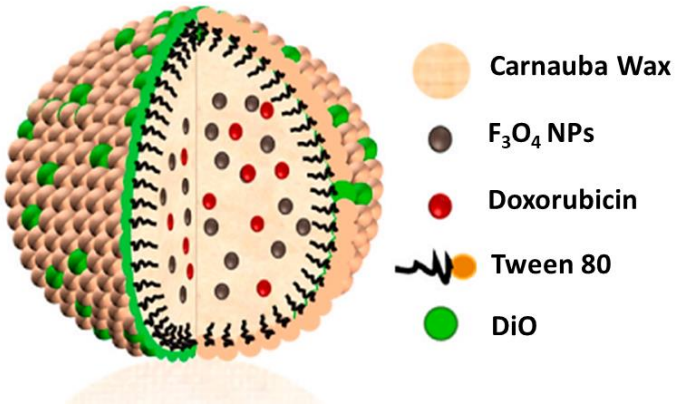

Figure 9. *Schematic representation of the magnetic lipid nanocomposite vehicles (mLNVs) described by García-Hevia et al. (Figure adapted from reference 33)*

In their study, the scientists efficiently co-encapsulated MNPs (F_3O_4) for MRI imaging and MH therapy, along with the potent anticancer drug doxorubicin (DOX), within the lipid matrix, as represented in **Figure 9**. The hybrid nanocomposite carrier demonstrated synergistic blend of MH-induced effects coupled with MRI's diagnostic capabilities, and by applying an AMF, they accomplished a precise control over DOX release, and localized thermal ablation of tumour cells. This strategic incorporation of thermotherapy and chemotherapy presents an advanced approach for treating solid tumours, achieving remarkable antitumoural effects and minimized toxicity.[33]

As a fluorescent reporter for *in vitro* investigations, this lipid phase additionally included a lipophilic fluorescent dye, 3,3'-dioctadecyloxacarbocyanine perchlorate (DiO), and an approved alkylphenolic surfactant (Tween 80) for stabilize the entire structure in water. To combine diagnostic, drug delivery and therapy in a single platform (**Figure 10**), each of these components and their corresponding proportions were carefully chosen, providing a non-invasive imaging capability by MRI for diagnosis and follow-up of the tumour (MNPs) and by fluorescent optical imaging (DiO), a encapsulation of chemotherapeutic drugs to a hydrophobic core (natural wax), a control over drug release process (MH-induction), and a synergistic combination of chemo (DOX) and thermal (MH) therapies to enhance antitumoural efficiency with minimal side effects.[33]

As a result, the combination mLNVs-DOX formulation by García-Hevia *et al*. exhibited controlled size and stability, magnetic and optical properties, what showed a potent cytotoxicity against malignant melanoma cells (*in vitro* and *in vivo*), even at low DOX doses, showcasing its potential for effective drug delivery and imaging applications.

Magnetic nanocarriers play a crucial role in the field of DDS for transport and release chemotherapeutics on the specific tumour site, including in TAM-targeting. Biological or physicochemically altered nano-drugs have the advantage of more precise locational drug release and less damaging side effects on healthy tissue.[68] Therefore, the possibility of TAM-targeting therapy is made possible by nanocarrier technology.[15]

1.3.3 Applications for TAM-targeting

Markers present on the surface of macrophages can act as useful therapeutic target areas. The macrophage mannose receptor (CD206) is one of those, much expressed by selected populations of macrophages, which has been widely investigated as biomarker for targeting TAMs.[57,69] Therefore, some advanced TAM-targeting immune-nanomedicine has been applied, including in lipid-based NPs.[15]

Although, inorganic-organic hybrid nanovehicles with theranostic potential have not yet been investigated for TAM-targeted techniques, holding in a single platform active targeting, non-invasive imaging and controlled drug delivery capabilities.[57] Thereby, Scialla *et al*. created a new targeted hybrid nanovehicle to improve the prognosis of triple-negative breast cancer (TNBC) by targeting TAMs. This nanovehicle is capable of enhancing MRI contrast, regulating temperature through MH and responding to pH changes to target TAMs, in combination with controlled drug delivery.[57]

In this study, mLNVs based on a natural hydrophobic matrix (Carnauba wax) were designed, in which was encapsulated SPIONs (F_3O_4), the chemotherapeutic drug (DOX) and a fluorescent dye (DiO), showed in **Figure 10**. The whole structure was stabilized in water, in not just one emulsifier, as García-Hevia *et al*. did with Tween80,[33] but with three main particle surface modifying molecules to functionalize the mLNVs, causing water stability with pH-responsive targeting capabilities for TAMs: a *O*-stearoyl mannose (M-C18), a PEG-hydrazone-C18 (PHC) and a PEG-amide-C18 (PAC).[57]

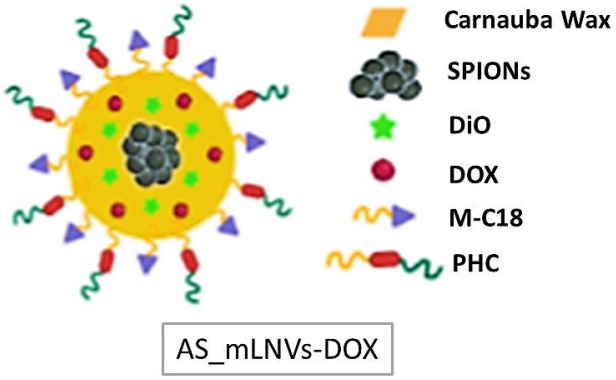

Figure 10. *Schematic representation of the magnetic lipid nanocomposite vehicles (mLNVs) described by Scialla et al. (Figure adapted from reference 57)*

M-C18 was the active targeting ligand used, and one of the modifying molecules to functionalize the mLNVs, designed to selectively target TAMs through mannose-mannose receptor recognition. On the other hand, the PHC consisted of a PEGylated alkyl C18 chain held together through an acid-sensitive hydrazone bond (hydrazone bond breaks down at pH lower than 6,8), in other words, a pH-responsive molecule. PAC is identical to PHC, but with acid-insensitive characteristics because the hydrazine bond has been replaced with a peptide bond, and for that reason, PAC was used as a negative control. Altogether, Scialla *et al*. synthesized two different nanoformulations: M-C18 mLNVs containing PHC as acid-sensitive (AS_mLNVs); and the M-C18 mLNVs containing PAC as acid-insensitive (AI_mLNVs), like in **Figure 10**.[57]

Due to the long PEG chain, PHC was expected to provide a shielding effect at physiological pH (7,4) on the M-C18 at the mLNV's surface, preventing the recognition by the particular mannose receptor on M2 macrophages surface. However, in the TME, lower pH conditions would disrupt the acid-sensitive chemical bond of PHC, exposing the mannose ligand by removing this PEG protection, causing TAMs uptake of mLNVs (**Figure 11**).[57,70]

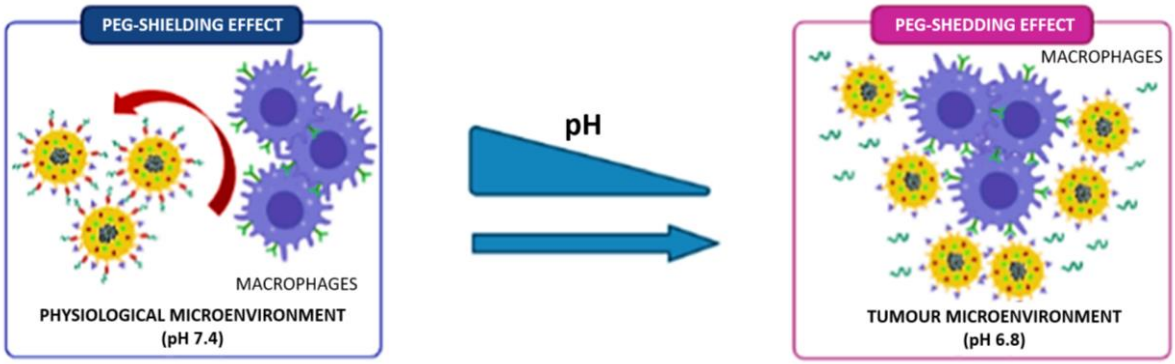

Figure 11. *pH-Triggered TAMs targeting via mannose receptor recognition. (Figure adapted from reference 57)*

As a result, a preferential targeting of the pH-sensitive formulations to M2 macrophage pro-tumoural phenotype was subsequently shown *in vitro*, confirming the breakdown of the acid-sensitive PHC and the activation of the mannose-mannose specific recognition. It was also observed a anti-tumour efficacy both in DOX-loaded mLNV and on DOX alone, however DOX-mLNV dramatically reduced the adverse effects induced by the free drug.[57]

This specific formulation demonstrated great biocompatibility, therapeutic efficacy against cancer, specifically in TNBC, with image-guided therapies and noticeably reduced target toxicity, being also a step forward on TAM-targeting therapy.[57]

Targeting peptides are, therefore, a promising alternative for delivering diagnostic agents and anticancer drugs. They benefit from non-immunogenicity, rapid blood clearance, and improved tumour penetration because of their small size. Since they are simple to produce and can attach to many substances for targeted administration, peptides are useful tools in modern personalized medicine.[27] Therefore, to increase the selectivity of TAM targeting, Cieslewicz *et al*., as mentioned earlier, examined a peptide library and identified M2pep (YEQDPWGVKWWY), shown in **Figure 4**, as a potential replacement for the conventional ligands, which demonstrated toxicity to the pro-tumoural M2-like phenotype in TAMs.[26] Yet, there is still room for improvement in terms of drug loading capacity and M2 macrophage-binding.

Thus, Pang *et al*. assumed that polymeric NPs may be an effective partner of M2pep for targeted drug delivery to M2-like TAMs (**Figure 12**), due to the fact that their surface can accommodate M2pep's multivalent binding, and that the matrix can hold a variety of payloads, from tiny compounds to macromolecules.[24]

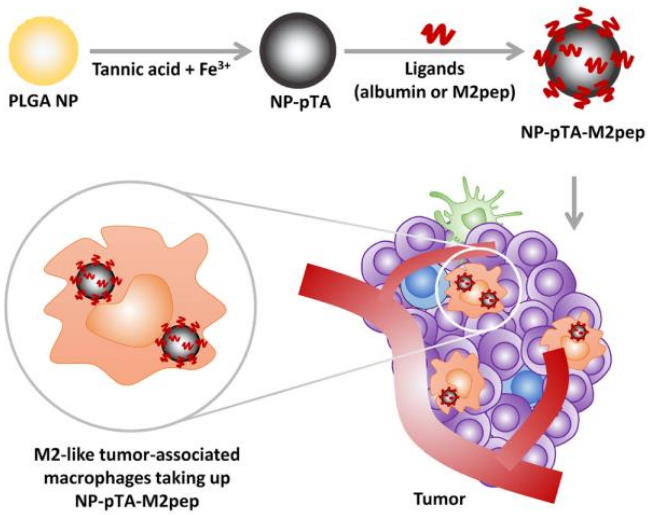

Figure 12. *Schematic illustration of M2pep-coated NPs and their interaction with TAMs. (Figure adapted from reference 24)*

In this paper, they modified poly(lactic-co-glycolic acid) nanoparticles (PLGA NP) with M2pep, due to its frequent use for drug carrier by their biocompatibility and biodegradability, by the simple tannic acid-Fe^{3+} based surface modification method.[24] Tannic acid (TA) is a polyphenol commonly found in plants, accommodating multiple phenol functional groups, that can be deposited on the surface of NPs and serve as an intermediary layer that provides additional functionality.[71] TA instantaneously interacts with Fe^{3+} in a neutral aqueous intermediate to establish an TA-Fe^{3+} complex (pTA) layer on the surface of NPs, which accommodates thiol- or amine-terminated ligands, including peptide ligands, like M2pep.[24]

Pang *et a*l. proceeded with PLGA NP modified with M2pep via TA-Fe^{3+} complex (NP-pTA-M2pep) and a helper albumin-coated nanoparticles (NP-pTA-Al), as shown in **Figure 12**.[24] Since albumin (Al) has been used as a blocking agent to decrease non-specific binding, it was selected as a control considering it has low affinity for TAMs and little interactions with macrophages.[72] They tested how the PLGA NP-pTA-M2pep interacted with macrophages of different phenotypes *in vitro* and *in vivo*, which itself did not show significant results, but when conjugated with a tyrosine kinase inhibitor (PLX3397) that helps to reduce TAMs population, helped attenuate tumour growth with significance, compared to when it was incorporated into albumin-modified PLGA NP, and even a significant delay in tumour growth as compared to free PLX3397 at the equivalent dose, improving its effect. These findings suggest that M2pep-coated NPs are an effective way to deliver drugs to tumour-supportive TAMs (M2 phenotype) and regulate their activities. Several types of NPs have been investigated for this purpose, such as mSLN.[24]

Chapter 2

Results and Discussion

2. Results and Discussion

This work was developed within the scope of project "UnTAM – Unleashing the tumour-associated macrophage (TAM) workforce to fight against cancer from the inside" (PTDC/QUI-OUT/3143/2021), funded by the FCT and currently ongoing at the Chemistry Centre of the University of Minho and the International Iberian Nanotechnology Laboratory.

The main aim of this project is to develop a new magnetic drug delivery system to target macrophages in cancer therapy, based on the proposed delivery vehicle shown in **Figure 13**. This formulation will be directed specifically to TAMs and will re-programme their phenotype from an M2 (tumour-promoting) to an M1 phenotype (anti-tumour). This transition will activate the immune response against tumours by the recruitment of T cells and NK cells (**Figure 14**), which are crucial for recognizing and eliminating tumoural cells. This can be achieved by combining a TAM-targeted DDS to deliver chemotherapeutic drugs, with an external triggering of drug release. Therefore, it is intended to develop a hybrid lipid-based MDDs able to target M2 TAMs specifically, by incorporation of a targeting peptide and encapsulation of immunomodulating drugs, along with magnetic iron oxide nanoparticles (MIONs). As targeting peptide, it will be used the previously mentioned M2pep, that has already been shown to specifically target M2 macrophages and slow tumour growth. The attachment of M2pep to the lipid-based NPs can be carried out by anchoring it to phospholipids through their hydrophobic tails.

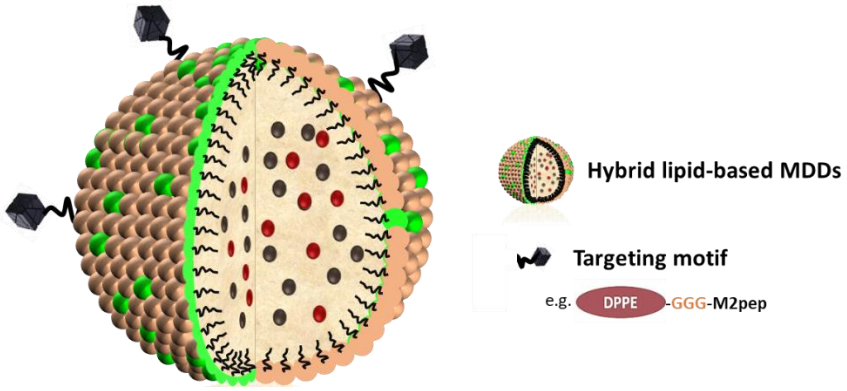

Figure 13. *Proposed delivery vehicle.*

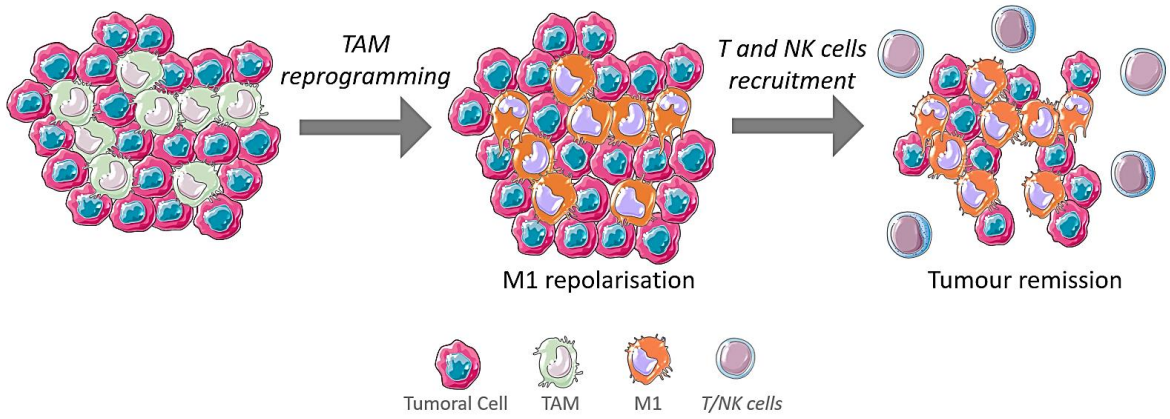

Figure 14. *Schematic illustration of TAMs polarization into the M1-like phenotype by the recruitment of T and NK cells leaving to tumour remission.*

It was also proposed to accomplish an M2pep substrate labelled with a fluorophore as a control, to follow the peptide to its target (M2 macrophages), enabling a better understanding of the complex chemical events occurring within TAMs.

In this way, the aim of this thesis was the synthesis of the targeting M2pep and several conjugates, functionalized with a fluorophore and phospholipids. Only the obtained M2pep-phospholipid conjugates were anchored on the final hybrid MDDs (**Figure 13**). The synthesis of the lipid-based NPs was carried out by an effective, green, and simple method, to incorporate simultaneously MNPs and the targeting peptide M2pep into a natural and biocompatible lipid matrix, to selectivity target M2-like TAMs.

2.1 Synthesis and Characterization

2.1.1 Precursors

2.1.1.1 Rhodamine B derivatives **1a-c**

In order to investigate the selectivity of M2pep towards M2-like TAMs using fluorescence-based techniques, it was proposed to attach a fluorescent probe, with the adequate photophysical properties, to the target peptide.

Attaching a fluorescent probe to a targeting ligand has been a widely used tool for cell processes imaging.[73] Xanthene derivatives are the most often used fluorophores in contemporary biological and medical research, and rhodamine B (RhoB) has been reported as a helpful label for peptides and proteins to help visualize inside cells, due to being chemically robust and usually affordable.[74,75] For this reason, RhoB was chosen to be attached to the target peptide.

The structure of M2pep, previously mentioned, has a chain of 12 amino acids with a free carboxylic group at the C-terminal and a free amine group at the N-terminal, allowing the possibility of coupling RhoB on either side. As RhoB has a free carboxylic group in its structure (in its open form), it could only react directly with the N-terminal of the M2pep. To have the option of coupling RhoB also at the C-terminal of the peptide, the synthesis of precursor **1a** was carried out.

In this sense, the rhodamine precursor **1a** was synthesized through a reaction between RhoB and a diamine (1,3-diaminopropane) by heating in ethanol at reflux for 10 h (**Scheme 3**). The residue obtained in this reaction was submitted to a liquid-liquid extraction and then purified by a dry flash chromatography with methanol (MeOH)/ dichloromethane (DCM) (3:97, v/v) as eluent, and the pure precursor **1a** was obtained as a salmon pink solid in 53% yield. This synthesis was replicated twice, with yields of 33% and 75%.

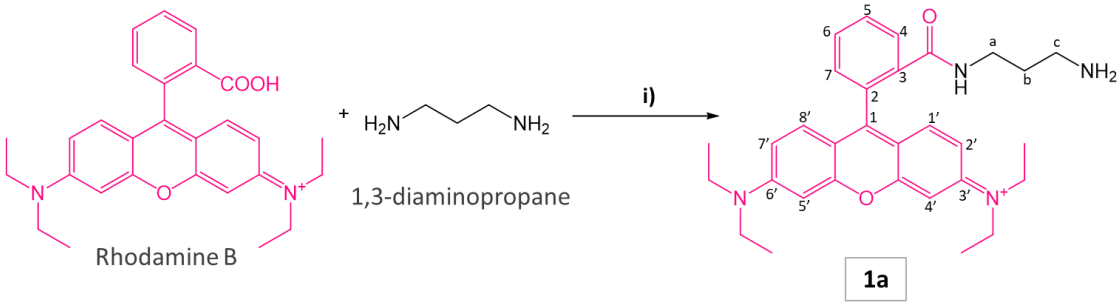

Scheme 3. *Synthesis of precursor* ***1a****:* ***i)*** *ethanol, reflux, 10 h.*

Precursor **1a** was characterized by ^{1}H NMR spectroscopy and mass spectrometry (MS). The obtained ^{1}H NMR spectra in DMSO-d_6 showed a triplet and a multiplet a 1.06 and 3.30 ppm, respectively, corresponding to the CH_3 and CH_2 groups, respectively, of the four ethyl groups linked to nitrogen of the xanthene ring. The diamine CH_2 groups appeared as

triplets at 1.34 and 3.04 ppm and a multiplet centred at 2.56 ppm, confirming the binding of diamine to RhoB. Signals corresponding to the aromatic protons of the xanthene ring appeared as a multiplet between 6.30-6.36 ppm, with integration for 6 H corresponding to the ring protons. The remaining aromatic protons appeared as multiplets at higher chemical shifts (6.97-7.78 ppm), being the H-4 the most deprotected due to the mesomeric effect from the amide group. The RhoB diamine **1a** was also characterized by ESI-MS, with a peak at *m/z* 500 which corresponds to the estimated molecular ion $[M+H]^+$ (MW_{calc}=499.30 g/mol).

Having the option of RhoB with the free amine group (precursor **1a**) to react with the acid terminal of M2pep, another precursor was also synthesized from precursor **1a**, to allow more flexibility and less hindrance in the attachment. The precursor **1b** was prepared by the reaction of the previous synthetized precursor **1a** and maleic anhydride, by heating at reflux in chloroform for 22 h (**Scheme 4**). The first attempt to purify the crude product obtained was undertaken with a column chromatography on silica gel with MeOH/DCM (1:100, v/v) as eluent,[76] which was unsuccessful, as the intended compound eluted together with impurities. So, another purification by column chromatography was made with another eluent, ethyl ether/ethyl acetate (AcOEt) (5:5, v/v), that resulted in a pink solid of precursor **1b** in an approximate 36% yield, but still with some contaminants.

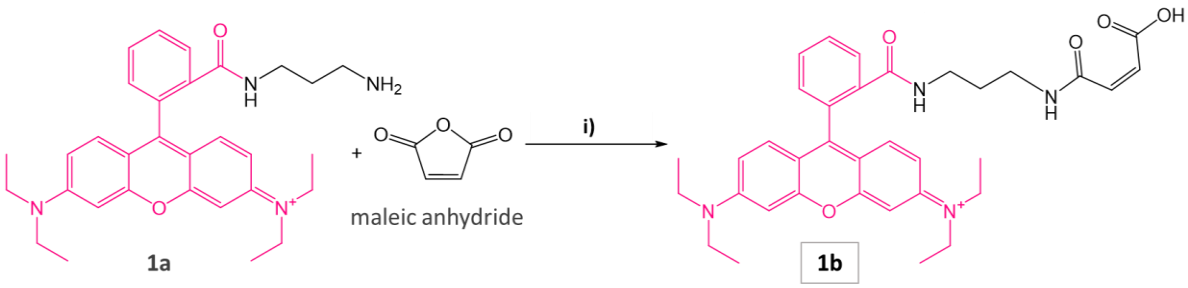

Scheme 4. *Synthesis of precursor* ***1b****:* ***i)*** *chloroform, reflux, 22 h.*

Precursor **1b** was also characterized by ^{1}H NMR spectroscopy and MS. In the ^{1}H NMR spectra, there was still evidence of contamination. However, the MS analysis showed a peak at *m/z* 598, corresponding to the $[M+H]^+$ ion, which proves the presence of precursor **1b** in the solid, even with several impurities. Hence, this compound was not used for subsequent coupling to M2pep since the purification of this compound needs to be optimized.

Another alternative of RhoB precursor was considered: react the RhoB with an amino acid, that could be later coupled to the peptide M2pep. In this sense, the simplest amino acid was chosen, glycine (Gly), which has no side chains. Thus, the synthesis of precursor **1c** was attempted through a coupling between RhoB and glycine, protected at its terminal carboxylic acid with a *tert*-butyl ester group, to ensure reaction at the free amino group, as represented in **Scheme 5**. The preparation of precursor **1c** was accomplished by solution-phase chemistry in DMF described by Kraft and co-workers,[77] using *N*-ethyl-*N*'-(3-dimethylaminopropyl) carbodiimide hydrochloride (EDC.HCl) and *N*-hydroxysuccinimide (NHS) as coupling and additive reagents, respectively, in the presence of triethylamine (Et_3N), to neutralize the HCl in EDC. The impure precursor **1c** was obtained as a pink solid, after solvent evaporation.

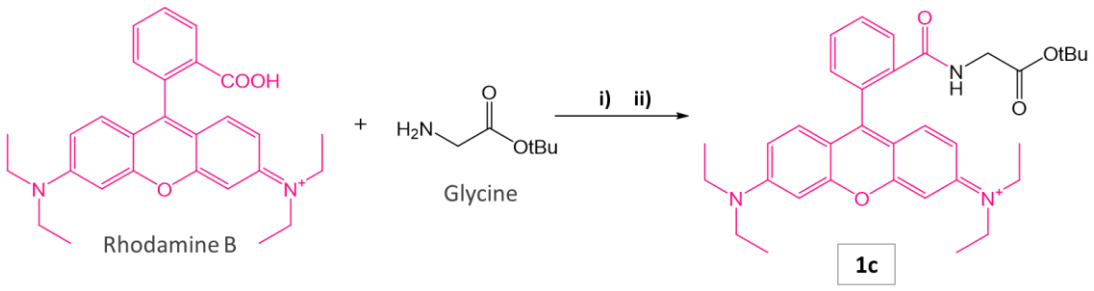

Scheme 5. *Synthesis of precursor* ***1c****: i) NHS, EDC.HCl, Et_3N, dry DMF, 0°C, 30 min;* ***ii)*** *Gly(OtBu), room temperature, 7 days.*

Before making any attempt at purification, the solid obtained was analyzed by MS, which showed a major peak at *m/z* 443 that did not fit with the expected molecular weight. This peak belonged to free RhoB, thus proving that the coupling of RhoB with glycine did not occur.

Having attempted to synthesize these three different precursors from RhoB, only precursor **1a** was successfully achieved and purified, which will be coupled later to M2pep.

2.1.1.2 Phospholipid derivatives **2a-b**

In order to attach the peptide M2pep to the lipid based MDDs, it was necessary to incorporate a hydrophobic chain. For this purpose, the phospholipids 1,2-dipalmitoyl-*sn*-glycero-3-phosphoethanolamine (DPPE) and 1,2-dioleoyl-*sn*-glycero-3-phosphoethanolamine (DOPE) were chosen to be linked to M2pep.

Phospholipids are the main constituent of the lipid bilayers that make up cell membranes. They are known for being soluble in both water and oil (amphiphilic nature) since they have a polar head (phosphate group) and a hydrophobic end (two hydrocarbon tails, usually made of fatty acids).[78] Because of their nature, they have been widely used in DDS, providing biocompatibility, and enabling communication with the environment around cells.[79,80] For these reasons, the phosphoethanolamines DPPE and DOPE were chosen, that were already employed in previously DDS studies.[36,45] Their hydrophobic tails have different length and saturation: DPPE has two fully saturated 16-carbon chains, whereas DOPE has two 18-carbon chains with a double bond between C9 and C10.

Considering that in both phospholipids, the polar head is functionalized with a free amine group, they already can be directly bound to the M2pep C-terminal. Although, bearing in mind the same reasoning as for the synthesis of RhoB precursors, for the possibility of binding DPPE and DOPE also at the M2pep N-terminal, both phospholipids were covalently linked to succinic anhydride to generate a free carboxylic group (**Schemes 6** and **7**).

The DPPE precursor **2a** was obtained by reacting DPPE with succinic anhydride,[81] as presented in **Scheme 6**. The reaction occurred for 5 hours at room temperature, in the presence of Et_3N. The mixture was then acidified and submitted to a liquid-liquid extraction. As DPPE was difficult to dissolve, purification was done by preparative layer chromatography (PLC) with a mixture of chloroform ($CHCl_3$), MeOH and water (H_2O) (65:25:4, v/v) as eluent. The pure DPPE-SA **2a** was then obtained as a white pale solid in 51% yield. A second attempt resulted in a yield of 57%.

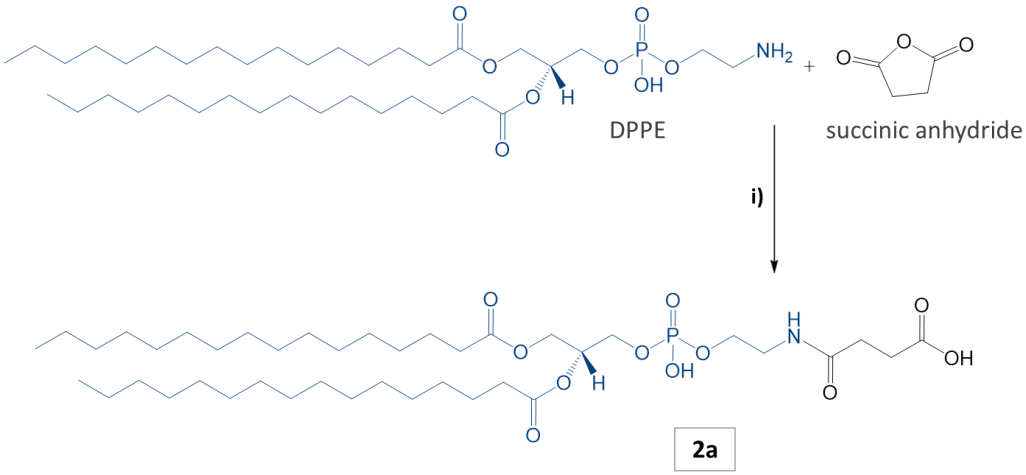

Scheme 6. *Synthesis of precursor DPPE-SA* ***2a****:* ***i)*** *Et_3N, $CHCl_3$/MeOH (9:1), room temperature, 5 h.*

It was not possible to characterize the precursor **2a** by ^{1}H NMR spectroscopy, as it proved difficult to solubilize in all deuterated solvents available in the laboratory. Even so, by MS it was possible to obtain a spectrum which showed peaks that correlated with the expected molecular ion of precursor **2a**.

The synthesis of precursor **2b** was done by the same method,[81] by reacting DOPE with succinic anhydride in the presence of Et_3N, for about 5 hours at room temperature (**Scheme 7**). The reaction mixture was also acidified and submitted to a liquid-liquid extraction. DOPE was much easier to dissolve, so purification was done by column chromatography on silica gel with $CHCl_3$/MeOH (8:2, v/v) as eluent, that resulted in an oily off-white solid in 37% yield. This synthesis was replicated once more, with a yield of 87%.

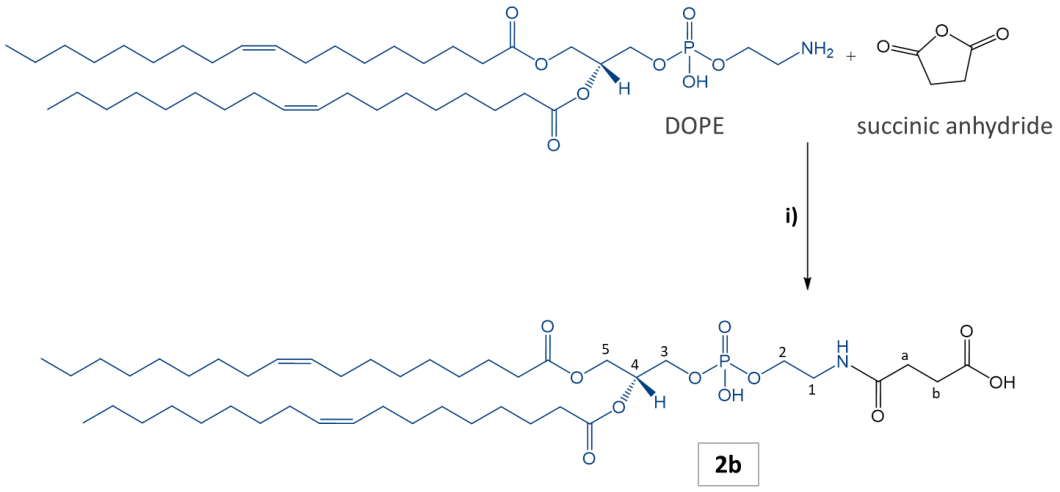

Scheme 7. *Synthesis of precursor DOPE-SA* ***2b****:* ***i)*** *Et_3N, $CHCl_3$/MeOH (9:1), room temperature, 5 h.*

The purified DOPE-SA **2b** was characterized by ^{1}H NMR spectroscopy and MS, which confirmed its structure and purity. In the ^{1}H NMR spectra it is possible to observe the presence of all protons in the two hydrocarbon chains, with the protons of the double bond appearing at 5.42-5.36 ppm. The protons corresponding to the linked succinic anhydride, corresponding to H-a and H-b, appeared at 2.48 and 2.68 ppm, respectively. By MS it was also possible to see the peak that is in accordance with the calculated molecular weight.

2.1.2 M2pep-GGG **3b** and GGG-M2pep **3d**

Having synthesized the precursors, the desired targeting peptide M2pep was then obtained through microwave-assisted solid-phase peptide synthesis (MW-SPPS) applying the 9-fluorenylmethyloxycarbonyl (Fmoc) strategy.

The basic concept of the SPPS is to covalently link the first amino acid to a solid support, which is an insoluble polymeric resin, and increase the peptide chain by incorporating the remaining amino acids through coupling and deprotection sequences. After the synthesis, the peptide is cleaved from the resin, with or without the protecting groups at the side chains of the amino acids, depending on the type of resin used.[82] The M2pep synthesis was undertaken using a Wang resin, that requires a concentrated trifluoroacetic acid (TFA) solution which simultaneously cleaves the peptide from the resin and the usual protecting groups at the side chains of the synthesized peptide.[83]

The M2pep is a 12 amino acid sequence (Tyr-Glu-Gln-Asp-Pro-Trp-Gly-Val-Lys-Trp-Trp-Tyr), most of which have bulky side chains, and therefore it was important to ensure that its accessibility after anchoring to the lipid shell of the DDS was maximized, so it was decided to add a spacer, namely three glycines (Gly-Gly-Gly). Considering that the peptide can be linked by either its N- or C-terminal, the M2pep was synthesized with the triple glycine spacer at either termini, M2pep-GGG **3b** and GGG-M2pep **3d** (**Scheme 8**).

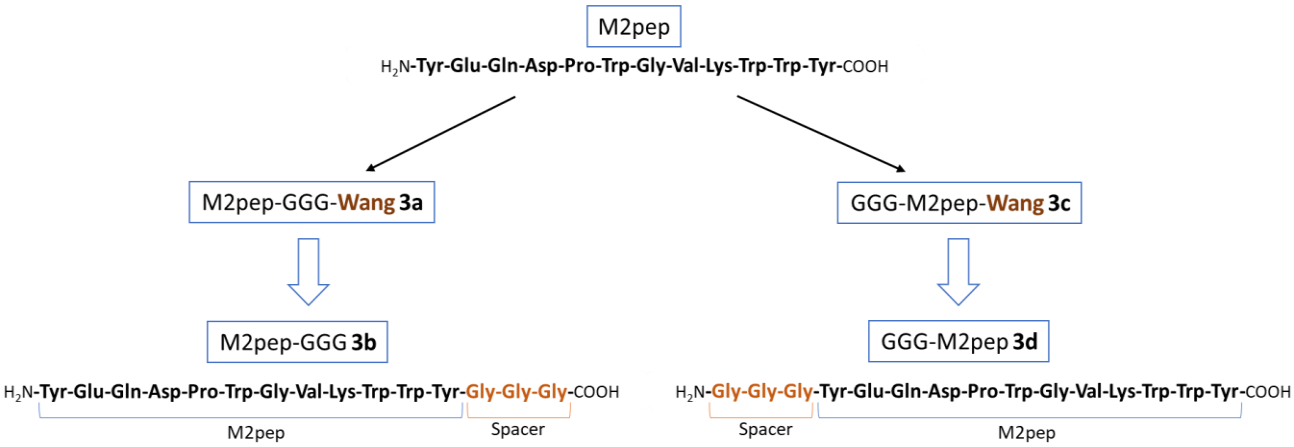

Scheme 8. *Synthesis of M2pep-GGG-Wang resin **3a** and M2pep-GGG **3b**, and GGG-M2pep-Wang **3c** and GGG-M2pep **3d**.*

These two M2pep variations in **Scheme 8** were subsequently used for coupling with the previously synthesized precursors, either with the peptide still bound to the resin (SPPS) or with the free peptide (synthesis in solution).

The synthesis of M2pep-GGG **3b** had been carried out previously at the research group, using an automatic peptide synthesizer. Standard Fmoc solid-phase peptide synthesis was performed on a 0.25 mmol scale using a Wang resin preloaded with a glycine (Fmoc-Gly-Wang) with a degree of functionalization of 0.51 mmol/g. Since the first amino acid was already coupled, the remaining amino acids glycine (Fmoc-Gly-OH), tyrosine (Fmoc-Tyr(tBu)-OH), glutamic acid (Fmoc-Glu(OtBu)-OH), glutamine (Fmoc-Gln(Trt)-OH), aspartic acid (Fmoc-Asp(OtBu)-OH), proline (Fmoc-Pro-OH), tryptophan (Fmoc-Trp(Boc)-OH), valine (Fmoc-Val-OH) and lysine (Fmoc-Lys(Boc)-OH) were sequentially coupled, with their respective protecting groups (**Scheme 9**). The Fmoc group deprotection was performed with a solution of 20% of piperidine in dimethylformamide (DMF). The fully deprotected M2pep-GGG **3b** was then cleaved from the resin with a mixture of TFA/H_2O/triisopropylsilane (TIS) (95:2.5:2.5, v/v), (**Scheme 9**), for subsequent peptide labelling by solution synthesis, and M2pep-GGG resin **3a** was used in SPPS.

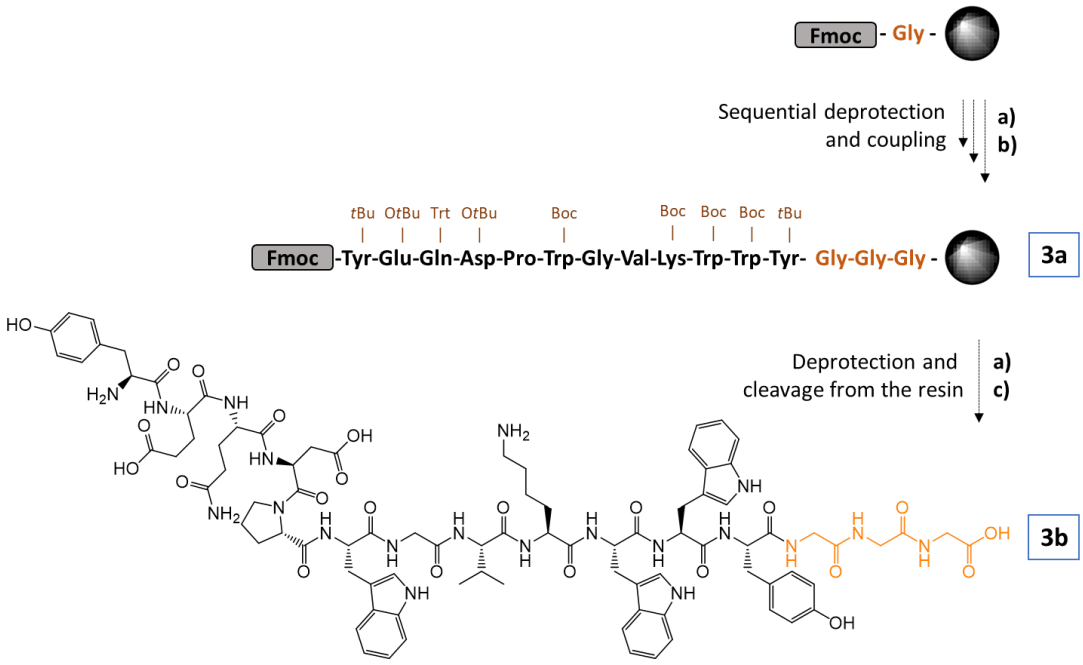

Scheme 9. *Solid phase peptide synthesis microwave-assisted of M2pep-GGG* ***3b****:* ***a)*** *20% of piperidine in DMF;* ***b)*** *Fmoc-amino acid-OH, Oxyma, DIC, DMF;* ***c)*** *TFA/H2O/TIS (95:2.5:2.5, v/v).*

In all couplings carried out, it was necessary to use a coupling reagent, like carbodiimides, to activate the carboxylic acid to react with the amine of the next amino acid to be coupled, forming an amide bond (peptide bond). In carbodiimide-mediated coupling reactions, additives are usually used to avoid side reactions and racemization of the activated amino acid.[84,85] The coupling reagent used in all amino acid couplings was *N*,*N*-diisopropylcarbodiimide (DIC) and the additive ethyl 2-cyano-2-(hydroxyimino)acetate (Oxyma) was used.

The synthesis of the GGG-M2pep **3d** was done on a manual peptide synthesizer, starting from a preloaded Fmoc-Tyr(tBu)-Wang resin, with a degree of functionalization of 0.52 mmol/g. As the first amino acid of peptide **3d** (Tyr), was already linked to the resin, the Fmoc group was then cleaved with a 20 % solution of piperidine in DMF, using the pre-defined programs on the CEM-Discover SPS equipment. After deprotection, the resin was washed, and the remaining amino acids were coupled always after the deprotection of the Fmoc group of the previous coupled amino acid. In this way, the amino acids lysine (Fmoc-Lys(Boc)-OH), valine (Fmoc-Val-OH), glycine (Fmoc-Gly-OH), tryptophan (Fmoc-Trp(Boc)-OH), proline (Fmoc-Pro-OH), aspartic acid (Fmoc-Asp(OtBu)-OH), glutamine (Fmoc-Gln(Trt)-OH), glutamic acid (Fmoc-Glu(OtBu)-OH), tyrosine (Fmoc-Tyr(tBu)-OH), and the last three glycines

were sequentially coupled, using DIC and Oxyma. After Fmoc group deprotection of the last amino acid, cleavage from the resin **3c** with the mixture of TFA/H_2O/TIS (95:2.5:2.5, v/v), afforded the fully deprotected GGG-M2pep **3d** (**Scheme 10**).

This synthesis was monitored by a 2,4,6-trinitrobenzenesulfonic acid solution (TNBS) test to verify the existence of free amino groups at the resin surface and, consequently, the effectiveness of the coupling. This solution reacts with the amino groups to produce a red product that indicates the presence of free amino groups, thus indicating that the previous coupling was incomplete. Throughout the various couplings performed, the TNBS test was performed after some couplings, which could be potentially more problematic due to side chain bulk or steric hindrance.

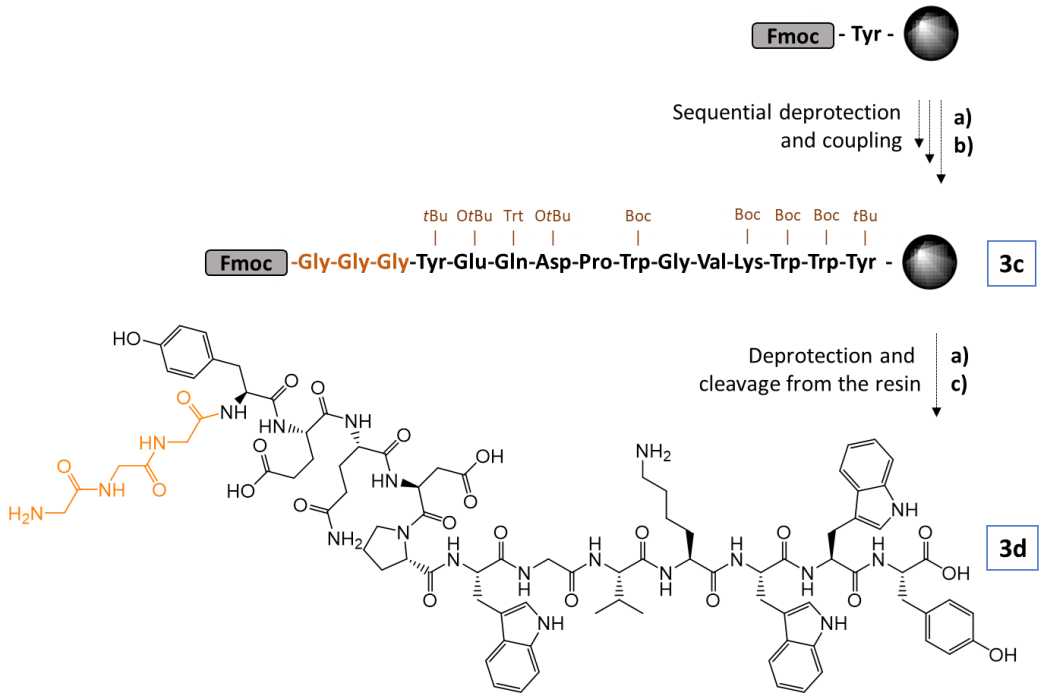

Scheme 10. *Solid phase peptide synthesis microwave-assisted of M2pep-GGG* ***3d****:* ***a)*** *20% of piperidine in DMF;* ***b)*** *Fmoc-amino acid-OH, Oxyma, DIC, DMF;* ***c)*** *TFA/H2O/TIS (95:2.5:2.5, v/v).*

Only part of the on-resin peptides **3a** and **3c** were cleaved to proceed with characterization of free peptides **3b** and **3d**, respectively, and therefore it was not possible to calculate the yield of these syntheses. The structure of these obtained peptides was confirmed by MS, UV-Vis absorption and Fourier-transform infrared spectroscopy (FTIR). The confirmation of the structure by ^{1}H NMR was not feasible in the available 400 MHz equipment, considering the overall complexity of the molecule, so it was not undertaken.

The M2pep-GGG **3b** was submitted to a high-resolution MS, which confirmed its structure. A low-resolution analysis was also made, and the spectra showed the peak corresponding to the double charged molecular ion with the mass of $[M^+]/2$.

In order to further confirm the structure of the obtained peptides, UV-Vis absorption spectroscopy and FTIR were also used. The UV-Vis absorption spectrum of M2pep-GGG **3b** was obtained at pH 7 phosphate buffer, to approximately replicate the physiological pH, and displayed bands of similar appearance to the absorption curves of Trp and Tyr (**Figure 15 a)**), at about 280 nm, the only amino acids with side chains that show absorption in the UV-Vis zone. This proves the presence of both amino acids in the structure of the peptide. The M2pep-GGG **3b** was also analysed by FTIR, which allowed the identification of the most important bands corresponding to the functional groups N-H and C=O bonds, respectively, as observed in **Figure 15 b)**. Similar characteristics were observed in the UV absorption and FTIR spectra of GGG-M2pep **3d** (spectra not shown).

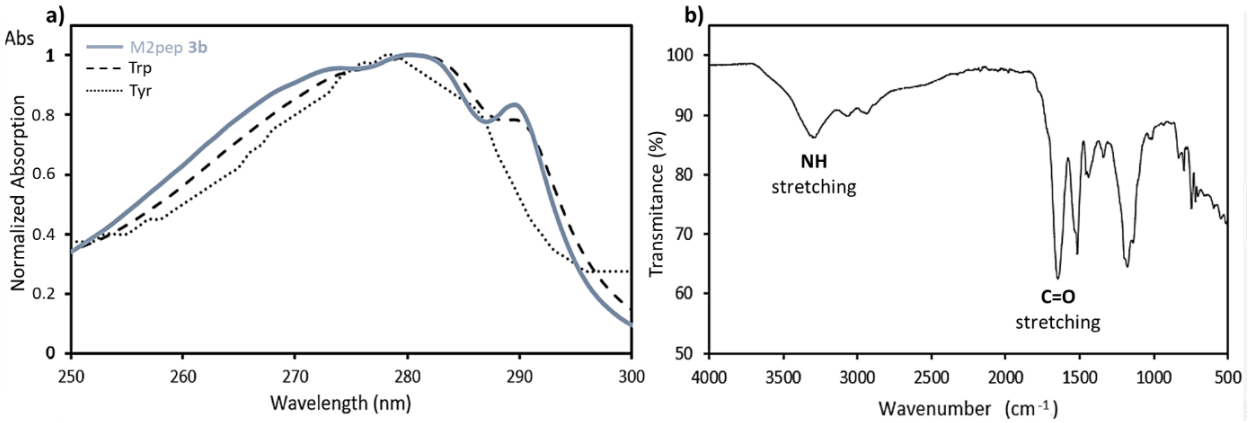

Figure 15. a) *Normalized UV-Vis absorption of M2pep* ***3b*** *(1.0 x 10^{-5} M) in phosphate buffer at pH 7;* ***b)*** *FTIR of M2pep* ***3b.***

A qualitative analysis was also carried out by high performance liquid chromatography (HPLC) to confirm the purity of both peptides. This analysis was carried out using a C18 reverse-phase column with H_2O/acetonitrile (ACN) (40:60, v/v) with 0.1% of TFA as eluent and flow 0.2 mL/min, which showed a unique peak at about 13 minutes (**Figure 16**), which indicates high purity in both peptides **3b** and **3d**. In this way, it was possible to confirm the efficient coupling between amino acids and that the cleavage conditions efficiently removed the side chain protecting groups of both peptides, as expected.

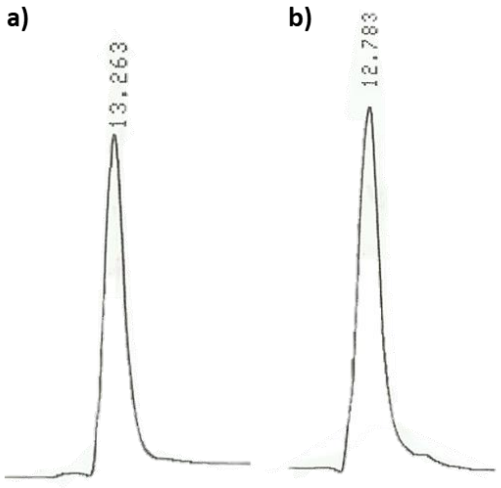

Figure 16. *Analytical HPLC chromatograms with eluent H_2O/ACN (40:60, v/v) with 0.1% TFA at 0.2 mL/min for* ***a)*** *M2pep-GGG* ***3b*** *and* ***b)*** *GGG-M2pep* ***3d****.*

2.1.3 M2pep linked to fluorophores **4a-d**

In this work, it was also envisaged to connect a fluorescent probe derived from RhoB to the target peptide to study the selectivity of M2pep towards M2-like TAMs using fluorescence-based techniques. These fluorescent probes find applications in various fields, including bioimaging, offering an *in situ*, real-time, and non-invasive analysis.[86] Particularly for peptides, RhoB proved to be a useful fluorescent label.[74]

To obtain M2pep labelled with RhoB, compound **1a** (bearing an amino group) was coupled to the acidic terminal of M2pep-GGG **3b**, through an amide bond. Considering that two M2pep's were accomplished, each having a terminal spacer of three Gly's on opposite sides, M2pep-GGG **3b** and GGG-M2pep **3d**, it seemed more appropriate to first attempt the linking of RhoB **1a** to the peptide with the spacer in its C-terminal.

Thus, the coupling of RhoB **1a** with the free peptide M2pep-GGG **3b** was carried out by solution synthesis for 5 days at room temperature, using EDC.HCl and NHS as coupling reagents, in the presence of Et_3N (**Scheme 11**). To avoid cross-reactions, this reaction was carried out using only 1 equivalent of each reagent to ensure that coupling preferably occurred at the more exposed C-terminal of free peptide **3b**, rather than at the side chains of Asp and Glu. A pink solid was then precipitated with ethyl ether, and isolated by filtration.

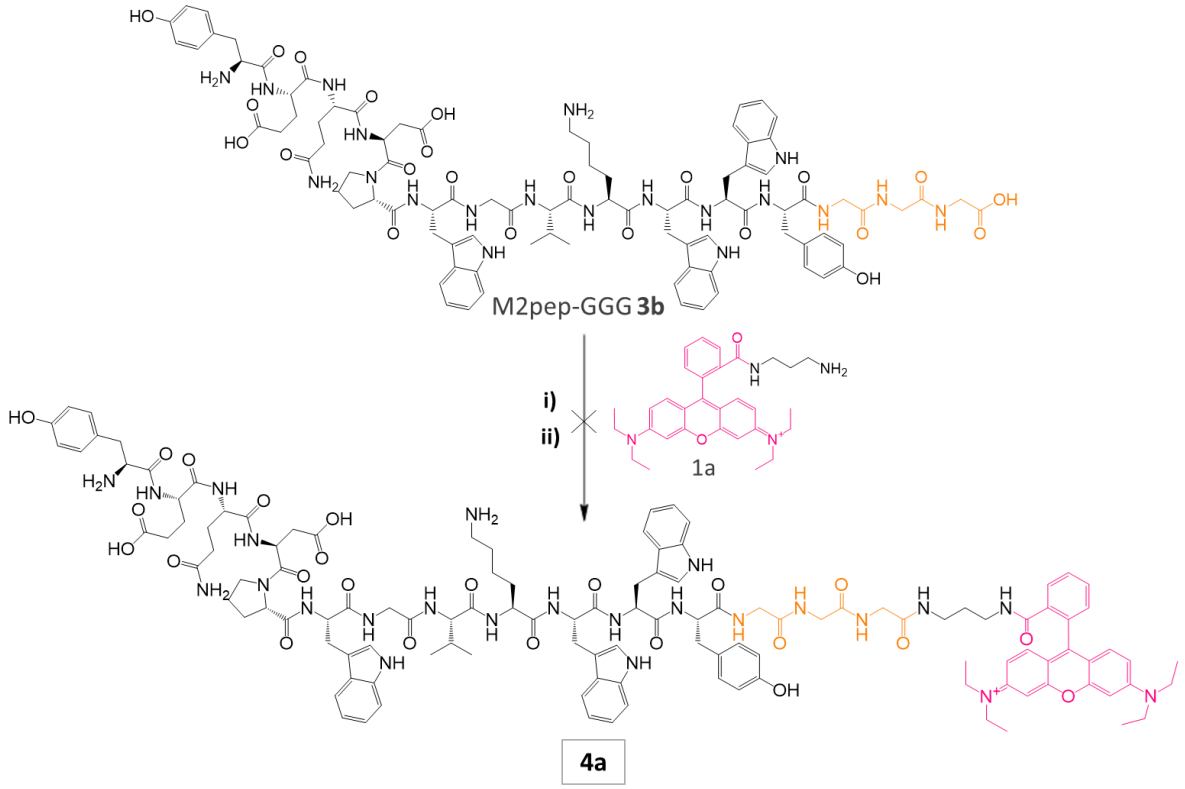

Scheme 11. *Synthesis attempt of peptide* ***4a****:* ***i)*** *NHS, EDC.HCl, Et_3N, dry DMF, 0°C, 30 min;* ***ii)*** *precursor* ***1a****, room temperature, 5 days.*

Before proceeding to the purification, the obtained solid was first characterized by MS to verify whether the desired peptide **4a** had been successfully synthesized. It was concluded that the coupling did not actually occur, probably due to inaccessibility of the peptide reactive terminal.

Another attempt was made with M2pep-GGG **3b** regarding coupling at its N-terminal with RhoB, which has a free carboxylic group. So, the reaction was made with activation of the RhoB acidic terminal with NHS/EDC.HCl (**Scheme 12**). This coupling was performed for about 7 days at room temperature, with 1 equiv. of each reagent to avoid the reaction of the activated acidic group of RhoB with the side chain of Lys.

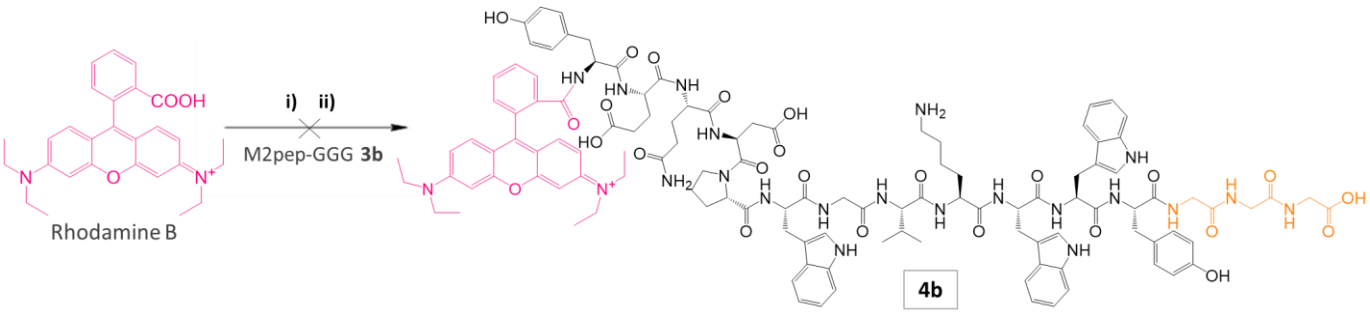

Scheme 12. *Synthesis attempt of RhoB-M2pep-GGG* ***4a****:* ***i)*** *NHS, EDC.HCl, Et_3N, dry DMF, 0°C, 30 min;* ***ii)*** *M2pep-GGG* ***3b****, room temperature, 5 days.*

After work-up with diethyl ether, the precipitated pink solid was isolated by filtration. Once again, there was no evidence by MS of the desired coupled product **4b**. In this case, maybe the spatial impediment between the carboxylic group of RhoB and the amino group of Tyr (both are bulky) could explain the lack of reaction.

Considering that the RhoB fluorophore was used in both attempts to synthesize peptide **4a** and **4b**, and neither of them worked, it was decided to change to another fluorophore of the cyanine type, commonly used in the research group, namely a carboxylated pentamethine cyanine (Cy5), that is also widely used in bioimaging, and therefore considered an excellent probe for obtaining fluorescence images.[87] The structure of carboxy-Cy5 also has a free carboxylic group, enabling the coupling with the N-terminal of the peptide.

Therefore, the coupling of carboxy-Cy5 with the same peptide M2pep-GGG **3b** was carried out for 6 days at room temperature, with activation of the carboxy-Cy5 acidic terminal with NHS/EDC.HCl (**Scheme 13**). When the reaction ended, a blue solid was precipitated with ethyl ether, and isolated by filtration. It was not possible to characterize the obtained compound due to insolubility in most solvents tested (including deuterated solvents), and therefore it was not possible to conclude whether the coupling happened or not.

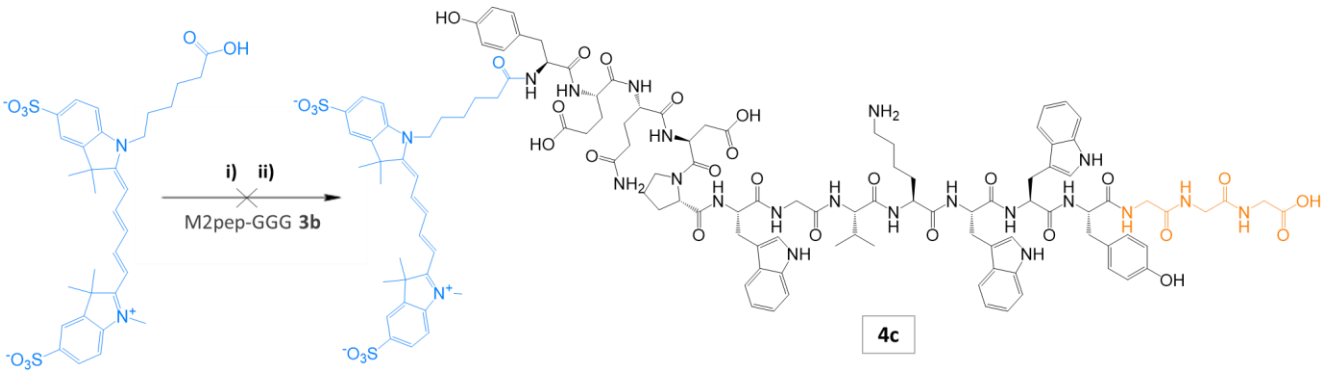

Scheme 13. *Synthesis attempt of Cy5-M2pep-GGG* ***4c****:* ***i)*** *NHS, EDC.HCl, Et_3N, dry DMF, 0°C, 30 min;* ***ii)*** *M2pep-GGG* ***3b****, room temperature, 6 days.*

Thereby, it was settled that the issue with the three earlier attempts would be the synthesis' solution-based method. Considering that the M2pep is a long peptide with 15 amino acids (with the spacer), without the protecting groups, it is likely that the peptide may acquire a conformation that hinders the access to the reaction site and prevents coupling reactions.

Thus, it was decided to repeat the coupling of RhoB but using microwave-assisted solid phase synthesis, which means that the reaction was carried out with the peptide still bound to the solid support, with the side chain protecting groups.

Therefore, after the coupling of the last amino acid of M2pep-GGG-Wang **3a** and the respective Fmoc deprotection, RhoB was coupled to the free amine group using DIC/Oxyma, following the standard SPPS conditions. Cleavage of the peptide from the resin was done by treatment with a cocktail of TFA/H_2O/TIS (95:2.5:2.5, v/v), resulting peptide **4d** (RhoB-M2pep-GGG as a pink solid (**Scheme 14**). A TNBS test was run on the resin after coupling of RhoB, to ensure that the NH_2 groups were unavailable, which showed no color in the resin, indicating that the coupling occurred successfully.

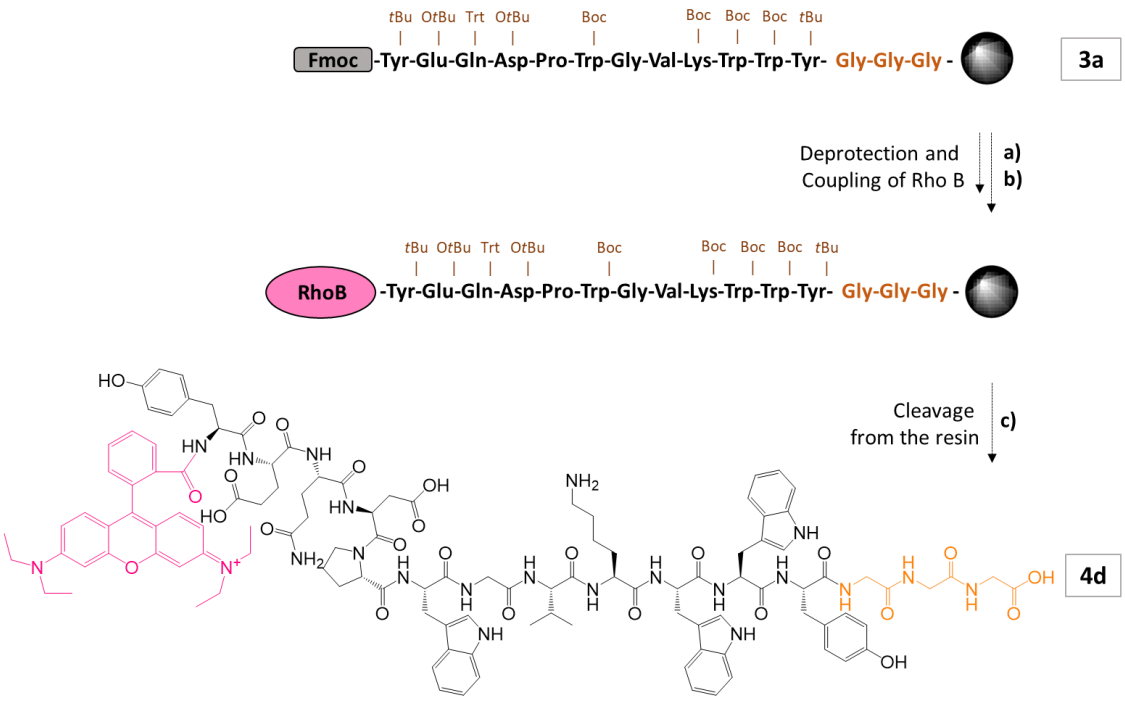

Scheme 14. *Solid phase peptide synthesis microwave-assisted of RhoB-M2pep-GGG* ***4d****:* ***a)*** *20% of piperidine in DMF;* ***b)*** *RhoB, Oxyma, DIC, DMF;* ***c)*** *TFA/H_2O/TIS (95:2.5:2.5, v/v).*

After optimization of the conditions for purification in an analytical HPLC, peptide **4d** was subjected to semi-preparative HPLC separation. The eluent was a mixture of ACN/H_2O (1:1, v/v) with a flow rate of 1.0 mL/min and detection of UV-Vis absorption at 540 nm. The sample was dissolved in 10 mL of eluent and divided into 10 aliquots for injection and the fraction with an average retention time of 29 min was isolated and collected.

The solid, obtained after freeze-drying the combined fractions, was isolated with a yield of 6% (19 mg) and MS analysis (positive and negative ionisation) confirmed it was peptide **4d**, highlighting the fragment with *m/z* 1133 that results from the loss of the triple glycine spacer and the cleavage at the Asp-Pro bond.

RhoB exhibits an equilibrium between two distinct forms: a fluorescent open form **A** and a non-fluorescent lactone form **B**, as depicted in **Scheme 15**. In acidic environments, pink-coloured form **A** predominates, while colourless form **B** dominates in basic conditions.[2] Since RhoB is only fluorogenic in acidic conditions, it is an interesting quality for monitoring the TME which has been shown to hold an acidic environment.[57]

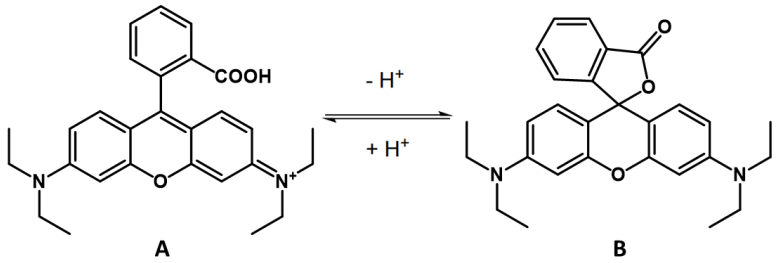

***Scheme 15**. Structure of RhoB in equilibrium between its open form **A** and closed form **B**.*

To replicate the acidic environment of the TME, solutions of free M2pep-GGG **3b** and RhoB-M2pep-GGG **4d** were prepared in phosphate buffer at pH 5.6. These solutions were compared by UV-Vis absorption and fluorescence spectroscopy (**Figure 17**).

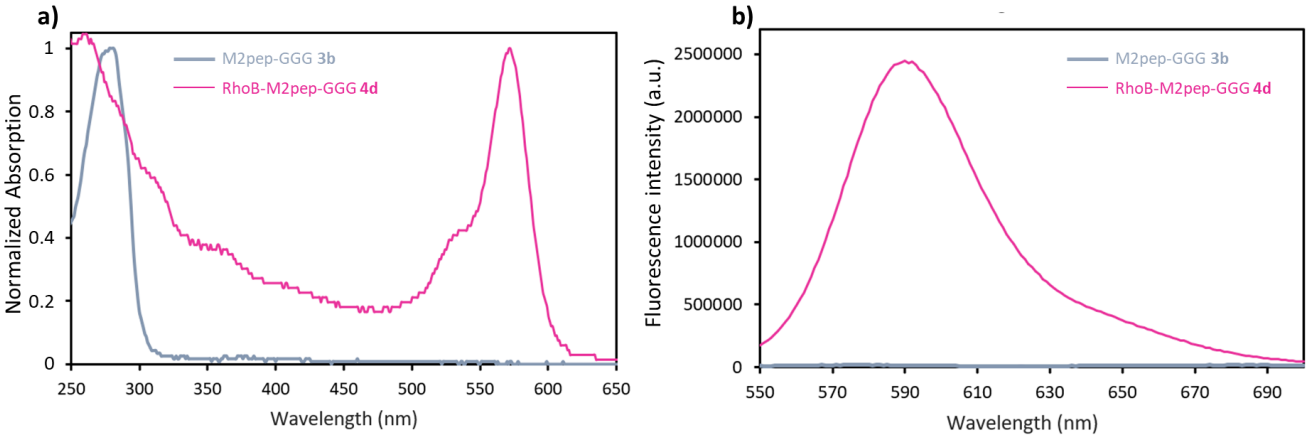

***Figure 17. a)** Normalized UV/Vis absorption and **b)** fluorescence spectra of RhoB-M2pep-GGG **4d** and M2pep-GGG **3b** (1.0 x 10^{-5} M) in phosphate buffer at pH 5.6.*

The absorption spectra showed an intense absorption band at 280 nm for M2pep-GGG **3b**, whereas for RhoB-M2pep-GGG **4d**, it was visible a dominant band with a maximum absorption around 570 nm, responsible for the pink colour solution and ascribed to the presence of RhoB (**Figure 17 a**). The absorption band at about 260-280 nm observed for both peptides can be attributed to the presence of Trp and Tyr residues. In the non-normalized fluorescence spectrum (**Figure 17 b**) it was clearly confirmed that the conjugation of RhoB with M2pep-GGG (peptide **4d**) dramatically enhanced the fluorescence intensity, in comparison with M2pep-GGG **3b** alone, showing a wavelength of maximum fluorescence at about 590 nm. Therefore, peptide **4d** could be used as an efficient probe to target M2 macrophages in cancer diagnosis.

2.1.4 M2pep linked to phospholipids **5a-e**

In order to anchor the M2pep derivatives to the lipid-coated NPs, it was necessary to incorporate a hydrophobic section into the peptide that could attach to the hydrophobic surface of the DDS. For this purpose, phospholipids DPPE and DOPE were chosen, and their amphiphilic nature allows binding to the peptide through their polar phosphoetanolamine group and attachment to the lipid surface through their hydrophobic tails.

Given that previous syntheses in solution between M2pep and the fluorophores (RhoB and Cy5) were not successful, priority was given to microwave-assisted solid phase synthesis, which has the advantage of reacting the peptide while still in the solid support, with the respective protecting groups of the side chains of the amino acids, avoiding secondary reactions.

With the peptide still attached to the resin, only the N-terminal amine group is available for coupling. For this reason, precursors of both DPPE and DOPE were previously synthesized, by linking the phospholipid to succinic anhydride (SA), to afford a carboxylic acid terminal, precursors **2a** (DPPE-SA) and **2b** (DOPE-SA).

Microwave-assisted solid phase synthesis was performed on GGG-M2pep-Wang **3c** with coupling of precursors **2a** and **2b** using DIC/Oxyma after deprotection of the Fmoc group of the last coupled amino acid. Five coupling cycles with of 5 minutes each (P= 25 W, T= 75 °C) were done and, at the end, a TNBS test was run on the resin to monitor the coupling of the phospholipids. The TNBS test was positive, and the reaction mixture was stirred for another 48 hours at room temperature. A new TNBS test was negative, which established that the phospholipid had coupled. The final peptides were then cleaved from resin with a cocktail solution of a TFA/TIS/H_2O (95:0.25:0.25, v/v), as represented in **Scheme 16**.

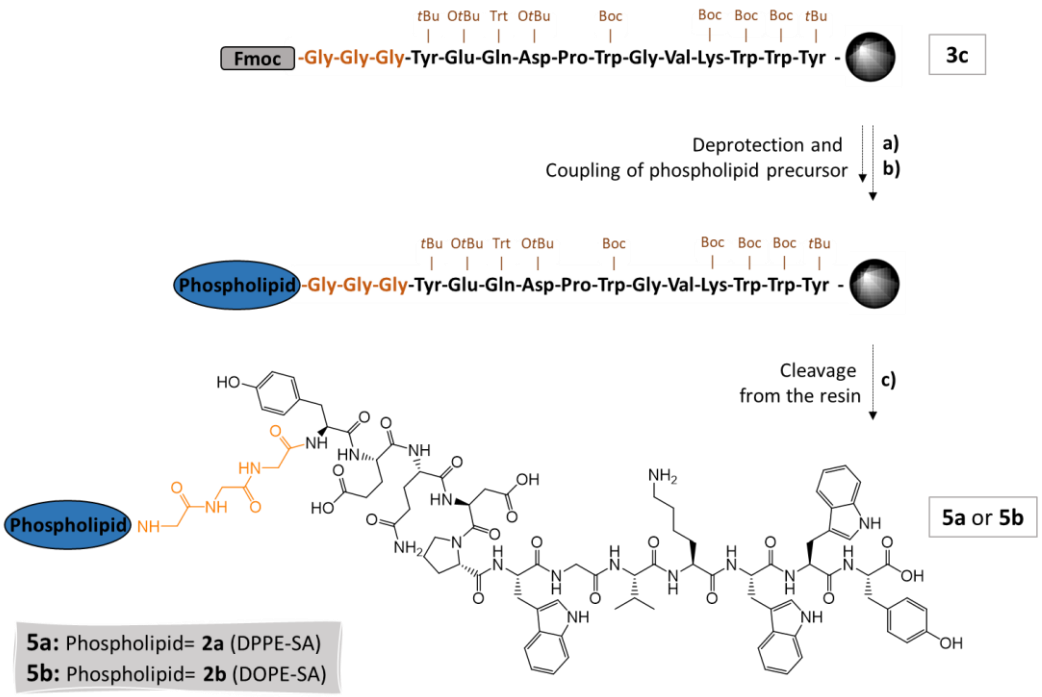

Scheme 16. *Microwave-assisted solid phase peptide synthesis of DPPE-SA-GGG-M2pep* ***5a****:* ***a)*** *20% piperidine in DMF;* ***b)*** *precursor 2a, Oxyma, DIC, DMF;* ***c)*** *TFA/H_2O/TIS (95:2.5:2.5, v/v); and DPPE-SA-GGG-M2pep* ***5b****:* ***a)*** *20% piperidine in DMF;* ***b)*** *precursor 2b, Oxyma, DIC, DMF;* ***c)*** *TFA/H_2O/TIS (95:2.5:2.5, v/v).*

The TFA used in the cleavage from Wang resin must be removed before biological studies, because it is toxic to cells.[88,89] It is easy to remove TFA by evaporation under a stream of nitrogen or in a rotary evaporator, but it is more challenging to remove the trifluoroacetate counter anions, which interact strongly with cationic peptides,[88] like at the ε-amino group of Lys, which is present in M2pep. TFA ions should be substituted for a biocompatible counterion, such as chloride.[89] Thus, after the synthesis of the peptides, an exchange procedure was made with a 0.1 M hydrochloric acid solution followed by freeze-drying, resulting in the chloride salts of peptide **5a** (DPPE-SA-GGG-M2pep) and peptide **5b** (DOPE-SA-GGG-M2pep), as crude light brownish solids in global yield of 77 and 61%, respectively. The final structures of the peptides **5a** and **5b**, represented in the **Figure 18**, were then confirmed by MS (negative ionisation), with a peak at *m/z* 1300 corresponding to $[M\text{-}2H]^{2+}$ (molecular ion with +2 charge) for **5a**. For **5b**, there were peaks at *m/z* 1070 (C-terminal fragment from scission at Tyr-Glu, with decarboxylation of Glu, and Trp-Tyr), 956 (fragment from indole loss of fragment 1070), and 842 (fragment from indole loss of fragment 842). Tandem MS spectra on fragment with *m/z* 1070 corroborated the relationship between these three fragments.

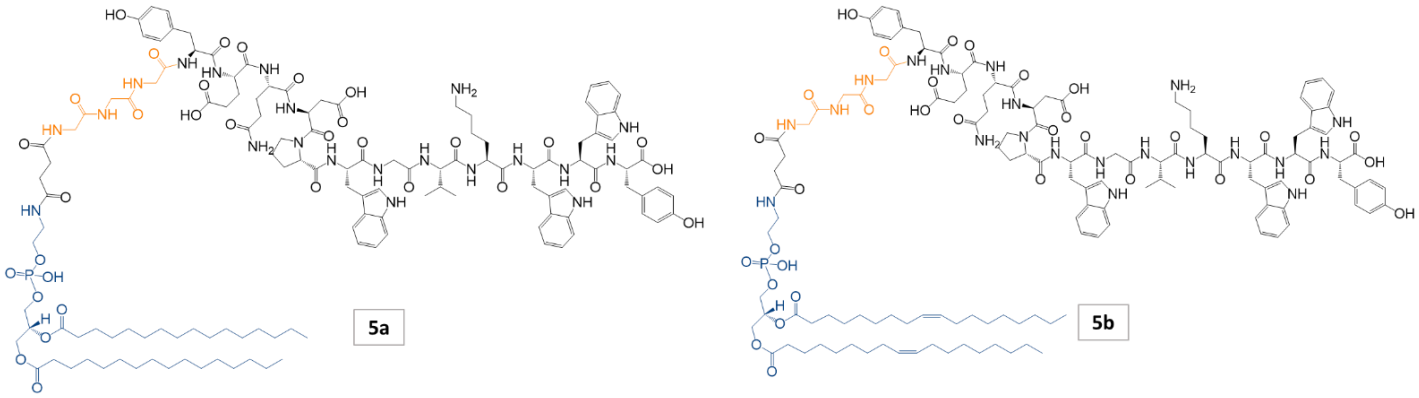

Figure 18. *Structure of peptides* ***5a*** *(DPPE-SA-GGG-M2pep) and* ***5b*** *(DOPE-SA-GGG-M2pep).*

The same solid-phase approach was performed on M2pep-GGG-Wang **3a**, with the triple glycine spacer at the peptide C-terminal. Only precursor **2b** was chosen for this coupling, as it easier to solubilize than **2a**. The coupling of DOPE-SA **2b** was done using DIC/Oxyma and subsequently cleaved from resin with the same cocktail of 95% TFA. The same exchange procedure was made with a 0.1 M HCl solution, and a brown crude solid was obtained intending to be peptide **5c** (DOPE-SA-M2pep-GGG), as shown in **Scheme 17**, as a crude light brownish solid in 21% yield.

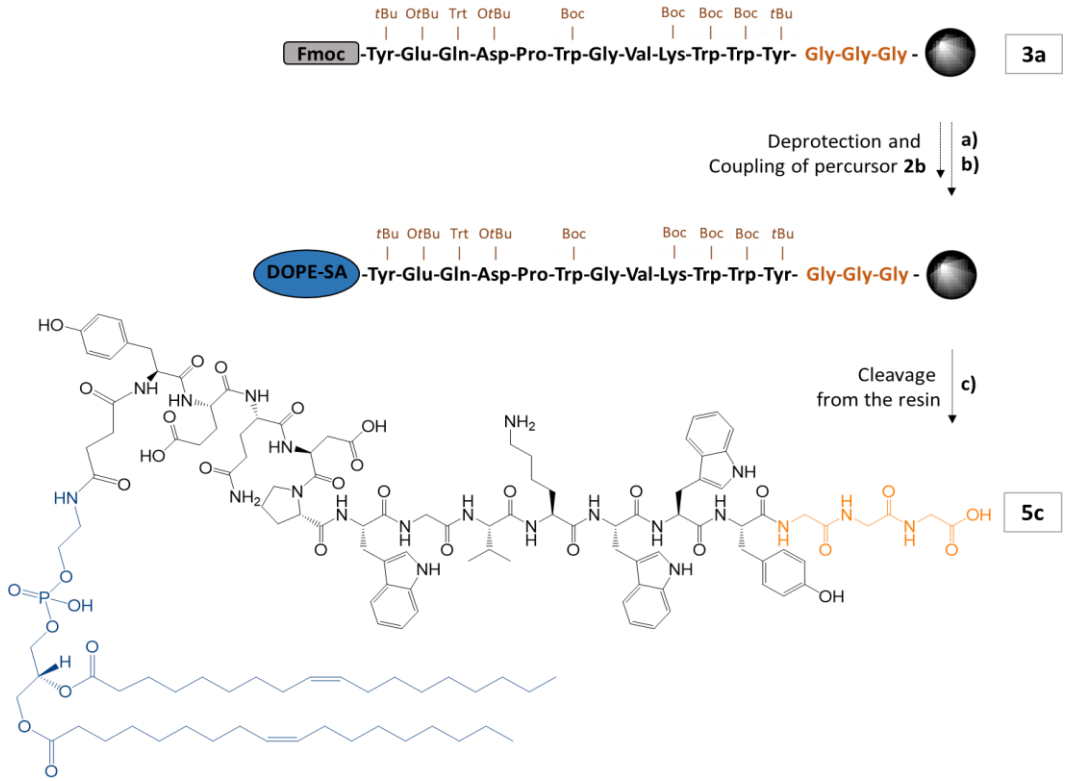

Scheme 17. *Microwave-assisted solid phase peptide synthesis of DPPE-SA-M2pep-GGG* ***5c****:* ***a)*** *20% piperidine in DMF;* ***b)*** *precursor* ***2b****, Oxyma, DIC, DMF;* ***c)*** *TFA/H_2O/TIS (95:2.5:2.5, v/v).*

Since the molecular weight of the synthesized peptides exceeded the analysis range of the available MS equipment (only masses up to 2000), the molecular ion peak was not visible, but peaks of lower mass were seen, that may correspond to the molecular ion with additional charges and the fragmentation of the molecule. Considering the length of the peptides, there are many possibilities for fragmentation. For example, peptide **5c** (MW_{calc}= 2654,10 g/mol) was detected with peaks that corresponded to the masses of two fragments produced by scission at the Gly - Val bond, with *m/z* 1703 and 951.

Comparing peptide **5b** (DOPE-SA-GGG-M2pep) with peptide **5c** (DOPE-SA-M2pep-GGG), where only the triple Gly spacer position changes, both were successfully obtained, yet linking directly to the spacer (peptide **5b**) obtained a significantly higher yield. This could be because the reaction of the phospholipid with a less hindered amino acid, such as Gly, is much easier than at an amino acid with a bulky side chain, like Tyr in peptide **5c**. Therefore, linking to the spacer appears to be more promising.

Further characterization of peptides **5a**, **5b** and **5c** was performed using UV-Vis absorption spectroscopy and FTIR. The absorption results were obtained at pH 7, to approximately replicate the physiological pH, and showed that the spectra have similar appearance to the absorption curve of M2pep-GGG **3b** (**Figure 19 a**), around 280 nm, attributed to the presence of Trp and Tyr. The peptides **5a**, **5b** and **5c** were also analysed by FTIR, which allowed the identification of the most important bands corresponding to the functional groups N-H and C=O. In Figure **19 b)** it is shown the FTIR spectrum of peptide **5c**, as a representative example.

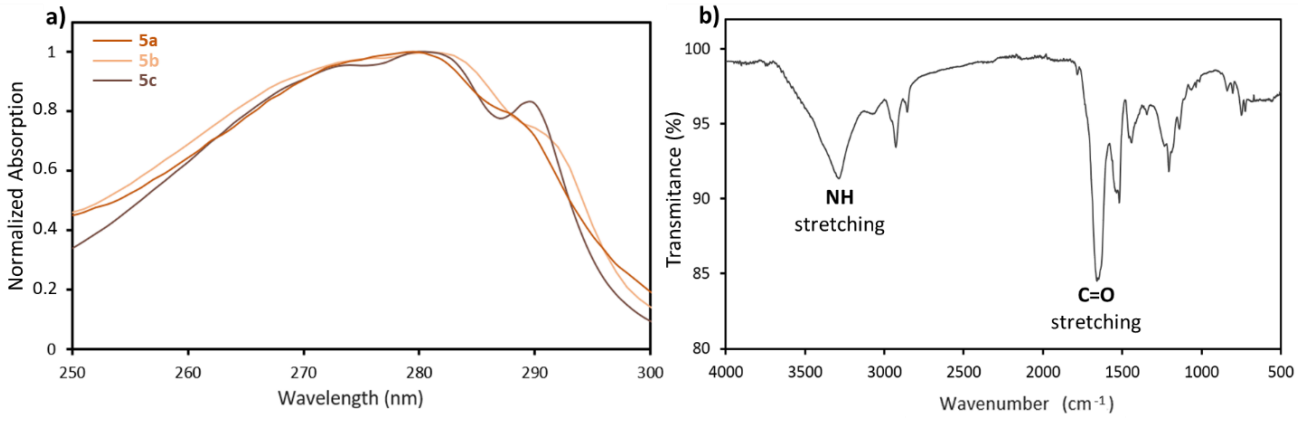

Figure 19. a) *Normalized UV/Vis absorption spectra of peptide **5a**, **5b** and **5c** (1.0 x 10^{-5} M) in phosphate buffer at pH 7;* ***b)*** *FTIR spectrum of peptide **5c**.*

Bearing still in mind the possibility of reacting the phospholipids DPPE and DOPE to the C-terminal of the M2pep, the coupling in solution was studied. This coupling had to be done in solution phase, since in solid phase synthesis the C-terminal of the peptide is blocked by the solid support. Therefore, the coupling of DPPE and DOPE to the free M2pep-GGG **3b** was carried out in a solution synthesis, using EDC.HCl as coupling reagent and NHS as additive, to activate the acidic terminal of the peptide, in the presence of Et_3N and heating at 40 °C for 18 h (**Scheme 18**). After work-up, crude light brownish solids were obtained by precipitation with diethyl ether, and isolated by filtration.

The solids obtained were characterized by MS, which showed that the desired peptides **5d** and **5e** were not present. This demonstrates that solution-based synthesis is not effective when coupling other moieties to M2pep, as the side chains of the amino acids are unprotected and none of the previous attempts produced the desired final peptide. The solution synthesis could only work if the peptide was protected, which is not possible with SPPS with Wang resin.

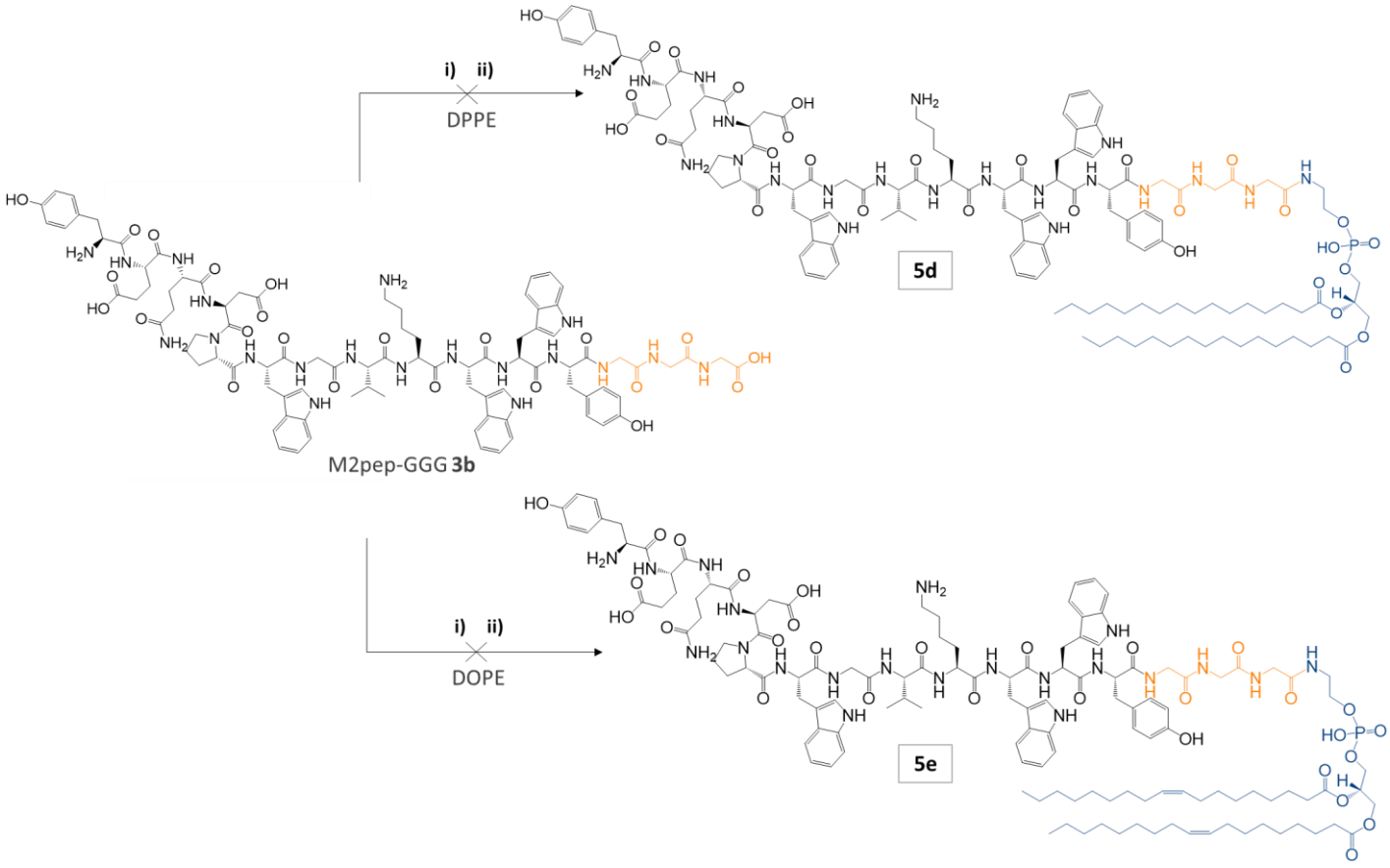

Scheme 18. *Synthesis attempt of M2pep-GGG-DPPE* ***5d****: **i)** NHS, EDC.HCl, Et_3N, dry DMF, 0°C, 30 min; **ii)** DPPE, 40 °C, 18 h. Synthesis attempt of M2pep-GGG-DOPE* ***5e****: **i)** NHS, EDC.HCl, Et_3N, dry DMF, 0°C, 30 min; **ii)** DOPE, 40 °C, 18 h.*

Attempts were also made in the research group to synthesize M2pep using the 2-chlorotrityl resin, a hyper-acid sensitive resin in which the cleavage of the protected peptide is possible with a very low acid percentage in the cleavage cocktail (typically 1%), but the resin seems to suffer premature release of the growing peptide throughout the synthesis. In the near future, a new synthesis will be attempted by adding a small percentage of an amine (0.1 equiv of DIPEA relative to the Oxyma) to the Oxyma solution to ensure a basic media throughout the whole synthesis procedure.

In this manner, based on the results achieved so far, peptides **5a** (DPPE-SA-GGG-M2pep), **5b** (DOPE-SA-GGG-M2pep) and **5c** (DOPE-SA-M2pep-GGG) were studied in the subsequent attachment to the lipid surface of the MDDs.

2.2 Synthesis of the magnetic solid lipid nanoparticles (mSLNs)

The main goal of this dissertation is to develop a hybrid lipid-based MDDs able to target M2 TAMs specifically by incorporation the targeting peptide M2pep, and encapsulation immunomodulating drugs and MIONs. Since these MIONs are inserted into the MNPs category and are within a lipid-base, we can describe the resulting systems as mSLNs.

These mSLNs will consist of a lipid base matrix for the incorporation of the remaining components (**Figure 20**). The matrix used was Carnauba Wax, already approved by FDA for its application in humans, which possesses a very high melting point (82–86 °C) and presents in its composition natural phospholipids providing enhanced biodegradability and biocompatibility, making it an attractive option for the formulation of the mSLNs.[33,57] The MNPs used were magnetite NPs coated with oleic acid (F_3O_4@OA) and their incorporation was possible due to the high affinity between the oleate-coating and the hydrophobic wax. In the wax was also incorporated, to be in the wax-water interface, a lipophilic fluorescent optical tracer (DiO), a green fluorophore very used as fluorescent reporter for *in vitro* studies, to be able to track the intracellular applications of the mSLNs.

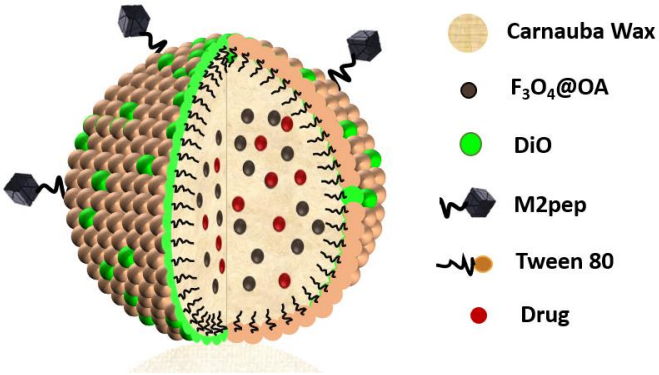

Figure 20. *Schematic representation of the proposed mSLNs.*

The final structure was stabilized in water by an FDA-approved surfactant (Tween 80). The attachment of the targeting M2pep to the mSLNs was possible by the hydrophobic tails of the phosphoethanolamines DPPE and DOPE, previously linked to the M2pep. The obtained peptides **5a** (DPPE-SA-GGGM2pep), **5b** (DOPE- SA-GGGM2pep) and **5c** (DOPE- SA-M2pepGGG), which were previously synthesized by microwave-assisted SPPS, were the more promising obtained peptides with both M2pep and the phospholipid chain. Therefore, these three peptides will be used for the attachment to the mSLNs.

In the final formulation, immunomodulating drugs will be incorporated into the lipid-based structure, to promote the decrease of M2 TAMs in the tumour environment. However, for the optimization process of the M2pep containing mSLNs, it was decided to refrain from drug use to save resources.

Knowing which components would be used, the preparation of the mSLNs proceeded by a simple modified melt emulsification method (**Scheme 19**), providing a stable formulation by mixing an organic with an aqueous phase to obtain the final mSLN. All the hydrophobic components of the mSLN were combined with the wax to form the organic phase, and water and Tween 80 formed the aqueous phase. The hydrophobic F_3O_4@OA (previously prepared by the research group following a standard co-precipitation protocol), and the lipophilic fluorescent dye (DiO), having both a hydrophobic segment, were added to the organic phase, and combined with the wax.

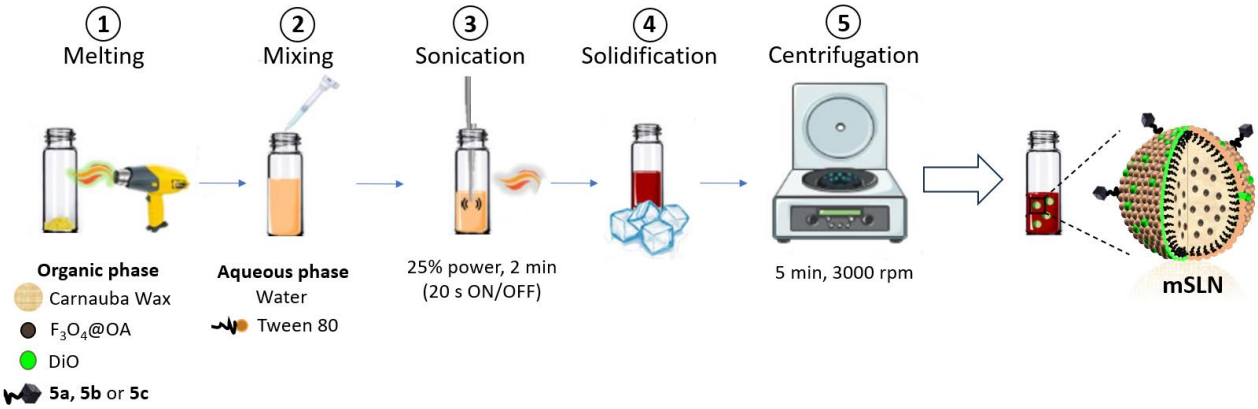

Scheme 19. *Schematic representation of the melt emulsification procedure followed for the preparation of the mSLNs. (Figure adapted from reference 33)*

The next component of the mSLN formulation added was the synthetized M2pep (**5a**, **5b** or **5c**) that also had a hydrophobic portion (DPPE or DOPE), thus being also added in the organic phase. The complete organic phase was heated until the wax melted, and all the solvent had evaporated. The aqueous phase was then added, presenting a much simpler composition, being formed only by water and the surfactant Tween 80 (**Scheme 19**).

The mixture was sonicated for 2 min at 20 s working intervals, at 25% power, and immediately immersed in ice, to solidify the mSLNs. They were then centrifuged resulting in the desired particles dispersed in the aqueous supernatant (**Scheme 19**). This procedure was the same for the synthesis of mSLNs with M2pep **5a**, **5b** and **5c** individually, obtaining the structure illustrated in **Figure 3**. In addition to these main syntheses, was also prepared one control, which was synthesized with all the other components, except the peptide (**Figure 21**).

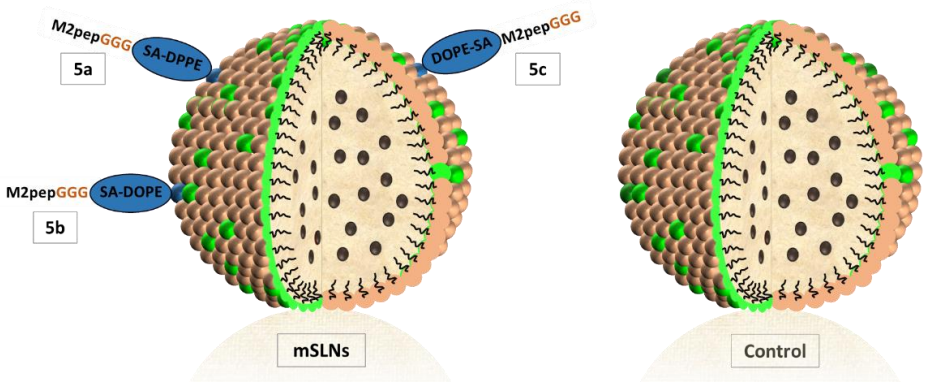

Figure 21. *Representation of the prepared mSLNs: mSLN **5a** (with peptide **5a**), mSLN **5b** (with peptide 5b), mSLN **5c** (with peptide **5c**) and the control (without peptide).*

The amount of each component of the formulation of the mSLNs was carefully thought out to obtain a final stable structure with the desired characteristics. The summary of the composition of each mSLNs synthesized, is reported in **Table 1**.

Table 1. *Summary of the composition of the prepared mSLNs.*

mSLNs	Tween80*	DiO*	F_3O_4@OA*	M2pep 5a*	M2pep 5b*	M2pep 5c*
Control	10 %	0.125 %	20 %	____	____	____
5a	10 %	0.125 %	20 %	2.5 %	____	____
5b	10 %	0.125 %	20 %	____	2.5 %	____
5c	10 %	0.125 %	20 %	____	____	2.5 %

- Each component of the mSLNs is added in proportion to 100 mg of wax (% w/ w_{wax}).

2.2.1 Physico-Chemical Characterization

The resulting mSLNs were firstly characterized using dynamic light scattering (DLS). This technique is widely used to characterize NPs to determine their size or hydrodynamic diameter (D_h) from the diffraction of a laser by the particles in a solution. DLS also gives the polydispersity index (PI), which indicates the homogeneity of a solution: the higher the value, the more polydisperse is the sample, and values above 0.4 indicate that the sample has a very heterogeneous distribution of particle size.[90] The zeta potential (Zpot) is also available in DLS characterization, giving the stability output of the NPs by measuring their surface charge. Zpot higher than +30 and inferior than −30 mV is considered as stable, having sufficient repulsive forces to achieve better physical colloidal stability, however, beyond these electrostatic interactions, there exist other types of stabilization.[41,91] The Dh, PDI and Zpot of the obtained mSLNs, is shown in **Table 2**.

All the mSLNs formulations revealed a PDI below 0.4, appropriate for biomedical applications,[33] indicative of a relatively homogenous population size, and no significant differences were observed between the PDI values of the functionalized mSLNs with M2pep and the control. The Dh was around 200 nm among all synthesized particles, except for mSLN **5a** which turned out to be a slightly smaller (179.7 nm).

Table 2. *Average D_h (nm), PDI and Zpot (mV), estimated by DLS, and encapsulated iron concentration (mg/mL and %), measured by ICP-AES, of the prepared mSLNs.*

	DLS			ICP-AES	
mSLNs	**D_h (nm)**	**PI**	**Zpot (mV)**	**[Fe] (mg/mL)**	**Fe encapsulated (%)**
Control	219.0 ± 11.0	0.24 ± 0.05	-16.1 ± 2.5	0.465	8
5a	179.7 ± 11.1	0.31 ± 0.06	-20.3 ± 0.2	0.400	7
5b	216.9 ± 10.4	0.29 ± 0.01	-14.9 ± 1.2	0.259	4
5c	224.7 ± 7.5	0.22 ± 0.03	-34.8 ± 2.4	0.332	6

The Zpot values were all negative, which is attributed to the presence of fatty acids from the carnauba wax and tween stabilization. Despite that, only the mSLN **5c** possesses a highly negative Zpot (-34.8), which contributes to particles repelling each other, improving colloidal stability. The mSLN **5a** has a less negative Zpot value (-20.3), and the mSLN **5b** and control show an even lower, but similar, negative value (-14.9 and -16.1, respectively). mSLNs **5a** and **5c**, both with the presence of M2pep coupled with the same phospholipid (DOPE), were the ones that presented the most negative Zpot values, although with a significant difference between them. The variation between the two can be attributed to how M2pep's amino acids are connected to the mSLN, which helps to explain this distinction: while mSLN **5c** has the neutral glycine spacer in the outside of the particle, the mSLN **5a** has a tyrosine, presenting different polarities, which may explain the influence on hydrodynamic size and surface charge. Despite this change in the surface charge, all the nanoformulations exhibited effective colloidal stability.

Furthermore, the technique inductively coupled plasma atomic emission spectroscopy (ICP-AES) was applied to each mSLN, which allows the quantification of several elemental species.[92] In this manner, the ICP measurements provided confirmation and quantification of the iron that was present in the resulting formulations (**Table 1**), and the percentage of encapsulated iron showed that the iron encapsulation on to the mSLNs was very efficient, given that only 20% of NPs was initially added.

The mSLNs were also characterized by transmission electron microscopy (TEM) to study their dispersion and morphology.[41] TEM micrographs (**Figure 22**) revealed the successful incorporation of the magnetite NPs within the lipid core of all nanoformulations, seen as visible hypointense (darker) small spots within the wax matrix, and showed the spherical shape of the particles.

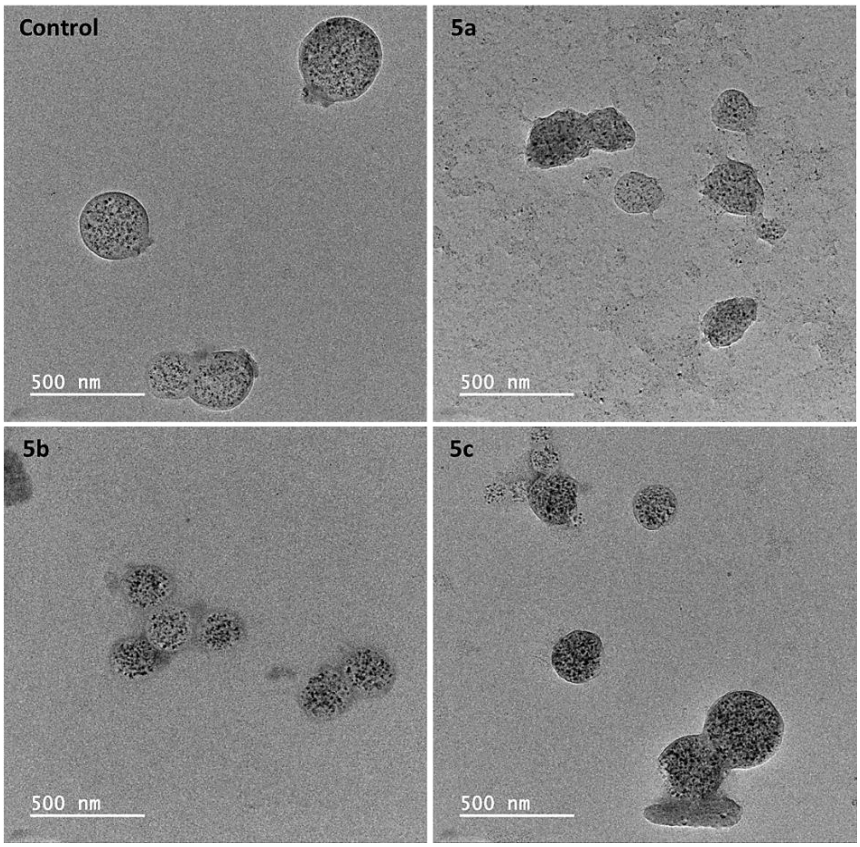

Figure 22. *TEM micrographs of the obtained mSLNs (scale bars correspond to 500 nm):* ***Control*** *(mSLN control);* ***5a*** *(mSLN* ***5a****);* ***5b*** *(mSLN* ***5b****) and* ***5c*** *(mSLN* ***5c****).*

An additional characterization by fluorescence spectrophotometry was also made with the mSLNs **5a** and **5b**, to evaluate the incorporation of DiO fluorophore into the obtained particles. It was possible to confirm the presence of DiO in both particles (and control), according to the spectrum shown in **Figure 23 a)**, with an emission band being observed at a wavelength of approximately 500 nm, which is in agreement with the fluorescence properties of DiO.[93] The emission band did not have any significant shift relative to the control band, stating that there was no challenge encapsulating DiO in the presence of M2pep.

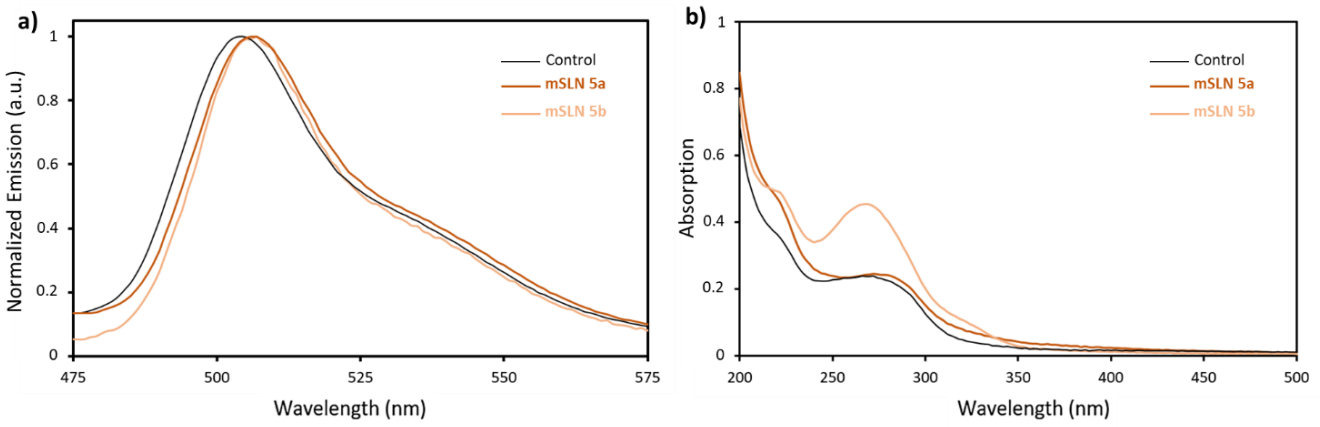

Figure 23. a) *Normalized fluorescence spectra and* ***b)*** *UV-Vis absorption (before purification) of mSLNs* ***5a*** *and* ***5b****, and control, in water.*

The aqueous solution of mSLNs before purification by centrifugation was also submitted to a UV-Vis absorption qualitative analysis, trying to obtain confirmation of M2pep's incorporation into the final nanoformulations. In the obtained spectra (**Figure 23 b**) is easy to observe that the control already shows a strong base absorption, to which mSLN **5a** is very close, and therefore settle that the majority of M2pep **5a** was encapsulated into the particle. On the other hand, M2pep **5b** was not fully incorporated, which may explain why its Zpot value is so similar to the control. The incorporation of more peptide in mSLN **5a** also can explain the size difference of this particle compared to the others by DLS. The larger the presence of peptide (ligand), the more surfactant is available for the particle to be stabilized, the lower the size.

Considering that it was not possible to trace a calibration curve, due to solubility problems with peptides **5a** and **5b**, it was not conceivable to quantify the exact concentration of non-encapsulated M2pep in the final formulations, leading only to this qualitative analysis.

In summary, the synthesized mSLNs showed good colloidal stability in a spherical shape with an average 200 nm diameter, with suitable iron concentration, and confirmation of the encapsulation of DiO fluorophore and the target M2pep.

The presence of peptide M2pep will allow selective targeting of M2-like TAMs to reprogram their phenotype from predominantly M2 to M1, triggering an immune response against cancer, while the efficient co-encapsulation of the MNPs will enable MRI's diagnostic

capabilities and MH-induced effects, allowing a *quasi*-real-time monitoring of the process and a precise control over anticancer drug release, by applying an AMF.

Once this synthesis is optimized and the M2pep encapsulated in the final mSLNs is actually quantified, tests will begin to encapsulate this peptide together with immunomodulating drugs, as it has already been proven that the combination of target peptides, such M2pep, and chemotherapeutic agents effectively target TAMs and potentialize the anti-tumour effect of chemotherapy, with less toxicity.[22,24,29]

Chapter 3

Conclusions and Perspectives

3. Conclusions and Perspectives

The first aim of this thesis was the synthesis and characterization of targeting peptide M2pep and several conjugates, functionalized with a RhoB fluorophore, to selectively target M2 macrophages by fluorescence-based techniques, and phospholipids (DPPE and DOPE) to be anchored on the final hybrid MDDs.

RhoB derivatives were initially synthesized by a reaction between a diamine and the fluorophore, obtaining the precursor **1a** with yields of 53, 33 and 75%, and characterization by ^{1}H NMR spectroscopy and MS confirmed the presence of the desired structure. The precursor **1b** was prepared by the reaction of previous precursor **1a** and maleic anhydride, giving the final compound, confirmed by MS, with a yield of 36%, but still with contaminants, meaning the purification of this precursor must be subsequently optimized. The last RhoB precursor **1c** was attempted to be synthesized through a coupling between RhoB and a glycine by solution synthesis using EDC.HCl and NHS, however characterization by MS showed that the coupling was unsuccessful. So, only precursor **1a** was successfully achieved and purified, which was later coupled to M2pep.

Precursors of the phospholipids DPPE and DOPE were synthesized by the same method, by reacting the phospholipid with succinic anhydride, giving the precursor **2a** (DPPE-SA) with yields of 51 and 57%, and precursor **2b** (DOPE-SA) with yields of 37 and 87%. Both were positively characterized by MS, but as precursor **2b** showed less solubility problems, it also allowed confirmation of its structure and purity by ^{1}H NMR spectroscopy.

The peptides M2pep with the triple glycine spacer were then synthetized by MW-SPPS in a Wang resin, applying the Fmoc strategy. The M2pep-GGG **3b** was obtained using an automatic peptide synthesizer and GGG-M2pep **3d** synthesis was performed on a manual peptide synthesizer. These M2pep were subsequently used for coupling with the synthesized precursors, either with the peptide still bound to the resin with protecting groups (SPPS) or with the free peptide without the protecting groups (synthesis in solution). The structure and purity of the obtained peptides **3b** and **3d** was confirmed by high and low-resolution MS, UV-Vis absorption spectroscopy, FTIR and HPLC.

Initially, attempts were made with the aim of coupling the precursor **1a**, fluorophore RhoB and another type of fluorophore (Cy5) to the termini of M2pep **3b** in solution synthesis (peptide **4a**, **4b** and **4c**, respectively), yet none of them succeeded. Considering that the free M2pep has 15 amino acids (with the glycine spacer), without the protecting groups of the side chains, it is likely that the peptide may acquire a conformation that hinders the access to the reaction site and prevents coupling reactions. It was then decided to perform microwave-assisted solid phase synthesis by conjugating the free N-terminal of the M2pep-GGG Wang **3a** and RhoB using DIC/Oxyma. The labelled peptide **4d** (RhoB-M2pep-GGG), was purified by semi-preparative HPLC and obtained in 6% yield. Its structure was confirmed by MS and UV-Vis absorption, and fluorescence spectroscopy showed clearly that the conjugation of RhoB with M2pep-GGG (peptide **4d**) dramatically enhanced the fluorescence intensity of M2pep, and therefore, can be used as an efficient probe to target M2 macrophages in cancer diagnosis. This fluorescent peptide is currently being used to target M2 macrophages in *in vitro* studies. In the future, it will be tested the RhoB labelling onto M2pep with the glycine's spacer at the reaction site (RhoB-GGG-M2pep), for a more effective coupling.

The phospholipids precursors were also covalently linked to M2pep, to incorporate a hydrophobic section into it, to anchor the M2pep onto the lipid-coated of the mSLNs. Priority was given to microwave-assisted solid phase synthesis, and so precursors **2a** and **2b** were coupled on the free N-terminal of the GGG-M2pep Wang **3c** using DIC/Oxyma, giving peptide **5a** (DPPE-SA-GGG-M2pep) and peptide **5b** (DOPE-SA-GGG-M2pep), in global yield of 77 and 61%, respectively. The same way, was coupled precursor **2b** on the M2pep-GGG Wang **3a**, providing peptide **5c** (DOPE-SA-M2pep-GGG) with 21% of global yield. When the triple Gly spacer is not at the coupling site, apparently there is a decrease in the final yield of the reaction (comparing peptide **5b** and **5c**), which can be explained by the fact that is easier to react the phospholipid with a less hindered amino acid, such as Gly, than with an amino acid with a bulky side chain, like Tyr. Therefore, linking onto the spacer appears to be more promising.

These peptides had difficulties in isolation and purification and consequently, due to lack of time, it was not possible to obtain the pure products, but it was still possible to recognize the structure of these conjugates by MS, UV-Vis absorption and FTIR. Moving

forward, it is determinant to find an effective method to purify these lipid peptides, for instance by using another type of semi-preparative column.

An attempt to synthetize the lipid M2pep was also performed with the possibility of coupling in solution the phospholipids DPPE and DOPE to the C-terminal of the free M2pep-GGG **3b**, but the desired product was not obtained.

In so doing, the synthesis of mSLNs was then performed with the more promising M2pep-lipid conjugates obtained by solid phase synthesis, peptides **5a**, **5b** and **5c**. The preparation of the mSLNs proceeded by a simple and green modified melt emulsification method, with incorporation of MNPs (F_3O_4@OA) and a fluorophore (DiO) in a carnauba wax matrix, and attachment of the targeting M2pep, giving a final stabilized structure in surfactant Tween 80. In addition of the synthesis of mSLNs **5a**, **5b** and **5c**, it was also prepared one control, with all the components except the peptide.

The synthesized mSLNs were characterized by DLS, ICP-AES, TEM, UV-Vis and fluorescence spectroscopy, and showed overall good colloidal stability in a spherical shape with an average 200 nm diameter, with suitable iron concentration (4-8%), and confirmation of the encapsulation of DiO and target M2pep, proving that the preparation method is indeed efficient.

It is important to be aware of the exact concentration of M2pep that was attached on to the mSLNs, since its presence was only proven qualitatively. Its quantification will eventually be carried out either by a UV-Vis calibration curve or even by HPLC.

This final nanoplatform is intended to efficiently encapsulate MNPs and more forward to encapsulate chemotherapeutic drugs, providing a combination of non-invasive imaging capability by MRI for the diagnosis and follow-up of the tumour, a good control over drug release, and even MH-inducing effects, simultaneously in the presence of the targeting peptide M2pep, being a step forward on TAMs targeting therapy.

Hereafter, the synthesis of M2pep-lipid conjugates will be tested with other phospholipids, such as 1,2-distearoyl-*sn*-glycero-3-phosphoethanolamine (DSPE), and even with a longer spacer like PEG, which have already been shown to attach efficiently onto lipid matrices of DDS.[40,57,94]

Chapter 4

Experimental section

4. Experimental section

4.1 General

The reagents and solvents used were commercially available (Acros Organics, Aldrich, Merck, AAPPTec) and used as received. Pre-functionalized Wang resins and all Fmoc-amino acids were purchased from AAPPTec and Iris Biotech. Phospholipids were purchased from TCI Chemicals. Sulfo-Cy5 was previously synthesized in the research group.[95]

Thin layer chromatography (TLC) was performed on silica gel plates 60, with fluorescence indicator F_{254} (Merck) and revealed by UV radiation (254 and 365 nm) in a CN-6 chamber (Vilber Lourmart) and in an iodine vapor chamber. Preparative layer chromatography (PLC) was performed on pre-coated PLC plates Silica Gel 60 F-254 (Merck). Column and dry flash chromatography were carried out using silica gel 60 of diameter 0.035-0.070 mm (Acros Organics).

Synthesis of M2pep-GGG **3a-b** was performed on an automatic peptide synthesizer (Liberty Blue 2.0, while the other solid phase syntheses were carried out on a manual Discover SPS peptide synthesizer, both from CEM Corporation.

Freeze-drying was done in a Labogene Scanvac CoolSafe 110-4 Pro equipped with a Welch CRVPro4 high vacuum pump.

The analytical HPLC comprised a Licrospher 100 RP18 analytical column (5 mm), Jasco PU-980 pump, Shimadzu SPDGAV UV/vis detector and a Shimadzu C-RGA Chromatopac recorder. Purification by semi-preparative HPLC was performed with a Europa Peptide 120 column C18 (5 µm) (Teknocroma) in a system composed of a Shimadzu LC-8A pump, coupled to a JASCO 875-UV UV-Vis detector and a Shimadzu C-RGA Chromatopac recorder.

The ^{1}H NMR spectra were obtained on a Bruker Avance III apparatus at an operating frequency of 400 MHz, using the solvent peak as an internal reference. The deuterated solvents used in NMR spectroscopy were $CDCl_3$ with 99.8% deuteration degree, containing 0.03% v/v of tetramethylsilane (EurisoTop), and DMSO-d_6 with a 99.8% deuteration degree, with 0.1% v/v tetramethylsilane (EurisoTop).

The UV-Vis absorption spectra were obtained on a UV/2501PC spectrophotometer (Shimadzu) and fluorescence emission spectra was obtained on a FluoroMax-4 (Horiba). Infrared spectra were obtained on a PerkinElmer Spectrum Two instrument with an ATR accessory in the 500-4000 cm^{-1} window.

High resolution MS, in positive ESI mode, was acquired on a QqTOF Impact IITM mass spectrometer (Bruker Daltonics). Low resolution ESI-MS analyses were performed on a Thermo Scientific LxQ Linear Ion Trap, equipped with an electrospray ionization source, in positive and negative mode.

4.2 Synthesis of Precursors

4.2.1 Rhodamine B precursors

4.2.1.1 Precursor **1a**

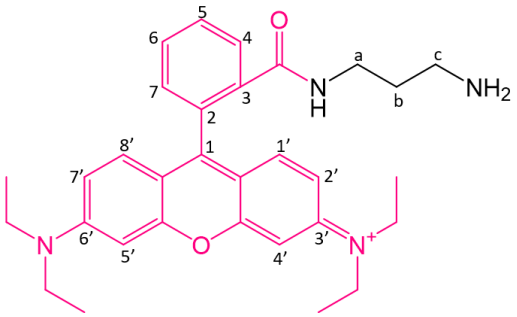

Rhodamine B (500 mg, 1.04 mmol, 1 equiv.) was dissolved in ethanol (25 mL) and 1,3-diaminopropane was added (865 µL, 5.22 mmol, 5 equiv.). The reaction was monitored by TLC, with MeOH/DCM (1:9, v/v) as eluent. The mixture was heated at reflux for 10 hours and then the solvent was removed under vacuum. The solid residue was dissolved in DCM (15 mL) and washed with distilled water (2 x 10 mL) and brine solution (2 x 10 mL). The organic layer was collected, dried over anhydrous magnesium sulphate ($MgSO_4$). The desiccant was filtered, and the organic filtrate was evaporated under reduced pressure. The obtained residue was submitted to a dry flash chromatography with MeOH/DCM (3:97, v/v) as eluent,

to obtain the pure precursor **1a** as a salmon pink solid (1st trial, 278 mg, 53%; 2nd trial, 171 mg, 33%; 3rd trial, 391 mg, 75%).

^{1}H RMN (400 MHz, DMSO-d_6): δ = 1.06 (t, J=6.8 Hz, 12H, 4×CH_3), 1.34 (t, J=6.8 Hz, 2H, CH_2-a), 2.48-2.57 (m, 2H, CH_2-b), 3.04 (t, J=6.8 Hz, 2H, CH_2-c), 3.29-3.32 (m, 8H, 4xCH_2), 6.30-6.36 (m, 6H, H-1' and H-8'+ H-2' and H-7'+ H-4' and H-5'), 6.97-6.99 (m, 1H, H-5), 7.46-7.52 (m, 2H, H-6 + H-7), 7.76-7.78 (m, 1H, H-4).

MS (ESI, positive mode): *m/z* 500 ([M+H]$^+$, 82%).

4.2.1.2 Precursor **1b**

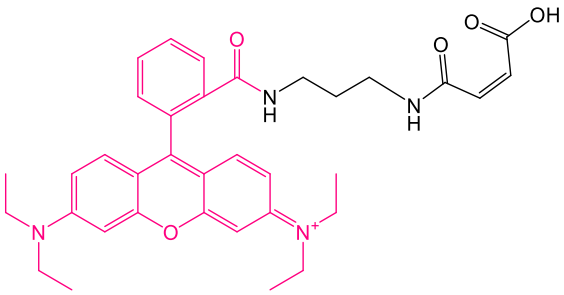

Precursor **1a** (278 mg, 0.557 mmol, 1 equiv.) was dissolved in chloroform (10 mL) and maleic anhydride (75,2 mg, 0.836 mmol, 1.5 equiv.) was added. The mixture was heated at reflux for 22 hours and then the solvent was removed by rotary evaporation under vacuum. The reaction was monitored by TLC, with MeOH/DCM (1:9, v/v) as eluent. The crude product was purified by column chromatography on silica gel with diethyl ether/AcOEt (5:5, v/v) as eluent, to get precursor **1b** as a pink solid (121 mg, 36%).

MS (ESI, positive mode): *m/z* 598 ([M+H]$^+$, 99%).

4.2.1.3 Precursor **1c**

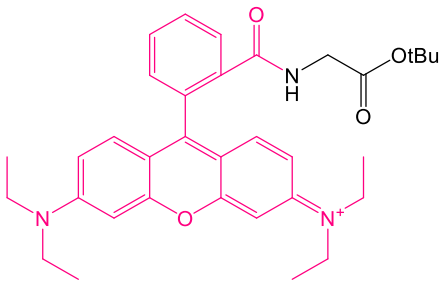

Rhodamine B (571 mg, 1.19 mmol, 2 equiv.) was dissolved in dry DMF (7 mL) and placed in an ice bath. After stirring for 5 min, NHS was added (137 mg, 2 equiv.) and after stirring for 10 min, EDC.HCl (228 mg, 2 equiv.) and Et_3N (248 µL, 1 equiv.) were added. The mixture was allowed to stir for another 30 min and then Gly(OtBu) was added (100 mg, 0,599 mmol, 1 equiv.) and allowed to stir for about 7 days at room temperature. Water was added and freeze-drying was carried out to afford an impure pink solid, mainly composed of unreacted rhodamine.

4.2.2 Phospholipid precursors

4.2.2.1 DPPE precursor **2a**

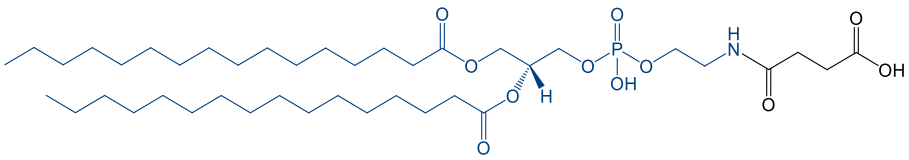

DPPE (100 mg, 0.144 mmol, 1 equiv.) and Et_3N (60 µL, 3 equiv.) were dissolved in 8 mL of $CHCl_3$/MeOH (9:1, v/v). Succinic anhydride (20 mg, 0.202 mmol, 1.4 equiv.) were dissolved DCM (in 8 mL) and added to the DPPE solution. The reaction mixture was stirred at room temperature for 5 hours. The reaction was monitored by TLC, with $CHCl_3$/MeOH/H_2O (65:25:4, v/v) as eluent, and then developed in an iodine chamber. The mixture was acidified by adding $CHCl_3$ (16 mL) and a 20 mM potassium phosphate buffer with pH 5.6 (16 mL) and then stirred for 30 minutes. The aqueous phase was washed with $CHCl_3$ (3 x 25 mL) and the combined organic phases were dried over anhydrous $MgSO_4$. The anhydrous $MgSO_4$ was filtered off and the organic solvent was evaporated under reduced pressure. The residue

was submitted to a PLC with $CHCl_3$/MeOH/H_2O (65:25:4, v/v) as eluent. The silica from the zone of the plate with R_f of 0.4 was scraped and washed with DCM/MeOH (9:1, v/v) (5 x 100 mL). The solvent was decanted, combined, and evaporated under reduced pressure. The precursor DPPE-SA **2a** was obtained as a white pale solid (1st trial, 15 mg, 51%; 2nd trial, 66 mg, 57%).

MS (ESI, positive mode): m/z 792 ($[M]^+$, 49%).

MS (ESI, negative mode): m/z 790 ($[M-H]^+$, 32%).

4.2.2.2 DOPE precursor **2b**

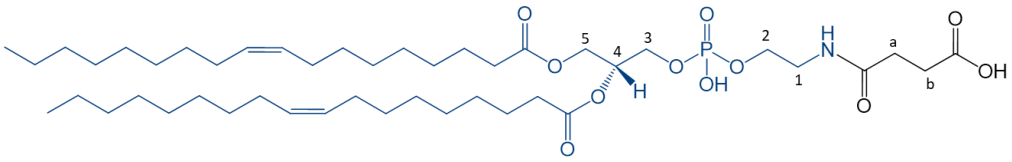

DOPE (100 mg, 0.134 mmol, 1 equiv.), succinic anhydride (18 mg, 0,188 mmol, 1.4 equiv.) and Et_3N (56 µL, 3 equiv.) were dissolved in 10 mL of $CHCl_3$/MeOH (9:1, v/v). The reaction mixture was stirred at room temperature for 5 hours. The reaction was monitored by TLC, with $CHCl_3$/MeOH/H_2O (65:25:4, v/v) as eluent and developed in an iodine chamber. The crude product obtained after evaporation of the solvent under reduced pressure was acidified by adding $CHCl_3$/MeOH (9:1, v/v) (5 mL) and dilute HCl solution at pH 5.5 (5 mL) and then stirred for 30 minutes. The aqueous phase was washed with $CHCl_3$ (3 x 10mL) and the combined organic phases were dried over anhydrous $MgSO_4$. The anhydrous $MgSO_4$ was filtered off and the organic solvent was evaporated under reduced pressure. The residue was purified by column chromatography on silica gel with $CHCl_3$/MeOH (8:2, v/v) as eluent, to get the precursor DOPE-SA **2b** as a viscous white pale solid (1st trial, 42 mg, 37%; 2nd trial,152 mg, 87%).

^{1}H RMN (400 MHz, $CDCl_3$): δ = 0.89 (t, J=6.4 Hz, 6H, 2×CH_3), 1.24-1.30 (m, 40H, 20×CH_2), 1.60 (s, 4H, 2×CH_2), 1.81-2.02 (m, 8H, 4×CH_2 next to C=C), 2.31 (d, J=7.6 Hz, 4H, 2×CH_2 next to C=O), 2.48 (br s, 2H, CH_2-a), 2.68 (br s, 2H, CH_2-b), 3.11 (br s, 2H, CH_2-1), 3.48 (br s, 2H, CH_2-2), 3.96-4.05 (m, 4H, NH + OH + CH_2-5 + CH_2-3), 4.16- 4.20 (m, 1H, CH_2-5 or CH_2-3), 4.36-4.40 (m, 1H, CH_2-5 or CH_2-3), 5.24-5.36 (m, 3H, CH-4 + 2xCH=).

MS (ESI, positive mode): *m/z* 867 (([M+Na]$^+$, 100%).

MS (ESI, negative mode): *m/z* 842 (([M-H]$^+$, 100%).

4.3. Microwave-assisted solid phase synthesis

4.3.1. General procedures

Deprotection of amino acids by cleavage of the Fmoc group

The resin was subjected to deprotection using a 20% piperidine solution in DMF (5 mL/g resin) for 30 s under microwave irradiation (P= 50 W, T= 75 °C). When the previous solution was discarded, a new solution of 20% piperidine in DMF (7 mL/g of resin) was added and allowed to react for 3 min under microwave irradiation (P= 50 W, T= 75 °C). The resin was washed four times with DMF.

NOTE: As the first amino acid of the desired peptide was already coupled to the resin (pre-loaded Wang resin), the loading of the resin was already determined.

Coupling of Fmoc-amino acids with DIC/Oxyma

The Fmoc-amino acid (5 equiv. relative to resin loading) was dissolved in 6 mL of dry DMF, DIC (5 equiv.) and Oxyma (5 equiv.) previously dissolved in the amount of dry DMF required and left under stirring for 4 min at room temperature. The mixture was added to the resin and the suspension was subjected to a microwave irradiation cycle of 4 min each (P= 25 W, T= 75 °C). After the reaction time, the resin was washed three times with DMF.

TNBS test

After the coupling step, a few beads of resin were collected and placed into a sample tube and 2 drops of a 10% *N*,*N*-Diisopropylethylamine (DIPEA) solution in DMF were added and 2 drops of 1% TNBS solution in DMF. After 10 minutes, the solvent was discarded and a few drops of DMF were added to the beads and the colour of the beads was assessed: if the beads showed a red colour, it meant there were free NH_2 groups and coupling was incomplete; otherwise, if the beads were colourless, the coupling was successful.

Peptide cleavage from the Wang resin

The resin was stirred with a TFA/TIS/H_2O solution (95:0.25:0.25, v/v) (5 mL/g resin) at room temperature for 2 hours. The suspension was filtered, and the resin was washed with neat TFA (3 x 0.5 mL) and filtered. The filtrates were combined, the solvent was concentrated under vacuum and cold ethyl ether was added to induce precipitation. and the mixture was kept in the refrigerator overnight. The mixture was centrifuged to isolate the solid formed, the supernatant decanted and the solid was dried in a vacuum desiccator.

4.3.2. M2pep-GGG **3b**

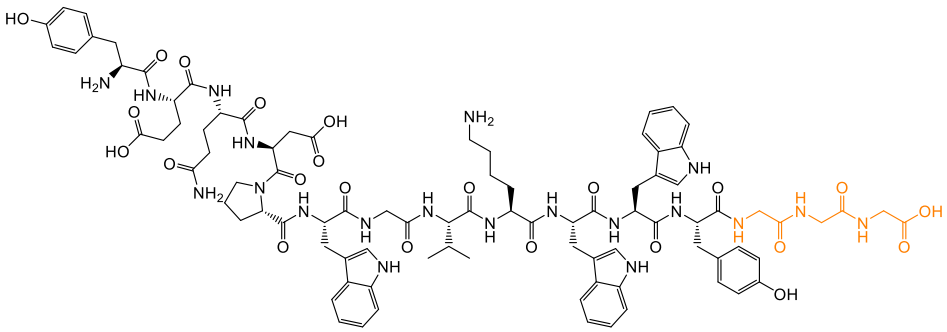

Fmoc-Gly-Wang resin with a degree of functionalization of 0.51 mmol/g (0,192 g), was suspended in DMF (5 mL) and peptide assembly was done considering the coupling/deprotection/cleavage steps previously described. The fully deprotected M2pep-GGG **3b** was obtained as a white solid, after cleavage from obtaining M2pep-GGG resin **3a**.

HRMS: (ESI, positive mode) *m/z* for $C_{89}H_{112}N_{20}O_{23}$, calculated 914.4099; found 914.9124 (+2 charge).

4.3.3. GGG-M2pep **3d**

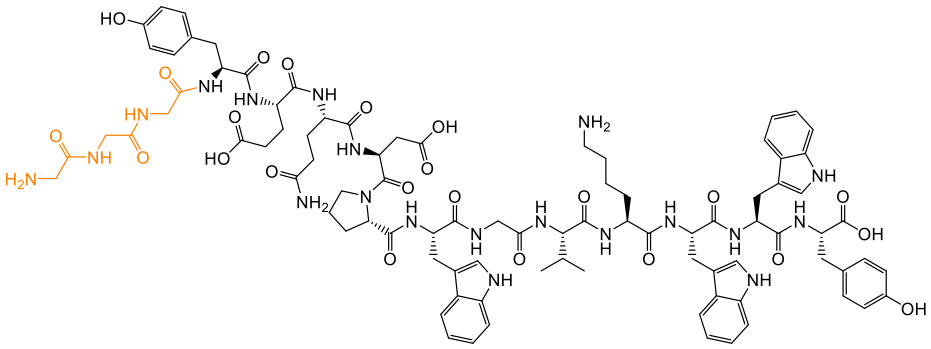

Fmoc-Tyr(tBu)-wang resin with a degree of functionalization of 0.52 mmol/g (0,192 g) was suspended in DMF (5 mL) and peptide assembly was done considering the coupling/deprotection/cleavage steps previously described. The fully deprotected GGG-M2pep **3d** was obtained as a yellowish white solid, after cleavage from GGG-M2pep resin **3c**.

MS (ESI, positive mode): *m/z* 915.03 (100%).

4.4. Synthesis of M2pep with a fluorophore

4.4.1. Peptide **4a**

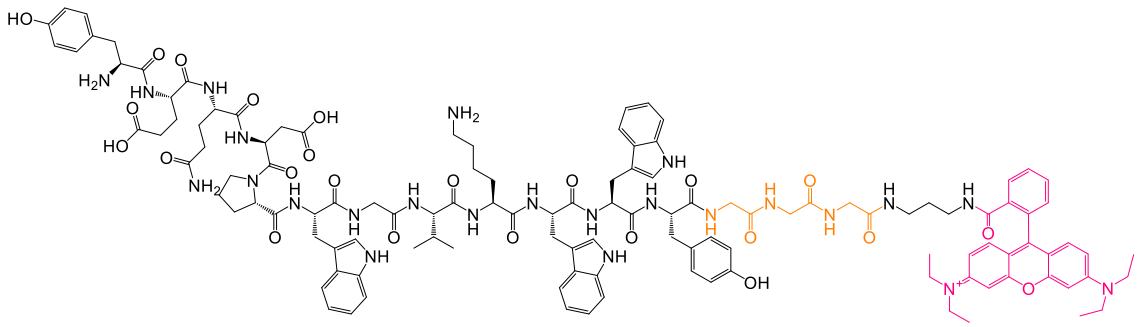

M2pep-GGG **3b** (50 mg, 0.0274 mmol, 1 equiv.) was dissolved in dry DMF (3 mL) and placed in an ice bath. After stirring for 5 min, NHS was added (3.2 mg, 1 equiv.) and after stirring for 10 min, EDC.HCl (5.3 mg, 1 equiv.) and Et_3N (3.8 µL, 1 equiv.) were added. The mixture was allowed to stir for another 30 min and then precursor **1a** was added (13.6 mg, 0.0274 mmol, 1 equiv.) and allowed to stir for about 5 days at room temperature. Diethyl

ether was added to the solution and the mixture kept in the refrigerator overnight. The solid was isolated by filtration and MS analysis confirmed that it was not the desired peptide.

4.4.2. Peptide **4b**

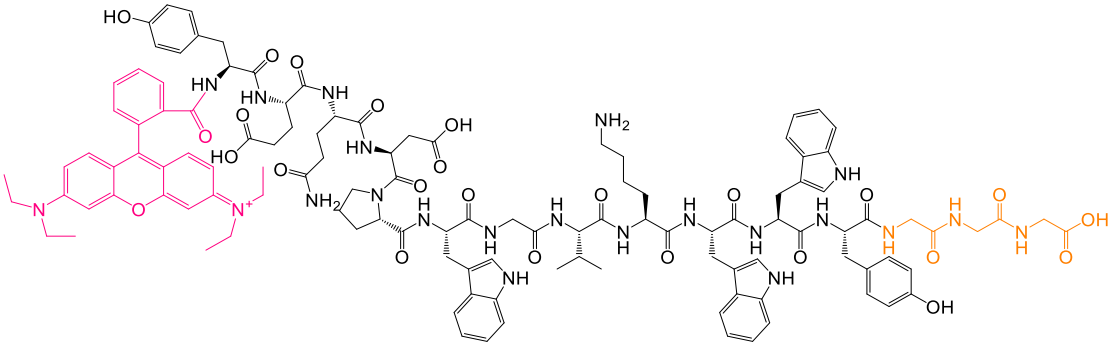

Rhodamine B (13 mg, 0.0274 mmol, 1 equiv.) was dissolved in dry DMF (3 mL) and placed in an ice bath. After stirring for 5 min, NHS was added (3.5 mg, 1 equiv.) and after stirring for 10 min, EDC.HCl (5.6 mg, 1 equiv.) and Et_3N (3.8 µL, 1 equiv.) were added. The mixture was allowed to stir for another 30 min and M2pep-GGG **3b** (50 mg, 0.0274 mmol, 1 equiv.) was added and allowed to stir for about 7 days at room temperature. Diethyl ether was added to the solution and the mixture kept in the refrigerator overnight. The solid was isolated by filtration and MS analysis confirmed that it was not the desired peptide.

4.4.3. Peptide **4c**

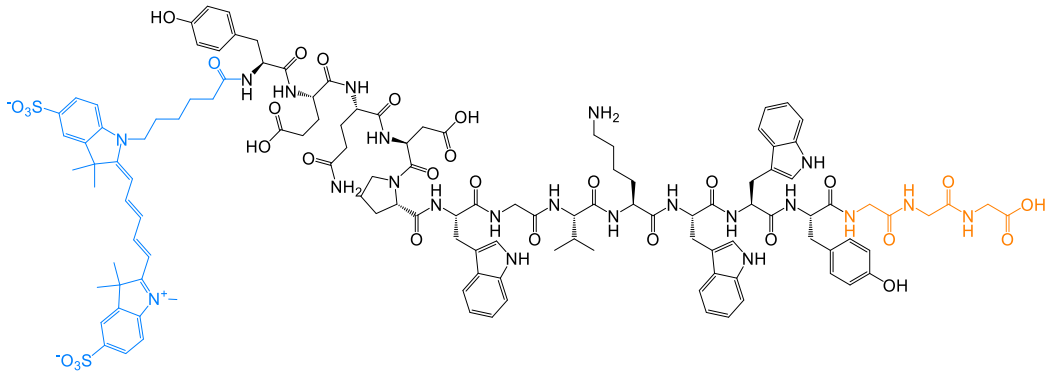

Carboxy-Cy5 (22.2 mg, 0.0346 mmol, 1 equiv.) was dissolved in dry DMF (3 mL) and placed in an ice bath. After stirring for 5 min, NHS was added (3.1 mg, 1 equiv.) and after stirring for 10 min, EDC.HCl (5.2 mg, 1 equiv.) and Et_3N (3.8 µL, 1 equiv.) were added. The mixture was allowed to stir for another 30 min and M2pep-GGG **3b** (36 mg, 0.0346 mmol, 1 equiv.) was added and allowed to stir for about 6 days at room temperature.

Diethyl ether was added to the solution and the mixture kept in the refrigerator overnight. The solid was isolated by filtration and it was not possible to confirm if it was the desired peptide due to insolubility in all the usual solvents.

4.4.4. Peptide **4d**

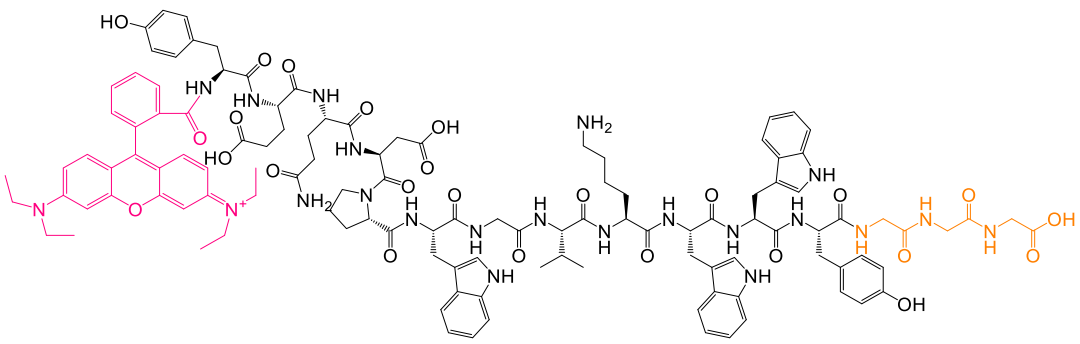

After deprotection of the last amino acid of M2pep-GGG-Wang **3a**, rhodamine B (492 mg, 1.02 mmol, 5 equiv. relative to resin loading) was dissolved in dry DMF (6 mL). Then DIC (160 µL, 5 equiv.) and Oxyma (146 mg, 5 equiv.) were added, previously dissolved in a small volume of dry DMF. The mixture was allowed to stir for 5 min and then added to the M2pep-GGG-Wang **3a** and subjected to coupling cycles (5x5 min, P= 25 W, T= 75 °C), letting it cool down between cycles. The resin was washed with DMF (3x) and then with MeOH (3x). This wash cycle was repeated 5 times. The peptide was then cleaved from the resin by the general solid phase synthesis procedures described above. The filtrate was concentrated in vacuum and diethyl ether was added to the residue and the mixture kept in the refrigerator overnight. After centrifugation, the obtained crude pink solid was dissolved in a mixture of ACN/H_2O (1:1, v/v) with 0.1% TFA (10 mL) and purified by HPLC using a semi-prep Europa C-18 column at a flow rate of 1.0 mL/min. The eluent mixture was filtered through a Millipore filter type HN 0.45 µm and ultrasonically degassed before use. The chromatogram was

traced by detection of UV/Vis absorption at 540 nm. Ten injections were performed and 17 fractions with different retention times were isolated, combined, and freeze-dried. The fraction with retention time at about 29 minutes proved to be peptide RhoB-M2pep-GGG **4d** in the form of a pink solid (19 mg, 6%).

MS (ESI, positive mode): *m/z* 1133 (100%) (corresponds to fragment resulting from loss of the triple Gly spacer and cleavage at the Asp-Pro bond).

4.5. Synthesis of M2pep with phospholipids

4.5.1. Peptide **5a**

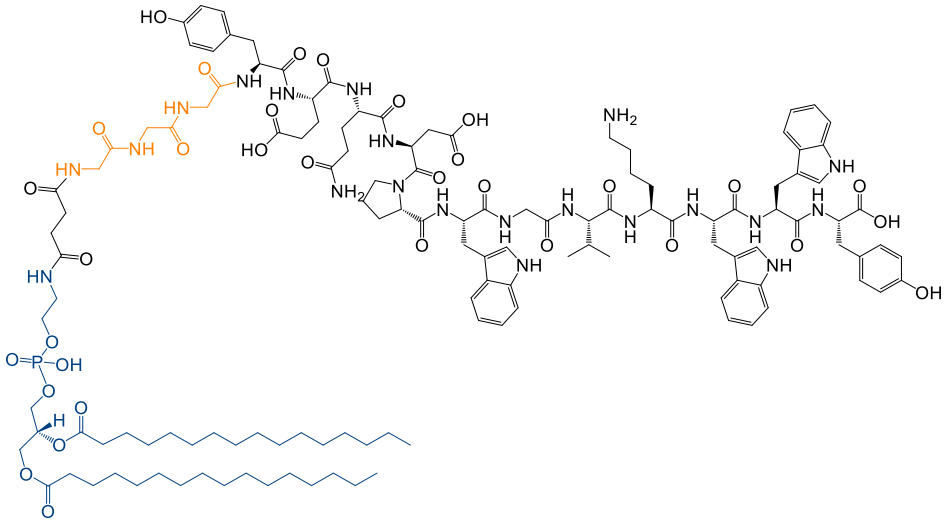

After deprotection of the last amino acid of GGG-M2pep-Wang **3c**, DPPE precursor **2a** (38 mg, 0.0475 mmol, 2.5 equiv. relative to resin loading) was dissolved in dry DMF (3 mL). Then DIC (7.3 µL, 2.5 equiv.) and Oxyma (6.7 mg, 2.5 equiv.) were added, previously dissolved in the required volume of dry DMF. The mixture was allowed to stir for 10 minutes at 40 °C and then added to the GGG-M2pep-Wand **3c** and the suspension was subjected to microwave irradiation cycles (5x5 min, P= 25 W, T= 75 °C), letting it cool down between cycles. After the microwave cycles, the resin was stirred for 48 hours at room temperature. The resin was washed with DMF (3x) and then with MeOH (3x). This wash cycle was repeated 4 times. The peptide was then cleaved from the resin by the general solid phase synthesis procedures described above. The filtrate was concentrated in vacuum and diethyl

ether was added to the residue and the mixture kept in the refrigerator overnight. After centrifugation, the obtained solid was dried and dissolved in 1 mL of a 0.1 M HCl solution, stirred for 5 min, and freeze-dried. This procedure was repeated two times and a light brownish solid proved to be peptide DPPE-SA-GGG-M2pep **5a** (39 mg, yield 77%).

MS (ESI, negative mode): *m/z* 1300 ($[M-2H]^{2+}$, 100%).

4.5.2. Peptide **5b**

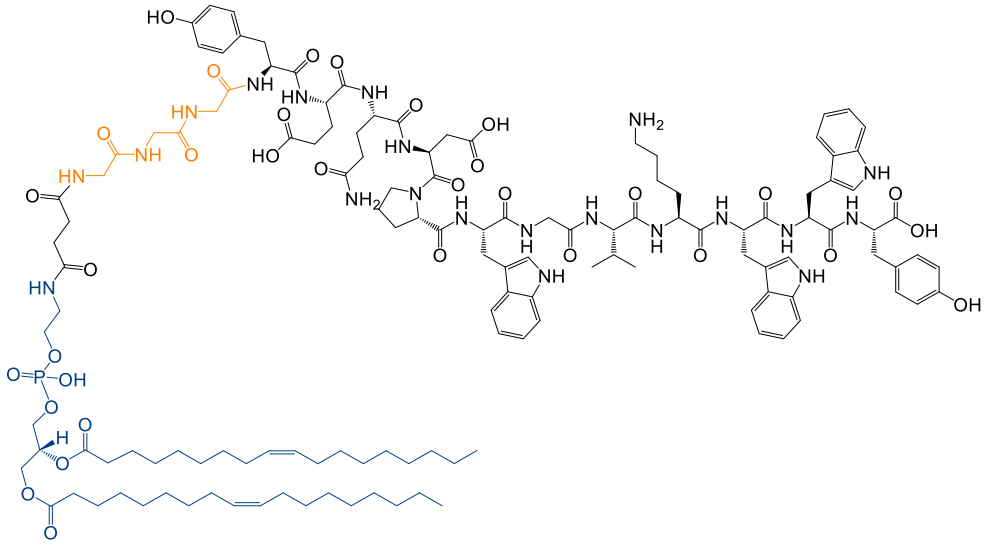

After deprotection of the last amino acid of GGG-M2pep-Wang **3c**, DOPE precursor **2b** (85 mg, 0.100 mmol, 2.5 equiv. relative to resin loading) was dissolved in dry DMF (5 mL). Then DIC (15.5 µL, 2.5 equiv.) and Oxyma (14.2 mg, 2.5 equiv.) were added, previously dissolved in the required volume of dry DMF. The mixture was allowed to stir for 10 minutes at 40 °C and then added to the GGG-M2pep-Wang **3c** and the suspension was subjected to microwave irradiation cycles (5x5 min, P= 25 W, T= 75 °C), letting it cool down between cycles. After the microwave cycles, the resin was stirred for 48 hours at room temperature. After the reaction time, the resin was washed with DMF (3x) and then with MeOH (3x). This wash cycle was repeated 4 times. The peptide was then cleaved from the resin by the general solid phase synthesis procedures described above. The filtrate was concentrated in vacuum and diethyl ether was added to the residue and the mixture kept in the refrigerator overnight. After centrifugation, the obtained solid was dried and dissolved in 1 mL of a 0.1 M HCl solution, stirred for 5 min, and freeze-dried. This procedure was repeated two times and a light brownish solid proved to be peptide DOPE-SA-GGG-M2pep **5b** (66 mg, yield 61%).

MS (ESI, negative mode): *m/z* 1070 (C-terminal fragment from scission at Tyr-Glu, with decarboxylation of Glu, and Trp-Tyr, 54%), 956 (fragment from indole loss of fragment 1070, 100%), and 842 (fragment from indole loss of fragment 842, 35%).

4.5.3. Peptide **5c**

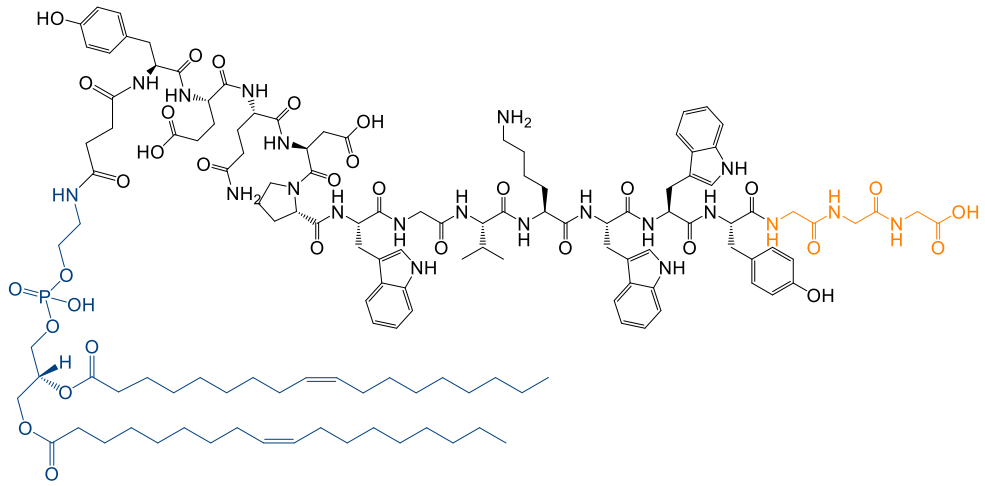

After deprotection of the last amino acid of M2pep-GGG-Wang **3a**, DOPE precursor **2b** (100 mg, 0.119 mmol, 2.5 equiv. relative to resin loading) was dissolved in dry DMF (7 mL). Then DIC (18.4 µL, 2.5 equiv.) and Oxyma (17 mg, 2.5 equiv.) were added, previously dissolved in the required volume of dry DMF. The mixture was allowed to stir for 10 minutes at 40 °C and then added to the M2pep-GGG-Wang **3a** and the suspension was subjected to microwave irradiation cycles (5x5 min, P= 25 W, T= 75 °C), letting it cool down between cycles. After the reaction time, the resin was washed with DMF (3x) and then with MeOH (3x). This wash cycle was repeated 4 times. The peptide was then cleaved from the resin by the general solid phase synthesis procedures described above. The filtrate was concentrated in vacuum and diethyl ether was added to the residue and the mixture kept in the refrigerator overnight. After centrifugation, the obtained solid was dried and dissolved in 1 mL of a 0.1 M HCl solution, stirred for 5 min, and freeze-dried. This procedure was repeated two times and a light brownish solid proved to be peptide DPPE-SA-M2pep-GGG **5c** (27 mg, yield 21%).

MS (ESI, negative mode): *m/z* 1703 (scission at the Gly - Val bond, 15%), 951 (scission at the Gly - Val bond, 25%).

4.5.4. Peptide **5d**

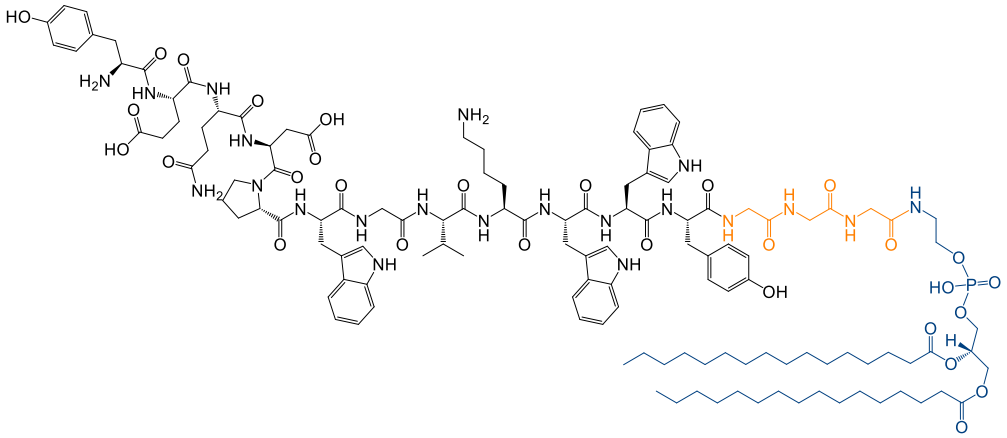

M2pep-GGG **3b** (54 mg, 0.0296 mmol, 1 equiv.) was dissolved in dry DMF (5 mL) and placed in an ice bath. After stirring for 5 min, NHS was added (9.5 mg, 3 equiv.) and after stirring for 10 min, EDC.HCl (16 mg, 3 equiv.) and Et_3N (11.4 µL, 3 equiv.) were added. The mixture was allowed to stir for another 30 min and DPPE was added (20,5 mg, 0.0296 mmol, 1 equiv.) and allowed to stir for about 18 hours at 40 °C. The reaction mixture was cooled to room temperature and diethyl ether was added and kept in the refrigerator overnight. The mixture was centrifuged to isolate the solid formed and then dried in a vacuum desiccator. A brown crude solid was obtained (262 mg) but it was not the desired peptide.

4.5.5. Peptide **5e**

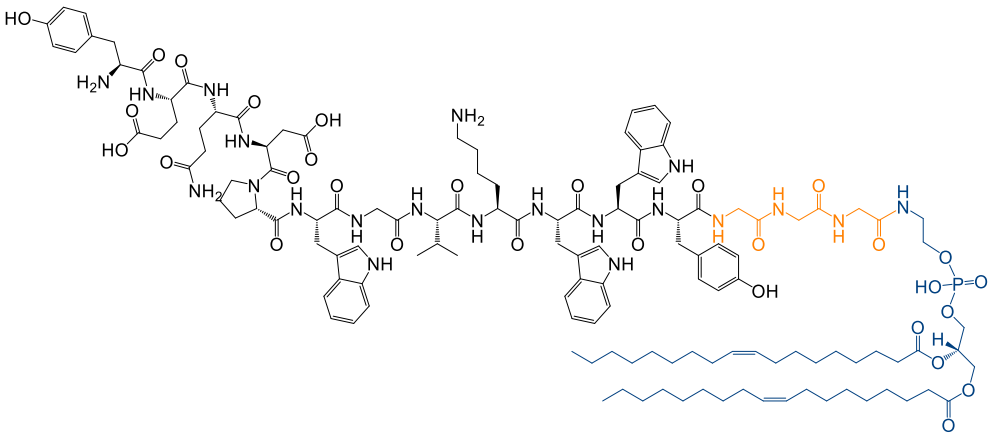

M2pep-GGG **3b** (52 mg, 0.0289 mmol, 1 equiv.) was dissolved in dry DMF (5 mL) and placed in an ice bath. After stirring for 5 min, NHS was added (10.7 mg, 3 equiv.) and after stirring for 10 min, EDC.HCl (16.6 mg, 3 equiv.) and Et_3N (12 µL, 3 equiv.) were added. The mixture was allowed to stir for another 30 min and DOPE was added (21.5 mg, 0.0289 mmol, 1 equiv.) and allowed to stir for about 18 hours at 40 °C. The reaction mixture was cooled to room temperature and then added ethyl ether and placed in the refrigerator overnight. The mixture was centrifuged to isolate the solid formed and then dried in a vacuum desiccator. A brown crude solid was obtained (215 mg) but it was not the desired peptide.

4.6. UV-Vis absorption and fluorescence spectroscopy

For all samples, solutions of $1x10^{-4}$ M were prepared in a phosphate buffer solution, and by diluting the concentrated solution, a solution in phosphate buffer was prepared with a concentration of $1x10^{-5}$ M. Solutions of M2pep-GGG **3b** and GGG-M2pep **3d** and of peptides **5a-c** were prepared with a phosphate buffer solution of pH 7, while peptide **4d** solution was made in a phosphate buffer at pH 5.6. In these measurements, absorption and fluorescence quartz cells with optical path of 1 cm were used.

The UV-Vis absorption spectra of peptides **3b** and **3d** and **5a-c** were plotted between 250 and 300 nm and the maximum absorption wavelength (λ_{abs}) was determined. The UV-Vis absorption spectrum of peptide **4d** was scanned between 250 and 600 nm. The fluorescence spectrum of the same solution of peptide **4d** was scanned, the excitation wavelength (λ_{exc}) was set at 540 nm and a slit of 3 nm was chosen and the maximum emission wavelength (λ_{emi}) was determined.

4.7. Synthesis of the mSLNs

This synthesis and characterization of solid lipid nanoparticles was carried out at INL as part of an ongoing collaboration within an FCT project with the Centre of Chemistry of the University of Minho.

The mSLNs were synthesized based on a modified melt emulsification method, where for every 100 mg of Carnauba wax were added a $CHCl_3$ solution of Fe_3O_4@OA (90 mg/mL of iron, total amount 20 % regarding wax), a 1 mg/mL $CHCl_3$ solution of DiO (0.125 % regarding wax) followed by the M2pep **5a** or **5b** or **5c** (2.5 % regarding wax). This organic phase was heated under a heat gun until the wax melted and all the $CHCl_3$ had evaporated. Then a 50 mg/mL water solution of Tween80 (10 % regarding wax) and a total of 2.250 mL of milli-Q water were added, making the aqueous phase. The sample was then ultrasonicated for 2 min at 20 s working intervals, at 25 % power, and immediately immersed in an ice bath until it was cold. The lipid NPs were centrifuged at 3000 rpm for 10 min, and only the supernatant was collected and reserved.

In addition to the three main syntheses, a control was also prepared, where the wax, Fe_3O_4@OA, DiO and Tween80 were added, except for the peptide M2pep. The entire procedure applied to control was the same as the described above.

4.7.1. Physico-Chemical Characterization

A DLS system was utilized to measure the Dh, PDI and ZP of the resulting mSLNs using a Horiba SZ-100 instrument. For this, the final solutions of the mSLNs were diluted in milli-Q water (1:100, v/v), and measured using a carbon electrode cell, at room temperature.

A further characterization of mSLNs morphology was performed by TEM on a JEM-2100-HT – JEOL microscope. The TEM images were collected in a 4 k CCD camera, at an accelerating voltage of 200 kV. The samples were prepared by dropping 7 µL of a diluted mSLNs water solution (solution prepared for DLS) onto a carbon coated copper TEM grid which was then allowed to dry at room temperature.

The concentration of iron encapsulated in mSLNs was quantified by ICP-AES in a spectrometer ICPE 9000 – SHIMADZU, and a stock solution with a known concentration was utilized to establish a calibration curve. The analysed samples were prepared by reacting overnight 100 µL of the mSLNs solution onto 900 µL of HCl (37 %), and then diluted in milli-Q water (1:10, v/v), making up to 10 mL of total volume. The samples were filtered by using 0.22 µm cut-off nylon-based hydrophilic syringe filters before the analysis. The iron concentration was then evaluated using the iron emission at 238 nm, for iron encapsulation estimation.

The M2pep that was not encapsulated was possible to be seen by UV-vis absorption analyses in a SpectroPhotoMeter - UV-2550 (SHIMADZU), between 200 and 500 nm, at 10 mm path length quartz cells. Sample preparation consisted of centrifugal filtering 500 µL of the resulting mSLNs solution using 30 kDa cut-off filters, and the obtained liquid was then diluted in milli-Q water (1:10, v/v). Fluorescent detection was also performed for the identification of DiO emission peak on the diluted mSLNs water solutions (solutions prepared for DLS), on a FluoMax-4 Spectrofluorometer (HORIBA), in an λ_{exc} of 465 nm and slit of 3 nm.

Chapter 5

References

5. References

(1) Chhikara, B. S.; Parang, K. Global Cancer Statistics 2022: The Trends Projection Analysis. *Chem. Biol. Lett.* **2023**, *10(1), 451*. https://pubs.thesciencein.org/journal/index.php/cbl/article/view/451.

(2) Hoenke, S.; Serbian, I.; Deigner, H.-P.; Csuk, R. Mitocanic Di- and Triterpenoid Rhodamine B Conjugates. *Molecules* **2020**, *25* (22), 5443. https://doi.org/10.3390/molecules25225443.

(3) Ferlay, J.; Colombet, M.; Soerjomataram, I.; Parkin, D. M.; Piñeros, M.; Znaor, A.; Bray, F. Cancer Statistics for the Year 2020: An Overview. *Int. J. Cancer* **2021**, *149* (4), 778–789. https://doi.org/10.1002/ijc.33588.

(4) Cerqueira, M.; Belmonte-Reche, E.; Gallo, J.; Baltazar, F.; Bañobre-López, M. Magnetic Solid Nanoparticles and Their Counterparts: Recent Advances towards Cancer Theranostics. *Pharmaceutics* **2022**, *14* (3), 506. https://doi.org/10.3390/pharmaceutics14030506.

(5) Cao, Y.; Qiao, B.; Chen, Q.; Xie, Z.; Dou, X.; Xu, L.; Ran, H.; Zhang, L.; Wang, Z. Tumour Microenvironment Remodeling via Targeted Depletion of M2-like Tumour-Associated Macrophages for Cancer Immunotherapy. *Acta Biomater.* **2023**, *160*, 239–251. https://doi.org/10.1016/j.actbio.2023.02.006.

(6) Ngambenjawong, C.; Gustafson, H. H.; Pineda, J. M.; Kacherovsky, N. A.; Cieslewicz, M.; Pun, S. H. Serum Stability and Affinity Optimization of an M2 Macrophage-Targeting Peptide (M2pep). *Theranostics* **2016**, *6* (9), 1403–1414. https://doi.org/10.7150/thno.15394.

(7) Marabelle, A.; Kohrt, H.; Caux, C.; Levy, R. Intratumoural Immunization: A New Paradigm for Cancer Therapy. *Clin. Cancer Res.* **2014**, *20* (7), 1747–1756. https://doi.org/10.1158/1078-0432.CCR-13-2116.

(8) Zhu, J.; Wang, J.; Li, Y. Recent Advances in Magnetic Nanocarriers for Tumour Treatment. *Biomed. Pharmacother.* **2023**, *159*, 114227. https://doi.org/10.1016/j.biopha.2023.114227.

(9) Yahaya, M. A. F.; Lila, M. A. M.; Ismail, S.; Zainol, M.; Afizan, N. A. R. N. M. Tumour-Associated Macrophages (TAMs) in Colon Cancer and How to Reeducate Them. *J. Immunol. Res.* **2019**, *2019*, 1–9. https://doi.org/10.1155/2019/2368249.

(10) Kaufmann, S. H. E. Immunology's Coming of Age. *Front. Immunol.* **2019**, *10*, 684. https://doi.org/10.3389/fimmu.2019.00684.

(11) Luz, R.; Nicolazzi, L.; Camara, N.; Braga, T. Macrophages: From Metchnikoff to 2020 and Ahead. In *Macrophages in the Human Body: A Tissue Level Approach.*; **2022**; pp 1–18.

(12) Stefater, J. A.; Ren, S.; Lang, R. A.; Duffield, J. S. Metchnikoff's Policemen: Macrophages in Development, Homeostasis and Regeneration. *Trends Mol. Med.* **2011**, *17* (12), 743–752. https://doi.org/10.1016/j.molmed.2011.07.009.

(13) Wynn, T. A.; Chawla, A.; Pollard, J. W. Macrophage Biology in Development, Homeostasis and Disease. *Nature* **2013**, *496* (7446), 445–455. https://doi.org/10.1038/nature12034.

(14) Komohara, Y.; Fujiwara, Y.; Ohnishi, K.; Takeya, M. Tumour-Associated Macrophages: Potential Therapeutic Targets for Anti-Cancer Therapy. *Adv. Drug Deliv. Rev.* **2016**, *99*, 180–185. https://doi.org/10.1016/j.addr.2015.11.009.

(15) Yang, Q.; Guo, N.; Zhou, Y.; Chen, J.; Wei, Q.; Han, M. The Role of Tumour-Associated Macrophages (TAMs) in Tumour Progression and Relevant Advance in Targeted Therapy. *Acta Pharm. Sin. B* **2020**, *10* (11), 2156–2170. https://doi.org/10.1016/j.apsb.2020.04.004.

(16) Obeid, E.; Nanda, R.; Fu, Y.-X.; Olopade, O. I. The Role of Tumour-Associated Macrophages in Breast Cancer Progression. *Int. J. Oncol.* **2013**, *43* (1), 5–12. https://doi.org/10.3892/ijo.2013.1938.

(17) Sica, A.; Schioppa, T.; Mantovani, A.; Allavena, P. Tumour-Associated Macrophages Are a Distinct M2 Polarised Population Promoting Tumour Progression: Potential Targets of Anti-Cancer Therapy. *Eur. J. Cancer* **2006**, *42* (6), 717–727. https://doi.org/10.1016/j.ejca.2006.01.003.

(18) Brown, J. M.; Recht, L.; Strober, S. The Promise of Targeting Macrophages in Cancer Therapy. *Clin. Cancer Res.* **2017**, *23* (13), 3241–3250. https://doi.org/10.1158/1078-0432.CCR-16-3122.

(19) Liu, Y.; Sun, D.; Fan, Q.; Ma, Q.; Dong, Z.; Tao, W.; Tao, H.; Liu, Z.; Wang, C. The Enhanced Permeability and Retention Effect Based Nanomedicine at the Site of Injury. *Nano Res.* **2020**, *13* (2), 564–569. https://doi.org/10.1007/s12274-020-2655-6.

(20) DeNardo, D. G.; Ruffell, B. Macrophages as Regulators of Tumour Immunity and Immunotherapy. *Nat. Rev. Immunol.* **2019**, *19* (6), 369–382. https://doi.org/10.1038/s41577-019-0127-6.

(21) Beltraminelli, T.; De Palma, M. Biology and Therapeutic Targeting of Tumour-Associated Macrophages. *J. Pathol.* **2020**, *250*, 573–592. https://doi.org/10.1002/path.5403.

(22) Figueiredo, P.; Lepland, A.; Scodeller, P.; Fontana, F.; Torrieri, G.; Tiboni, M.; Shahbazi, M.; Casettari, L.; Kostiainen, M. A.; Hirvonen, J.; Teesalu, T.; Santos, H. A. Peptide-Guided Resiquimod-Loaded Lignin Nanoparticles Convert Tumour-Associated Macrophages from M2 to M1 Phenotype for Enhanced Chemotherapy. *Acta Biomater.* **2021**, *133*, 231–243. https://doi.org/10.1016/j.actbio.2020.09.038.

(23) Benoit, M.; Desnues, B.; Mege, J.-L. Macrophage Polarization in Bacterial Infections. *J. Immunol.* **2008**, *181* (6), 3733–3739. https://doi.org/10.4049/jimmunol.181.6.3733.

(24) Pang, L.; Pei, Y.; Uzunalli, G.; Hyun, H.; Lyle, L. T.; Yeo, Y. Surface Modification of Polymeric Nanoparticles with M2pep Peptide for Drug Delivery to Tumour-Associated Macrophages. *Pharm. Res.* **2019**, *36* (4), 65. https://doi.org/10.1007/s11095-019-2596-5.

(25) Zang, X.; Zhang, X.; Hu, H.; Qiao, M.; Zhao, X.; Deng, Y.; Chen, D. Targeted Delivery of Zoledronate to Tumour-Associated Macrophages for Cancer Immunotherapy. *Mol Pharm.* **2019**, *16*, 2249–2258. https://doi.org/10.1021/acs.molpharmaceut.9b00261.

(26) Cieslewicz, M.; Tang, J.; Yu, J. L.; Cao, H.; Zavaljevski, M.; Motoyama, K.; Lieber, A.; Raines, E. W.; Pun, S. H. Targeted Delivery of Proapoptotic Peptides to Tumour-Associated Macrophages Improves Survival. *Proc. Natl. Acad. Sci.* **2013**, *110* (40), 15919–15924. https://doi.org/10.1073/pnas.1312197110.

(27) Le Joncour, V.; Laakkonen, P. Seek & Destroy, Use of Targeting Peptides for Cancer Detection and Drug Delivery. *Bioorg. Med. Chem.* **2018**, *26* (10), 2797–2806. https://doi.org/10.1016/j.bmc.2017.08.052.

(28) Liu, G. W.; Livesay, B. R.; Kacherovsky, N. A.; Cieslewicz, M.; Lutz, E.; Waalkes, A.; Jensen, M. C.; Salipante, S. J.; Pun, S. H. Efficient Identification of Murine M2 Macrophage Peptide Targeting Ligands by Phage Display and Next-Generation Sequencing. *Bioconjug. Chem.* **2015**, *26* (8), 1811–1817. https://doi.org/10.1021/acs.bioconjchem.5b00344.

(29) Li, K.; Liu, C.-J.; Zhang, X.-Z. Multifunctional Peptides for Tumour Therapy. *Adv. Drug Deliv. Rev.* **2020**, *160*, 36–51. https://doi.org/10.1016/j.addr.2020.10.009.

(30) Dhiman, N.; Awasthi, R.; Sharma, B.; Kharkwal, H.; Kulkarni, G. T. Lipid Nanoparticles as Carriers for Bioactive Delivery. *Front. Chem.* **2021**, *9*, 580118. https://doi.org/10.3389/fchem.2021.580118.

(31) Alibolandi, M.; Abnous, K.; Mohammadi, M.; Hadizadeh, F.; Sadeghi, F.; Taghavi, S.; Jaafari, M. R.; Ramezani, M. Extensive Preclinical Investigation of Polymersomal Formulation of Doxorubicin versus Doxil-Mimic Formulation. *J. Control. Release* **2017**, *264*, 228–236. https://doi.org/10.1016/j.jconrel.2017.08.030.

(32) Green, M. R.; Manikhas, G. M.; Orlov, S.; Afanasyev, B.; Makhson, A. M.; Bhar, P.; Hawkins, M. J. Abraxane®, a Novel Cremophor®-Free, Albumin-Bound Particle Form of Paclitaxel for the Treatment of Advanced Non-Small-Cell Lung Cancer. *Ann. Oncol.* **2006**, *17* (8), 1263–1268. https://doi.org/10.1093/annonc/mdl104.

(33) García-Hevia, L.; Casafont, Í.; Oliveira, J.; Terán, N.; Fanarraga, M. L.; Gallo, J.; Bañobre-López, M. Magnetic Lipid Nanovehicles Synergize the Controlled Thermal Release of Chemotherapeutics with Magnetic Ablation While Enabling Non-Invasive Monitoring by MRI for Melanoma Theranostics. *Bioact. Mater.* **2022**, *8*, 153–164. https://doi.org/10.1016/j.bioactmat.2021.06.009.

(34) García-Villén, F.; Carazo, E.; Borrego-Sánchez, A.; Sánchez-Espejo, R.; Cerezo, P.; Viseras, C.; Aguzzi, C. Clay Minerals in Drug Delivery Systems. In *Modified Clay and Zeolite Nanocomposite Materials*; Elsevier, **2019**; pp 129–166. https://doi.org/10.1016/B978-0-12-814617-0.00010-4.

(35) Zhang, X.; Chen, H.; Zhang, Y.; Huang, Q.; Feng, J.; Xing, H.; Fu, X.; Yan, X.; Zhang, Y.; Xu, Q.; Liang, J. HA-DOPE-Modified Honokiol-Loaded Liposomes Targeted Therapy for Osteosarcoma. *Int. J. Nanomedicine* **2022**, *Volume 17*, 5137–5151. https://doi.org/10.2147/IJN.S371934.

(36) Bilal, M.; Qindeel, M.; Raza, A.; Mehmood, S.; Rahdar, A. Stimuli-Responsive Nanoliposomes as Prospective Nanocarriers for Targeted Drug Delivery. *J. Drug Deliv. Sci. Technol.* **2021**, *66*, 102916. https://doi.org/10.1016/j.jddst.2021.102916.

(37) Abreu, A. S.; Castanheira, E. M.; Queiroz, M.-J. R.; Ferreira, P. M.; Vale-Silva, L. A.; Pinto, E. Nanoliposomes for Encapsulation and Delivery of the Potential Antitumoural Methyl 6-Methoxy-3-(4-Methoxyphenyl)-1*H*-Indole-2-Carboxylate. *Nanoscale Res. Lett.* **2011**, *6* (1), 482. https://doi.org/10.1186/1556-276X-6-482.

(38) Aslam, H.; Shukrullah, S.; Naz, M. Y.; Fatima, H.; Ullah, S.; Al-Sehemi, A. G. Multifunctional Magnetic Nanomedicine Drug Delivery and Imaging-Based Diagnostic Systems. *Part. Part. Syst. Charact.* **2021**, *38* (12), 2100179. https://doi.org/10.1002/ppsc.202100179.

(39) Fan, X.; Yuan, Z.; Shou, C.; Fan, G.; Wang, H.; Gao, F.; Rui, Y.; Xu, K.; Yin, P. cRGD-Conjugated Fe_3O_4@PDA-DOX Multifunctional Nanocomposites for MRI and Antitumour Chemo-Photothermal Therapy. *Int. J. Nanomedicine* **2019**, *14*, 9631–9645. https://doi.org/10.2147/IJN.S222797.

(40) Pasut, G.; Paolino, D.; Celia, C.; Mero, A.; Joseph, A. S.; Wolfram, J.; Cosco, D.; Schiavon, O.; Shen, H.; Fresta, M. Polyethylene Glycol (PEG)-Dendron Phospholipids as Innovative Constructs for the Preparation of Super Stealth Liposomes for Anticancer Therapy. *J. Control. Release* **2015**, *199*, 106–113. https://doi.org/10.1016/j.jconrel.2014.12.008.

(41) *Nanobiotechnology in Diagnosis, Drug Delivery, and Treatment*, 1st ed.; Rai, M., Razzaghi-Abyaneh, M., Ingle, A. P., Eds.; Wiley, **2020**. https://doi.org/10.1002/9781119671732.

(42) Xie, W.; Guo, Z.; Gao, F.; Gao, Q.; Wang, D.; Liaw, B.; Cai, Q.; Sun, X.; Wang, X.; Zhao, L. Shape-, Size- and Structure-Controlled Synthesis and Biocompatibility of Iron Oxide Nanoparticles for Magnetic Theranostics. *Theranostics* **2018**, *8* (12), 3284–3307. https://doi.org/10.7150/thno.25220.

(43) Zamay, G. S.; Zamay, T. N.; Lukyanenko, K. A.; Kichkailo, A. S. Aptamers Increase Biocompatibility and Reduce the Toxicity of Magnetic Nanoparticles Used in Biomedicine. *Biomedicines* **2020**, *8* (3), 59. https://doi.org/10.3390/biomedicines8030059.

(44) Chang, D.; Lim, M.; Goos, J. A. C. M.; Qiao, R.; Ng, Y. Y.; Mansfeld, F. M.; Jackson, M.; Davis, T. P.; Kavallaris, M. Biologically Targeted Magnetic Hyperthermia: Potential and Limitations. *Front. Pharmacol.* **2018**, *9*, 831. https://doi.org/10.3389/fphar.2018.00831.

(45) Sungsuwan, S.; Yin, Z.; Huang, X. Lipopeptide-Coated Iron Oxide Nanoparticles as Potential Glycoconjugate-Based Synthetic Anticancer Vaccines. *ACS Appl. Mater. Interfaces* **2015**, *7* (31), 17535–17544. https://doi.org/10.1021/acsami.5b05497.

(46) Liu, X.; Zhang, Y.; Wang, Y.; Zhu, W.; Li, G.; Ma, X.; Zhang, Y.; Chen, S.; Tiwari, S.; Shi, K.; Zhang, S.; Fan, H. M.; Zhao, Y. X.; Liang, X.-J. Comprehensive Understanding of Magnetic Hyperthermia for Improving Antitumour Therapeutic Efficacy. *Theranostics* **2020**, *10* (8), 3793–3815. https://doi.org/10.7150/thno.40805.

(47) Cędrowska, E.; Pruszyński, M.; Gawęda, W.; Żuk, M.; Krysiński, P.; Bruchertseifer, F.; Morgenstern, A.; Karageorgou, M.-A.; Bouziotis, P.; Bilewicz, A. Trastuzumab Conjugated Superparamagnetic Iron Oxide Nanoparticles Labeled with 225Ac as a Perspective Tool for Combined α-Radioimmunotherapy and Magnetic Hyperthermia of HER2-Positive Breast Cancer. *Molecules* **2020**, *25* (5), 1025. https://doi.org/10.3390/molecules25051025.

(48) Zhao, S.; Yu, X.; Qian, Y.; Chen, W.; Shen, J. Multifunctional Magnetic Iron Oxide Nanoparticles: An Advanced Platform for Cancer Theranostics. *Theranostics* **2020**, *10* (14), 6278–6309. https://doi.org/10.7150/thno.42564.

(49) Frantellizzi, V.; Conte, M.; Pontico, M.; Pani, A.; Pani, R.; De Vincentis, G. New Frontiers in Molecular Imaging with Superparamagnetic Iron Oxide Nanoparticles (SPIONs): Efficacy, Toxicity, and Future Applications. *Nucl. Med. Mol. Imaging* **2020**, *54* (2), 65–80. https://doi.org/10.1007/s13139-020-00635-w.

(50) Sanhaji, M.; Göring, J.; Couleaud, P.; Aires, A.; Cortajarena, A. L.; Courty, J.; Prina-Mello, A.; Stapf, M.; Ludwig, R.; Volkov, Y.; Latorre, A.; Somoza, Á.; Miranda, R.; Hilger, I. The Phenotype of Target Pancreatic Cancer Cells Influences Cell Death by Magnetic Hyperthermia with Nanoparticles Carrying Gemicitabine and the Pseudo-Peptide NucAnt. *Nanomedicine Nanotechnol. Biol. Med.* **2019**, *20*, 101983. https://doi.org/10.1016/j.nano.2018.12.019.

(51) Su, Z.; Liu, D.; Chen, L.; Zhang, J.; Ru, L.; Chen, Z.; Gao, Z.; Wang, X. CD44-Targeted Magnetic Nanoparticles Kill Head And Neck Squamous Cell Carcinoma Stem Cells In An Alternating Magnetic Field. *Int. J. Nanomedicine* **2019**, *14*, 7549–7560. https://doi.org/10.2147/IJN.S215087.

(52) Paliwal, R.; Paliwal, S. R.; Kenwat, R.; Kurmi, B. D.; Sahu, M. K. Solid Lipid Nanoparticles: A Review on Recent Perspectives and Patents. *Expert Opin. Ther. Pat.* **2020**, *30* (3), 179–194. https://doi.org/10.1080/13543776.2020.1720649.

(53) Piehler, S.; Dähring, H.; Grandke, J.; Göring, J.; Couleaud, P.; Aires, A.; Cortajarena, A. L.; Courty, J.; Latorre, A.; Somoza, Á.; Teichgräber, U.; Hilger, I. Iron Oxide Nanoparticles as Carriers for DOX and Magnetic Hyperthermia after Intratumoural Application into Breast Cancer in Mice: Impact and Future Perspectives. *Nanomaterials* **2020**, *10* (6), 1016. https://doi.org/10.3390/nano10061016.

(54) Belanova, A. A.; Gavalas, N.; Makarenko, Y. M.; Belousova, M. M.; Soldatov, A. V.; Zolotukhin, P. V. Physicochemical Properties of Magnetic Nanoparticles: Implications for Biomedical Applications In Vitro and In Vivo. *Oncol. Res. Treat.* **2018**, *41* (3), 139–143. https://doi.org/10.1159/000485020.

(55) Alavijeh, A.; Barati, M.; Barati, M.; Dehkordi, H. The Potential of Magnetic Nanoparticles for Diagnosis and Treatment of Cancer Based on Body Magnetic Field and Organ-on-the-Chip. *Adv. Pharm. Bull.* **2019**, *9*, 360–373. https://doi.org/10.15171/apb.2019.043.

(56) Xu, F.; Zhu, J.; Lin, L.; Zhang, C.; Sun, W.; Fan, Y.; Yin, F.; Van Hest, J. C. M.; Wang, H.; Du, L.; Shi, X. Multifunctional PVCL Nanogels with Redox-Responsiveness Enable

Enhanced MR Imaging and Ultrasound-Promoted Tumour Chemotherapy. *Theranostics* **2020**, *10* (10), 4349–4358. https://doi.org/10.7150/thno.43402.

(57) Scialla, S.; Hanafy, M. S.; Wang, J.-L.; Genicio, N.; Costa Da Silva, M.; Costa, M.; Oliveira-Pinto, S.; Baltazar, F.; Gallo, J.; Cui, Z.; Bañobre-López, M. Targeted Treatment of Triple-Negative-Breast Cancer through pH-Triggered Tumour Associated Macrophages Using Smart Theranostic Nanoformulations. *Int. J. Pharm.* **2023**, *632*, 122575. https://doi.org/10.1016/j.ijpharm.2022.122575.

(58) Song, H.; Wei, M.; Zhang, N.; Li, H.; Tan, X.; Zhang, Y.; Zheng, W. Enhanced Permeability of Blood–Brain Barrier and Targeting Function of Brain via Borneol-Modified Chemically Solid Lipid Nanoparticle. *Int. J. Nanomedicine* **2018**, *Volume 13*, 1869–1879. https://doi.org/10.2147/IJN.S161237.

(59) Satapathy, M. K.; Yen, T.-L.; Jan, J.-S.; Tang, R.-D.; Wang, J.-Y.; Taliyan, R.; Yang, C.-H. Solid Lipid Nanoparticles (SLNs): An Advanced Drug Delivery System Targeting Brain through BBB. *Pharmaceutics* **2021**, *13* (8), 1183. https://doi.org/10.3390/pharmaceutics13081183.

(60) Lingayat, V. J.; Zarekar, N. S.; Shendge, R. S. Solid Lipid Nanoparticles: A Review. *Nanosci. Nanotechnol. Res.* **2017**, 4, 67-72. https://doi.org/10.12691/nnr-4-2-5.

(61) Mirchandani, Y.; Patravale, V. B.; S., B. Solid Lipid Nanoparticles for Hydrophilic Drugs. *J. Control. Release* **2021**, *335*, 457–464. https://doi.org/10.1016/j.jconrel.2021.05.032.

(62) Zheng, G.; Zheng, M.; Yang, B.; Fu, H.; Li, Y. Improving Breast Cancer Therapy Using Doxorubicin Loaded Solid Lipid Nanoparticles: Synthesis of a Novel Arginine-Glycine-Aspartic Tripeptide Conjugated, pH Sensitive Lipid and Evaluation of the Nanomedicine in Vitro and in Vivo. *Biomed. Pharmacother.* **2019**, *116*, 109006. https://doi.org/10.1016/j.biopha.2019.109006.

(63) Bayón-Cordero, L.; Alkorta, I.; Arana, L. Application of Solid Lipid Nanoparticles to Improve the Efficiency of Anticancer Drugs. *Nanomaterials* **2019**, *9* (3), 474. https://doi.org/10.3390/nano9030474.

(64) Świętek, M.; Panchuk, R.; Skorokhyd, N.; Černoch, P.; Finiuk, N.; Klyuchivska, O.; Hrubý, M.; Molčan, M.; Berger, W.; Trousil, J.; Stoika, R.; Horák, D. Magnetic Temperature-Sensitive Solid-Lipid Particles for Targeting and Killing Tumour Cells. *Front. Chem.* **2020**, *8*, 205. https://doi.org/10.3389/fchem.2020.00205.

(65) Liu, Z.; Chen, K.; Davis, C.; Sherlock, S.; Cao, Q.; Chen, X.; Dai, H. Drug Delivery with Carbon Nanotubes for *In Vivo* Cancer Treatment. *Cancer Res.* **2008**, *68* (16), 6652–6660. https://doi.org/10.1158/0008-5472.CAN-08-1468.

(66) Jiménez-López, J.; García-Hevia, L.; Melguizo, C.; Prados, J.; Bañobre-López, M.; Gallo, J. Evaluation of Novel Doxorubicin-Loaded Magnetic Wax Nanocomposite Vehicles as Cancer Combinatorial Therapy Agents. *Pharmaceutics* **2020**, *12* (7), 637. https://doi.org/10.3390/pharmaceutics12070637.

(67) Moura, C. L.; Gallo, J.; García-Hevia, L.; Pessoa, O. D. L.; Ricardo, N. M. P. S.; Bañobre-López, M. Magnetic Hybrid Wax Nanocomposites as Externally Controlled Theranostic Vehicles: High MRI Enhancement and Synergistic Magnetically Assisted

Thermo/Chemo Therapy. *Chem. – Eur. J.* **2020**, *26* (20), 4531–4538. https://doi.org/10.1002/chem.201904709.

(68) Tapeinos, C.; Marino, A.; Battaglini, M.; Migliorin, S.; Brescia, R.; Scarpellini, A.; De Julián Fernández, C.; Prato, M.; Drago, F.; Ciofani, G. Stimuli-Responsive Lipid-Based Magnetic Nanovectors Increase Apoptosis in Glioblastoma Cells through Synergic Intracellular Hyperthermia and Chemotherapy. *Nanoscale* **2019**, *11* (1), 72–88. https://doi.org/10.1039/C8NR05520C.

(69) Lepland, A.; Malfanti, A.; Haljasorg, U.; Asciutto, E. K.; Pickholz, M.; Bringas, M.; Đorđević, S.; Salumäe, L.; Peterson, P.; Teesalu, T.; Vicent, M. J.; Scodeller, P. Depletion of Mannose Receptor–Positive Tumour-Associated Macrophages via a Peptide-Targeted Star-Shaped Polyglutamate Inhibits Breast Cancer Progression in Mice. *Cancer Res. Commun.* **2022**, *2* (6), 533–551. https://doi.org/10.1158/2767-9764.CRC-22-0043.

(70) Zhu, S.; Niu, M.; O'Mary, H.; Cui, Z. Targeting of Tumour-Associated Macrophages Made Possible by PEG-Sheddable, Mannose-Modified Nanoparticles. *Mol. Pharm.* **2013**, *10* (9), 3525–3530. https://doi.org/10.1021/mp400216r.

(71) Abouelmagd, S. A.; Meng, F.; Kim, B.-K.; Hyun, H.; Yeo, Y. Tannic Acid-Mediated Surface Functionalization of Polymeric Nanoparticles. *ACS Biomater. Sci. Eng.* **2016**, *2* (12), 2294–2303. https://doi.org/10.1021/acsbiomaterials.6b00497.

(72) Hyun, H.; Park, J.; Willis, K.; Park, J. E.; Lyle, L. T.; Lee, W.; Yeo, Y. Surface Modification of Polymer Nanoparticles with Native Albumin for Enhancing Drug Delivery to Solid Tumours. *Biomaterials* **2018**, *180*, 206–224. https://doi.org/10.1016/j.biomaterials.2018.07.024.

(73) Sengupta, S.; Krishnan, M. A.; Dudhe, P.; Reddy, R. B.; Giri, B.; Chattopadhyay, S.; Chelvam, V. Novel Solid-Phase Strategy for the Synthesis of Ligand-Targeted Fluorescent-Labelled Chelating Peptide Conjugates as a Theranostic Tool for Cancer. *Beilstein J. Org. Chem.* **2018**, *14*, 2665–2679. https://doi.org/10.3762/bjoc.14.244.

(74) Birtalan, E.; Rudat, B.; K. Kolmel, D.; Fritz, D.; B. L. Vollrath, S.; Schepers, U.; Brase, S. Investigating Rhodamine B-Labeled Peptoids: Scopes and Limitations Os Its Applications. *Pept. Sci.* **2011**, *96*, 694–701. https://doi.org/DOI 10.1002/bip.21617.

(75) Belko, N.; Maltanava, H.; Lugovski, A.; Ferreira, R. A. S.; Correia, S. F. H.; Shabunya, P.; Fatykhava, S.; Tabolich, A.; Kulahava, T.; Bahdanava, A.; Ferreira, M.; Tedim, J.; Poznyak, S.; Samtsov, M. pH-Sensitive Fluorescent Sensor for Fe(III) and Cu(II) Ions Based on Rhodamine B Acylhydrazone: Sensing Mechanism and Bioimaging in Living Cells. *Microchem. J.* **2023**, *191*, 108744. https://doi.org/10.1016/j.microc.2023.108744.

(76) Chen, H.; Zhou, B.; Ye, R.; Zhu, J.; Bao, X. Synthesis and Evaluation of a New Fluorescein and Rhodamine B-Based Chemosensor for Highly Sensitive and Selective Detection of Cysteine over Other Amino Acids and Its Application in Living Cell Imaging. *Sens. Actuators B Chem.* **2017**, *251*, 481–489. https://doi.org/10.1016/j.snb.2017.05.078.

(77) Wang, G. T.; Matayoshi, E.; Jan Huffaker, H.; Krafft, G. A. Design and Synthesis of New Fluorogenic HIV Protease Substrates Based on Resonance Energy Transfer. *Tetrahedron Lett.* **1990**, *31* (45), 6493–6496. https://doi.org/10.1016/S0040-4039(00)97099-0.

(78) Yang, Y.; Hu, B. Bio-Based Chemicals from Biorefining: Lipid and Wax Conversion and Utilization. In *Advances in Biorefineries*; Elsevier, 2014; pp 693–720. https://doi.org/10.1533/9780857097385.2.693.

(79) Nederberg, F.; Bowden, T.; Hilborn, J. Synthesis, Characterization, and Properties of Phosphoryl Choline Functionalized Poly ε-Caprolactone and Charged Phospholipid Analogues. *Macromolecules* **2004**, *37* (3), 954–965. https://doi.org/10.1021/ma035433b.

(80) Moghaddam, B.; McNeil, S. E.; Zheng, Q.; Mohammed, A. R.; Perrie, Y. Exploring the Correlation Between Lipid Packaging in Lipoplexes and Their Transfection Efficacy. *Pharmaceutics* **2011**, *3* (4), 848–864. https://doi.org/10.3390/pharmaceutics3040848.

(81) Schmitt, L.; Dietrich, C.; Tampé, R. Synthesis and Characterization of Chelator-Lipids for Reversible Immobilization of Engineered Proteins at Self-Assembled Lipid Interfaces. *J. Am. Chem. Soc.* **1994**, *116*, 8485–8491. https://doi.org/10.1021/ja00098a008.

(82) Keykavous, P.; Bharathi, K.; Haseena Banu, B. Applications of Peptide Coupling Reagents - An Update. *Int. J. Pharm. Sci. Rev. Res.* **2011**, 8, 108–119. https://doi.org/10.1002/chin.201147263.

(83) Guillier, F.; Orain, D.; Bradley, M. Linkers and Cleavage Strategies in Solid-Phase Organic Synthesis and Combinatorial Chemistry. *Chem. Rev.* **2000**, *100* (6), 2091–2158. https://doi.org/10.1021/cr980040+.

(84) Montalbetti, C. A. G. N.; Falque, V. Amide Bond Formation and Peptide Coupling. *Tetrahedron* **2005**, *61* (46), 10827–10852. https://doi.org/10.1016/j.tet.2005.08.031.

(85) Al-Warhi, T. I.; Al-Hazimi, H. M. A.; El-Faham, A. Recent Development in Peptide Coupling Reagents. *J. Saudi Chem. Soc.* **2012**, *16* (2), 97–116. https://doi.org/10.1016/j.jscs.2010.12.006.

(86) Li, X.; Zhao, S.; Li, B.; Yang, K.; Lan, M.; Zeng, L. Advances and Perspectives in Carbon Dot-Based Fluorescent Probes: Mechanism, and Application. *Coord. Chem. Rev.* **2021**, *431*, 213686. https://doi.org/10.1016/j.ccr.2020.213686.

(87) An, F.-F.; Kommidi, H.; Chen, N.; Ting, R. A Conjugate of Pentamethine Cyanine and 18F as a Positron Emission Tomography/Near-Infrared Fluorescence Probe for Multimodality Tumour Imaging. *Int. J. Mol. Sci.* **2017**, *18* (6), 1214. https://doi.org/10.3390/ijms18061214.

(88) Roux, S.; Zékri, E.; Rousseau, B.; Paternostre, M.; Cintrat, J.-C.; Fay, N. Elimination and Exchange of Trifluoroacetate Counter-Ion from Cationic Peptides: A Critical Evaluation of Different Approaches. *J. Pept. Sci.* **2008**, *14* (3), 354–359. https://doi.org/10.1002/psc.951.

(89) Sikora, K.; Neubauer, D.; Jaśkiewicz, M.; Kamysz, W. Citropin 1.1 Trifluoroacetate to Chloride Counter-Ion Exchange in HCl-Saturated Organic Solutions: An Alternative

Approach. *Int. J. Pept. Res. Ther.* **2018**, *24* (2), 265–270. https://doi.org/10.1007/s10989-017-9611-7.

(90) Takechi-Haraya, Y.; Ohgita, T.; Demizu, Y.; Saito, H.; Izutsu, K.; Sakai-Kato, K. Current Status and Challenges of Analytical Methods for Evaluation of Size and Surface Modification of Nanoparticle-Based Drug Formulations. *AAPS PharmSciTech* **2022**, *23* (5), 150. https://doi.org/10.1208/s12249-022-02303-y.

(91) Joseph, E.; Singhvi, G. Multifunctional Nanocrystals for Cancer Therapy: A Potential Nanocarrier. In *Nanomaterials for Drug Delivery and Therapy*; Elsevier, **2019**; pp 91–116. https://doi.org/10.1016/B978-0-12-816505-8.00007-2.

(92) Michalke, B.; Nischwitz, V. Speciation and Element-Specific Detection. in Liquid Chromatography. In *Liquid Chromatography*; Elsevier, **2013**; pp 633–649. https://doi.org/10.1016/B978-0-12-415806-1.00022-X.

(93) Cirulis, J. T.; Strasser, B. C.; Scott, J. A.; Ross, G. M. Optimization of Staining Conditions for Microalgae with Three Lipophilic Dyes to Reduce Precipitation and Fluorescence Variability. *Cytometry A* **2012**, *81A* (7), 618–626. https://doi.org/10.1002/cyto.a.22066.

(94) Alfaifi, A. A.; Heyder, R. S.; Bielski, E. R.; Almuqbil, R. M.; Kavdia, M.; Gerk, P. M.; Da Rocha, S. R. P. Megalin-Targeting Liposomes for Placental Drug Delivery. *J. Control. Release* **2020**, *324*, 366–378. https://doi.org/10.1016/j.jconrel.2020.05.033.

(95) Martins, C. D. F.; Raposo, M. M. M.; Costa, S. P. G. Synthesis and Characterization of a Water-Soluble Pentamethine Indocyanine Dye for Peptide Labeling. *Chem. Proc.* **2022**, *8*(1), 91. https://doi.org/10.3390/ecsoc-25-11768.